University of Crete

Quantum metrology in biochemical magnetometers

Kyriacos M. Vitalis

UNIVERSITY OF CRETE
DEPARTMENT OF PHYSICS

QUANTUM METROLOGY IN BIOCHEMICAL MAGNETOMETERS

by

Kyriacos M. Vitalis

A dissertation submitted in partial fulfillment of the requirements

for the degree of

Doctor of Philosophy in Physics

Supervisor:	Prof. I. K. Kominis	
Dissertation committee:	Prof. I. K. Kominis,	UoC
	Prof. X. Zotos,	UoC
	Prof. D. Charalambidis,	UoC

This research has been co-financed (01/04/2013-30/09/2015) by the European Union (European Social Fund – ESF) and Greek national funds through the Operational Program "Education and Lifelong Learning" of the National Strategic Reference Framework (NSRF) – Research Funding Program THALIS, and by the European Union's Seventh Framework Programme FP7-REGPOT-2012-2013-1 under grant agreement 316165.

Dedicated to my family:
my grandparents Avgoustis & Demetra,
my parents Michael & Soteroulla,
my siblings Demetris, Avgoustinos, Anna-Maria & Rafaelia

ABSTRACT

Radical-ion pairs and their reactions have triggered the study of quantum effects in biological systems. This is because they exhibit a number of effects best understood within quantum information science, and at the same time are central in understanding the avian magnetic compass and the spin transport dynamics in photosynthetic reaction centers. These pairs of biomolecular ions are recently shown to be biological open quantum systems. We show that the coupling of the radical-pair spin degrees of freedom to its decohering vibrational reservoir leads to a phononic Lamb shift of the radical-pair magnetic energy levels. The Lamb shift Hamiltonian is diagonal in the singlet-triplet basis, and results in a singlet-triplet energy splitting physically indistinguishable from an exchange interaction. This could have significant implications for understanding the energy level structure and the dynamics of photosynthetic reaction centers, which are intimately connected with the remarkable efficiency of photosynthesis.

Moreover, we address radical-pair reactions from the perspective of quantum metrology. Since the coherent spin-motion of radical pairs is effected by an external magnetic field, these spin-dependent reactions essentially realize a biochemical magnetometer. Using the quantum Fisher information, we find the fundamental quantum limits to the magnetic sensitivity of radical-pair magnetometers, arriving at a sensitivity $\delta B = \frac{2\mathrm{pT}}{\tau[1\mu s]\sqrt{\nu_0[10^{12}]}}$, given in terms of radical-pair lifetime τ and number of radical pairs ν_0. We then explore how well the usual measurement scheme considered in radical-pair reactions, the measurement of reaction yields, approaches the fundamental limits. In doing so, we find the optimal hyperfine interaction Hamiltonian that leads to the best magnetic sensitivity as obtained from reaction yields. This is still an order of magnitude smaller than the absolute quantum limit. Finally, we demonstrate that with a realistic quantum reaction control reminding one of Ramsey interferometry, here presented as a quantum circuit involving the spin-exchange interaction and a recently proposed molecular switch, we can approach the fundamental quantum limit within a factor of 2. Hence, this work opens the application of well-advanced quantum metrology methods to biological systems.

PUBLICATIONS

Invited article at the EPJ-Plus Topical Issue "Quantum Information and Complexity"
Lamb shift in radical-ion pairs produces a singlet-triplet energy splitting in photosynthetic reaction centers
K. M. Vitalis and I. K. Kominis, Europ. Phys. J. Plus 129, 187 (2014)

Quantum-limited biochemical magnetometers designed using the Fisher information and quantum reaction control
K. M. Vitalis and I. K. Kominis, Physical Review A 95, 032129 (2017)

"*You can know the name of a bird in all the languages of the world,*
but when you're finished, you'll know absolutely nothing whatever about the bird.
So let's look at the bird and see what it's doing – that's what counts.
I learned very early the difference between knowing the name of something
and knowing something."

— Richard P. Feynman

ACKNOWLEDGMENTS

I would like to thank my supervisor Prof. Iannis Kominis for the kind reception he has shown me, my enrollment in his research group in the Physics Department of the University of Crete, his rigorous scientific treatment and guidance which proved to be fruitful for my research and let me appreciate that quantum mechanics occurs in reality and not in the Hilbert space. I am most grateful for his constant support, and being available for discussion that enabled me to achieve a deeper understanding of the essential physics.

Special thanks to my parents, Michael & Soteroulla, for both their material and moral support and their unwavering belief in me. It is beyond any doubt that without their help, encouragement and unconditional love I would not have been able to accomplish my studies.

I am also thankful to my friends and all the members of our research group, especially George Soleas, Michael Hadjiconstantis, Christoforos Panagi, Pavlos Chrysanthou, Joseph Ioannou, Christos Elia, Constantinos Sofokleous, Marinos Kasapis, Argyris Dellis, Konstantinos Saliaris, Nikos Tsatrafyllis, Joniald Shena, Michalis Kritsotakis, Kostas Mouloudakis.

CONTENTS

LIST OF FIGURES

NOMENCLATURE

RPM Radical-Pair Mechanism

RP Radical Pair/Radical-ion Pair

DA Donor-Acceptor

LH Light Harvesting

LHC Light-Harvesting Complex

FMO Fenna-Mathews-Olson

RC Reaction Center

PRC Photosynthetic Reaction Center

BChl Bacteriochlorophyll

ET Electron Transfer

EPR Electron Paramagnetic Resonance

NMR Nuclear Magnetic Resonance

CIDEP Chemically Induced Dynamic Electron Polarization

CIDNP Chemically Induced Dynamic Nuclear Polarization

MFE Magnetic Field Effect

HOMO Highest Occupied Molecular Orbital

LUMO Lowest Unoccupied Molecular Orbital

ISC Inter-System Crossing

ME Master Equation

SOMO Singly Occupied Molecular Orbital

PVM Projector-Valued Measure

POVM Positive Operator-Valued Measure

CPM Completely Positive Map

RWA Rotating Wave Approximation

SQL Standard Quantum Limit

RMSE Root-Mean-Square Error

MLE Maximum Likelihood Estimation

QIP Quantum Information Processing

QFI Quantum Fisher Information

SLD Symmetric Logarithmic Derivative

GHZ Greenberger-Horne-Zeilinger

I

QUANTUM PHYSICS IN BIOLOGY

" *What is Life ?* "

— Erwin Schrödinger

1

INTRODUCTION

1.1. A BRIEF INTRODUCTION TO QUANTUM BIOLOGY

Nowadays, it is well accepted that the laws of quantum mechanics govern physics and chemistry, whereas it is not clear that the same holds for biology. Biology appears to remain in the classical domain, and hence quantum physics is actually unnecessary in most biological scenarios, e.g., on the level of proteins and cells. It seems that all processes, particularly on the physiological level, can and will be well understood in terms of classical biology. However, we suspect that life must, like everything else, be quantum at the atomic scale and hence we ask if this atomic scale matters. The debate goes back a long way. Erwin Schrödinger, a founding father of quantum mechanics, in his influential book "What is Life?" said that "quantum indeterminacy plays no biologically relevant role". Pascual Jordan, another albeit less recognized founder of quantum mechanics, was instead convinced that the "Secret of Organic Life" was to be found in quantum "organizing centers" that controlled the classical machinery around them.

Perhaps, the answer to this long-standing debate lies somewhere at the boundary between quantum and classical physics. A nanometer-scale system sits at this boundary, a challenging domain which prohibits so far exact calculations or confident approximations. The nanoscale domain is neither infertile nor inhabitable place, but quiet the contrary. Life has always been there, operating at the nanoscale for billions of years, endlessly varying and selecting the devices and programs that lead to survival. If we succeed in understanding these systems, then we will be able to synthesize bio-inspired devices (bio-engineering) that both mimic and advance natural processes. The convergence between molecular biology and nanotechnology could bring, in the near future, the emerging science of *quantum biology* [1–3] into mainstream. Quantum biology is a uniquely interdisciplinary field combining quantum physics, quantum information science, chemical physics (or physical chemistry), biochemistry, biophysics and biology.

The first key issue in the field of quantum biology is about the length scale where to explore quantum effects. In fact, quantum chemistry works very well for typical small

molecules on the order of less than 1 nm, i.e. with a small number of atoms. However, an exceptional amount of computational power would be required for typical proteins of about 5–10 nm. Usually, a hybrid classical-quantum method is exploited; a small region is treated quantum-mechanically, whereas the much larger surrounding is treated classically. A question that arises is whether quantum effects that are neglected in such calculations would affect the correctness of the predictions. Although it is found that the hybrid method results in great success, e.g. in supra-molecular chemistry, it is still not clear whether the treatment will be precise for complex proteins.

The second key issue in the field of quantum biology is whether and how quantum effects can sustain in biological systems. Biological systems are *open systems* (as supplied with energy), warm (namely at room temperature), wet and noisy with a huge number of collision events happening, so they are subject to a significant high level of environmental noise. However, quantum features such as *quantum coherence* and *quantum correlation*, i.e. *entanglement*[1], are fragile to thermal fluctuations and other noise sources. For example, quantum information processing (QIP) experiments that allow the observation of quantum effects, are usually performed under special, carefully controlled conditions such as carefully isolated setups, high vacuum and extremely low temperatures. This is in order to protect systems from the pernicious environmental noise, so that quantum effects be sustained for a sufficient long time with respect to the timescale over which the desired quantum operation takes place, even the absolute coherence time may be short.

Quantum coherence and entanglement have been experimentally identified in various systems such as ion traps, mechanical resonators, nitrogen vacancy centers in diamond, superconducting circuits, quantum dots etc. They are all crucial resources, i.e. helpful ingredients, for QIP. So, it is natural to ask whether quantum physics plays a non-trivial functional role in biology.

In recent years, scientists have been utilizing the concepts developed in quantum information science to explore quantum dynamics in biological systems. There is both theoretical and experimental evidence suggesting that a variety of organisms may harness some of the unique features of quantum mechanics (and also utilize environmental noise to harness such quantum features) to gain a biological advantage (compared to their classical competitors). These features go beyond trivial quantum effects, such as quantization of physical properties (energy, momentum etc.), and may include harnessing quantum coherence and entanglement on physiologically important timescales. Such findings support the early intuition of the founding fathers of quantum mechanics that biological systems should be influenced by the intricacies of quantum physics. Therefore, quantum biology is not about the "static", atomistic aspect of biological structure, but about dynamic effects related to quantum coherence and entanglement influencing biological function.

[1] Entanglement is a physical phenomenon that was the subject of a 1935 paper by Albert Einstein, Boris Podolsky, and Nathan Rosen, and several papers by Erwin Schrödinger shortly thereafter, describing what came to be known as the EPR paradox. Entangled states cannot accurately be described in terms of the properties of their component parts considered separately; instead, an entangle state must be described for the system as a whole. Moreover, the behavior of one part is (instantaneously) affected by what happens to the other part, even when they are separated by a large distance. Einstein and others considered such behavior to be impossible, and described this sort of thing as "spooky action at a distance".

Currently, the following four quantum biological mechanisms are explored: photosynthesis, magnetoreception (magnetic sensing), olfaction (sense of smell), general anaesthesia. In Chapter 2, we will review recent progress in this direction. It has been found that biological systems can perform certain tasks such as *photosynthesis* more efficiently, or realize a function such as *magnetoreception* in some avian species (migratory birds) by harnessing non-trivial quantum phenomena.

1.2. THIS THESIS

The contribution of this thesis to the general field of Quantum Biology is the following. There are some pairs of biomolecular ions, known as *Radical Pairs* (RPs), which are recently shown to exhibit a host of non-trivial quantum effects, providing a strong link between quantum physics and biology. In doing so, RPs have triggered the study of quantum effects in biological systems since they exhibit a number of effects best understood within quantum information science, and at the same time are central in understanding the avian magnetic compass and the spin transport dynamics in photosynthetic reaction centers (PRCs).

In Part II, we study the 'open' nature and the quantum dynamics of RPs which are located in the PRC of Photosystem I. Specifically, we show that the coupling of the RP spin degrees of freedom to its decohering vibrational reservoir leads to a phononic Lamb-shift-type singlet-triplet energy splitting, that is the physical magnetic energy levels of the RP are shifted relative to the levels of a 'bare' RP, which is an unphysical RP without the decohering vibrational states. Singlet and triplet RP states are shifted by a different amount, resulting in a singlet-triplet energy splitting, which is physically indistinguishable from an exchange interaction. This could have significant implications for understanding the energy level structure and the dynamics of PRCs, which are intimately connected with the remarkable efficiency of photosynthesis.

In Part III, we address RP reactions from the perspective of quantum metrology, opening the application of well-advanced quantum metrology methods to biological systems. Since the coherent spin-motion of RPs is effected by an external magnetic field, their spin-dependent reactions essentially realize a biochemical magnetometer. We find the fundamental quantum limits to the magnetic sensitivity of RP magnetometers by the means of a fundamental quantity of quantum parameter estimation, the so-called quantum Fisher information. We then find that the usual measurement scheme of reaction yields is sub-optimal, approaching the fundamental limits to within an order of magnitude. Finally, we demonstrate that with a realistic quantum reaction control, reminding one of Ramsey interferometry and modeled by a quantum circuit involving the exchange interaction and a recently proposed molecular photo-switch, we can approach the fundamental quantum limit within a factor of 2. The implementation of such a quantum-limited RP magnetometer will add into the Quantum Technology's gadgets a novel, state-of-the-art, magnetic-field-intensity biochemical quantum sensor.

2

QUANTUM PHENOMENA IN LIVING ORGANISMS

2.1. ENERGY TRANSPORT IN PHOTOSYNTHESIS

Photosynthesis is a process used by plants and other organisms (algae, bacteria) to convert (sun)light energy into chemical energy, which can then be utilized to fuel organisms' activities. This chemical energy is stored in carbohydrate molecules, such as sugars/glucose ($C_6H_{12}O_6$), which are made from carbon dioxide (CO_2) and water (H_2O). Photosythesis is largely responsible for producing and maintaining the oxygen content of the Earth's atmosphere, and supplies all of the organic compounds and most of the energy necessary for life on Earth, hence it is one of the most important biological processes.

From the point of view of physics, this energy, in the form of photons, is absorbed by *light-harvesting antennas*, consist of chlorophyll pigment molecules (giving plants their green color), which create an electronic excitation, called *exciton*. The exciton is then transported from each antenna to a *reaction center* (RC), where photo-chemical processing takes place and transforms the excitonic energy into a more stable chemical energy. The remarkable experimental observation is a photo-biological charge separation closed to 100% quantum efficiency[1], that is almost all of photon energy absorbed by the chlorophyll antennas is transferred to the RC and converted into a more stable electro-chemical form. A typical photosynthetic process is presented in Fig. 2.1.

Chlorophyll, e.g. chlorophyll-a $C_{55}H_{72}O_5N_4Mg$, is an eminently quantum object in which a metal atom (magnesium Mg) sits at the center of a highly delocalised cloud of electrons. The central part of the chlorophyll molecule is the porphyrin ring surrounding the magnesium atom, and it is the arrangement of electrons in this ring that allows chlorophyll to absorb solar energy. The photo-generated exciton can move around very efficiently in the system of connected chlorophylls, if they are sufficiently close to each other, and only

[1] Quantum efficiency is a measure of the probability that a single quantum, such as individual photon, is transformed into the desired output, such a charge-separation event, that converts the quantum's unstable energy into a more stable electric form, a process reminiscent of the charging of a capacitor. This energy can be utilized for future work.

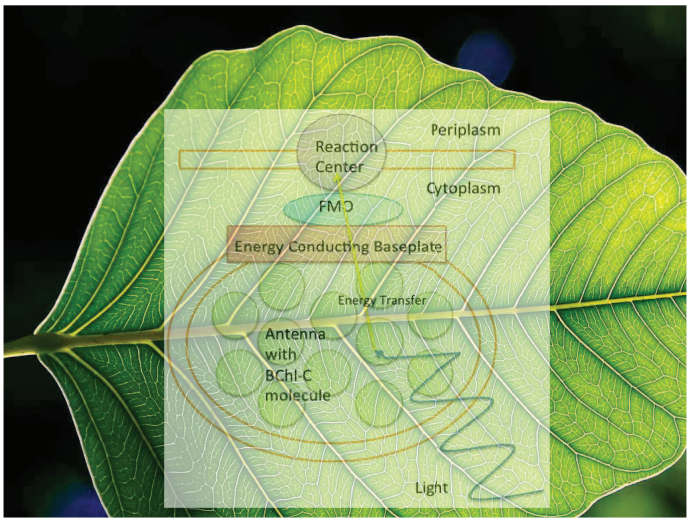

Figure 2.1: A light-harvesting chlorophyll antenna absorbs light as an electronic excitation (exciton), which is then transferred through an FMO complex (protein) to a photosynthetic reaction center; the FMO complex connects the photon-capturing antenna to the raction center by acting as a wire for energy transport. The FMO complex normally exists in a trimer of 3 complexes, each of which consists of 8 BChl-a molecules, and is connected to the chlorosome antenna through a baseplate. Excitations enter the FMO from this baseplate, exciting one of the BChl molecules into its 1^{st} singlet excited state. These molecules are close to each other ($\sim$ 1.5 nm) enabling the excitation energy to transfer from one BChl molecule to another, until it reaches the reaction center.

little of its energy is dissipated as heat. The exact exciton energy depends on the associated chlorophylls which have constant structure and, also, on their immediate molecular environment. If an exciton jumps from one set of chlorophylls to another with a smaller exciton energy, then this energy difference must be absorbed or generated by the environment in the form of vibrations, termed *phonons*. The precise biological structures and pigment constituents used, from the antenna to the RC and forward, vary between photosynthetic organisms. Most of them use arrangements of such chlorophyll molecules complexed with proteins.

One of the simplest and most well-studied examples is the light-harvesting apparatus of green-sulphur bacteria [1], into which the excitonic energy is transferred to the RC through a specialized protein called *Fenna-Mathews-Olson* (FMO) complex. Because of its relatively small size, water solubility and that it makes good crystals which enable the position of all its atoms to be known, the FMO complex yielded a rich scientific attention and as a result has been well characterized. What is remarkable is its observed high efficiency; almost every photon that is absorbed is successfully transferred to the RC even though the intermediate electronic excitations are very short-lived ($\sim$ 1 ns). This indicates that the exciton energy somehow finds an extremely efficient way to transfer to the RC. Indeed, G. S. Engel et al. [4] demonstrated experimentally that the energy transport timescale is on the order of ps. In 2007, G. R. Fleming and co-workers demonstrated evidence for quantum coherence in both the energy transfer in the FMO complex and in the bacterial RC [5]. Since then, the FMO complex has been one of the main subjects of research in quantum biology.

The same basic principles have been found to apply also to other protein complexes, such as light-harvesting complexes of photosynthetic bacteria, marine algae and plants.

These proteins transport excitons from one end to another via the chlorophyll molecules embedded in the protein by an efficient (and counter-intuitive) way: (i) the exciton does not usually reside on a single chlorophyll molecule but it is spread over several ones, (ii) the exciton follows at the same time different pathways which are mutually interfere in a wave-like fashion, (iii) the vibrational modes of the protein in which the chlorophylls are embedded are matched to the energy differences between excitons, so they can absorb or generate the correct amount of energy, and therefore facilitate exciton transport from one end to the other, almost without energy loss in between. In other words, as the exciton energy passes between molecules, a newly observed 'wave-like characteristic' allows the energy to simultaneously sample all the potential energy pathways and choose the most efficient one.

G. S. Engel et al. [4] performed their experiments at the cryogenic temperature of 77 K. Later experiments by E. Collini et al. and G. S. Engel et al. in 2010-11, have shown that the coherence in excitation transfer exists even near room temperature (~ 296 K). Photosynthesis usually performs at temperature above 273 K. A plausible question that naturally arises is why quantum coherence exists during excitonic transport and what is the role of it. And a plausible answer is because it may increase the energy transfer efficiency due to the aforementioned intriguing characteristics. A high transfer efficiency may be very important for life species which live in a weak light environment, such as green-sulphur bacteria.

A key to the survival of quantum coherence in this temperature regime is an interplay between the electronic energy levels and the energies of long-lived vibrational modes. If electronic levels of different chromophores are separated by an energy which corresponds to the energy of a vibrational mode, then we have a resonance which leads to mutual energy exchange, much like to that between coupled pendula of similar frequency. If a long-lived vibration is excited, then it can drive oscillations between electronic excitations in a light-harvesting antenna, thus enabling the pigments to share the same coherent modes. This is novel engineering: it is fair to say that no man-made device so far has made use of all these properties at these spatial and temporal scales concomitantly, and with such an efficiency.

As it has already been mentioned in [6], numerous theoretical models have been proposed to explain how and why excitonic transport is more efficient by using quantum coherence. For instance, some of them treat the environment as a Markovian thermal bath [7, 8]. Each site in the FMO complex interacts with an independent environmental bath. It was found that by combining the coherence of excitation transport and the thermal noise, the excitation may easily escape a local potential minima of the FMO and move to the RC.

However, as usual, there exists the opposite opinion which challenges the above conclusions. Recent analysis showed that the quantum enhancement of the transport efficiency might be only a few percent [9]. There is, also, the Förster model in which the exciton transfer between different sites is incoherent, and the superpositions/coherences are neglected. Therefore, it is still not clear and unambiguous whether quantum coherence is essential for Photosynthesis. Some works proposed classical models which can also have quantum-like oscillation behavior [10]. Hence, more studies are needed to clarify the role of quantum coherence in Photosynthesis [11, 12].

2.2. MAGNETORECEPTION IN BIRDS

For over 40 years, a wealth of data has made clear that birds posses a magnetic compass which helps them perform extraordinary features of navigation and migration by using the geomagnetic field, a phenomenon called *avian magnetoreception*. Although the molecular mechanism underlying this compass has been controversial for a long time, one thing has always been clear: the sensor must include either a ferromagnetic solid like magnetite, i.e. deposits of magnetic iron minerals, or a paramagnetic entity like an electronic spin.

Behavioral experiments on some avian species seem to rule out the magnetite-based mechanism. For example, European robins (*Erithacus rubecula*) have a magnetic sense that acts as an *inclination* compass insensitive to polarity [13], i.e. it cannot distinguish magnetic North from magnetic South pole, but just acquires directional information by interpreting the inclination of the magnetic field lines; 'poleward' pointing downward and 'equatorward' pointing upward [14]. However, most magnetite-based compass models operate as a polarity-sensitive sense [15]. So the current favorite and most attractive, at least in birds, is a mechanism involving electron spins, the so-called *Radical-Pair Mechanism* (RPM) proposed in 1978 by K. Schulten et al. [16] as a plausible biological chemical compass. A Radical Pair (RP) is typically a pair of bound molecules each has an unpaired electron.

Many behavioral experiments have been performed, revealing more and more intriguing properties of this non-polar magnetic sense. The navigation sense was shown to be :

(i) photoreceptor based, i.e. dependent on the presence of certain frequencies of ambient light[2] [15, 17] ,

(ii) sensitive to changes in the intensity of the external magnetic field [17, 18], and readjustment over time (as short as an hour) to these new intensities [18–20] ,

(iii) disrupted by magnetic pulses [21], and very weak (~ 50-100 nT) external radiofrequency magnetic fields oscillating at 1.3 MHz (resonant with the Zeeman splitting between the spin-up and spin-down states of radical electrons, i.e. the electronic spin-precession Larmor frequency, caused by the static geomagnetic field)[20]. Moreover, a recent study by S. Engels and co-workers revealed that the magnetic compass orientation in European robins is disrupted by the anthropogenic (urban) electromagnetic noise [22].

The precise operating principle of RPM is subtle and can be summarized in three main steps:

(**1**) Firstly, a photochemical reaction starts from the light activation of a photoreceptor and is followed by an electron transfer process leading to a spatially separated electron-pair (charge-separated state), that is a Radical Pair (RP). Each electron has spin (s=1/2) and

[2]These studies suggest that the magnetic compass operates best under blue and green light, whereas it is disrupted under yellow and red light with a fairly sharp transition between orientation and disorientation around 570 nm.

behaves like a quantum magnet. So an RP carries two unpaired electrons, the spin-state of which is the singlet (S) or the triplet ($T_0, T_\pm$). Usually, the generated RP is in the spin-correlated singlet state, which is also the spin-state of its neutral precursor molecule.

(**2**) Then, the RP spin-state is inter-converted between singlet and triplet under the combined effect of global and local magnetic interactions, namely the external Earth's magnetic field (Zeeman interaction) and the internal hyperfine interactions with the host nuclei, respectively. This quantum coherent process (also known as *Rabi flopping/cycle* with the driving field being, for instance, the hyperfine one) is sensitive to and controlled by both the intensity (magnitude) and orientation of the external magnetic field vector relative to the orientation of the local environment, principally made up of nuclear spins within the molecules. Hence, it is an interplay between symmetry and asymmetry in the interaction with the outside world that gives rise to this dynamical spin-coherence.

(**3**) Finally, the RP state is unstable and can decay to a more stable state. The singlet and triplet RPs undergo a chemical reaction and recombine spin-selectively, that is the charge recombination/reaction rate[3] depends on the spin states of the separated charges (radical electrons), which directly affects the products/yields of their reactions. These differing reaction yields are biologically detectable in principle; they constitute different 'chemical messengers'. Hence, if the relative weights of singlet and triplet states are sensitive to the angle of the external magnetic field, then there will be an angular modulation of the reaction products. In doing so, a biochemical compass is formed.

Now, how the PRM can be described as a paradigm of quantum biology? The singlet S and triplet-naught T_0 states are equivalent to the two out of four Bell states, which are maximally-entangled and thus highly desired in quantum information schemes. How much of a role does the quantum nature of these states play in RPM? A recent analysis of the lifetime and decoherence of these states suggests that the answer is quiet complex. Essentially, some dephasing models leave the sensitivity of the RP reactions to the external magnetic fields mostly intact. However, any kind of strong dephasing prevents the RP model from being able to explain the disruptive effects of very weak oscillating fields. The weaker the field, the longer is needed for it to have a significant effect. Hence, it was argued that quantum coherence of RP electron spins has to sustain for tens of microseconds, so that these disrupting feeble fields have enough time to take effect [23–25]. This is a quiet amazing result for an electron spin in a 'warm and wet' biological environment; it seems that this disruption due to external fields is a purely quantum phenomenon, and that both the quantum coherence and entanglement properties must be sustained for timescales 'exceeding the best man-made molecular systems'.

There are many studies on how quantum coherence and entanglement will enhance the performance of RPM. I. K. Kominis, by using density-matrix equation and quantum measurement theory, explained RP reactions by the quantum Zeno effect [26] and found their equivalence to a non-linear biochemical double-slit interferometer [27]. J. Cai et al. studied how quantum control could affect the performance of the chemical compass based

[3]The recombination rate should be much smaller than the singlet-triplet mixing rate to allow the RPM compass function.

on RPM, and also studied the role of entanglement in RPM [28]. It was shown that quantum coherence itself might not be very essential for the functioning of the RPM compass, whereas the interplay between quantum coherence and environmental noise (decoherence) is the key to achieve its high sensitivity. Later, J. Cai and M. B. Plenio by introducing the concept of global quantum coherence, they found that the essence of the RP compass can be understood in analogy to a quantum interferometer exploiting global quantum coherence, namely the more global quantum coherence the better performance of the RP compass [29]. Moreover, C. Y. Cai et al. found that the sensitivity of the RP biochemical compass could be greatly enhanced by quantum criticality (phase transition) of the environments of the two electrons in the RP [30]. The use of entanglement as a resource (helpful ingredient) for the orientation and navigability of migratory birds in the weak geomagnetic field remains an open question, whose answer will depend on the specific molecular realization of their chemical compass [28, 31–34].

There is a long history of experimental studies on magnetic-field sensitivity of RP reactions in solution [35]. However, in those early experiments the magnetic sensitivity was observed only for field strengths between 10 mT and several Tesla, i.e. much larger than the geomagnetic field of about 50 μT. Maeda et al. [36] demonstrated the most sensitive RP reaction so far. They synthesized a CPF molecular triad composed of linked carotenoid (C), porphyrin (P) and fullerene (F), and they reported sensitivities down to 50 μT. However, there was angular modulation only for stronger fields on the order of mT. Thus, the requirements of high magnetic field-sensitivity and high angular-sensitivity cannot be fulfilled at the same time. Recently, H. G. Hiscock et al. studied a modified multinuclear model for RPs and reported, for a magnetic field strength comparable to that of the Earth, a very sharp feature (spike) at the output of the sensor that could greatly increase the angular-sensitivity or, equivalently, the heading precision [37].

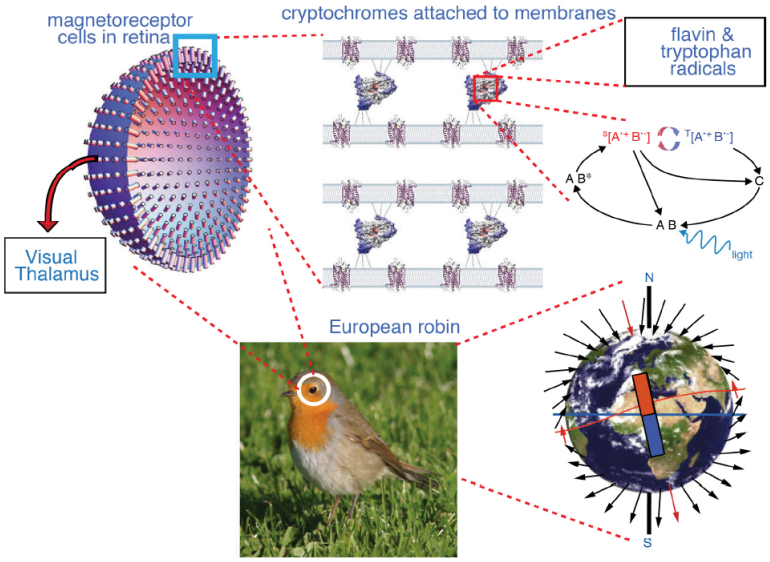

Figure 2.2: The 'quantum robin'. The reference direction provided by the Earth's magnetic field may be detected by cryptochrome molecules hosted in the birds' retina. According to the theory, light absorption generates long-lived flavin-tryptophan radical pairs. The products of their chemical reactions are determined by the orientation of the molecule with respect to the geomagnetic field vector. If cryptochromes are associated with the membrane disks of the outer segments of the photoreceptors, then an ordered structure could result and different reaction products in different locations of the retina could form an in-eye compass.

The precise nature of the RP that might be involved in this mechanism is as yet unknown. The prime and particularly intriguing candidate is a series of RP reactions that are known to happen within *cryptochrome* [14, 38, 39], a blue-light-sensitive photoreceptor flavoprotein. Since cryptochromes are resident in the bird's eye, particularly in the ganglion cell layer of the retina, they could induce a visual signal by which the bird navigates [20, 40]; it is likely that this mechanism inhabits the retina of the bird's eye enabling it to see the Earth's magnetic field as if it were light. Thus, there is a strong hypothesis that the RP reaction yield is further converted to nerve signal, and thus avian species may obtain information on the Earth's field to guide their migration. However, almost nothing is known about the biological circuitry connecting the RP yield to a neurological signal [41, 42].

Concluding, one of the principal models of magneto-detection in migrating birds rests on the quantum spin-dynamics of transient photo-generated radical pairs in ocular cryptochrome proteins. Experiments with birds have provided indirect and in cases conflicting evidence on the actual existence of the radical-pair mechanism. A recent study proposes a new experiment which can unambiguously identify the presence of the radical-pair magnetoreceptor in birds, and unravel some of its basic properties [43].

2.3. ELECTRON TRANSFER

Electron transfer (ET) is one of the most ubiquitous and fundamental phenomena in chemistry, physics and biology. Radiative and non-radiative ET processes correspond to a key elementary step in many important processes involving isolated molecules and supermolecules, ions and excess electrons in solution, condensed phase, surfaces and interfaces, electrochemical systems, solar cells etc. In nature, electron transfer, specifically photoinduced ET, is one of the most pivotal processes in photosynthesis; ET occurs in photosynthetic reaction centers (PRCs) where transfer of electrons is used to create charge imbalance across a membrane (transmembrane proton gradient), originating a proton pumping mechanism to produce adenosine triphosphate (ATP), the "molecular unit of currency". In chemical systems, ET at the metal surface with oxygen is responsible of the corrosion. Solid-state electronics depend on the control of the ET in semiconductors, and the new area of molecular electronics depends critically on the understanding and control of the transfer of electrons in and between molecules.

An ET is a type of quantum transition, in which an electron delocalizes from one stationary state and localizes in another stationary state, thereby inducing a change in the occupation number of both states. Any description of ET requires knowledge of the behavior and distribution of electrons around atomic nuclei. For an overview of the theory of electron transfer we refer the interested reader to [44].

The first studied ET reactions were self-exchange/isotopic[4] ET reactions of inorganic ions in aqueous solution [45]. The principal theoretical cornerstone for condensed phase ET was laid by Franck and Libby (1949–1952), who asserted that the *Franck–Condon prin-*

[4] For self-exchange/isotopic reactions the standard free energy (driving force) for the reactions is zero.

ciple[5] is applicable not only to the vertical radiative processes, but also to non-radiative horizontal ET. The factors determining ET rates have been tested extensively in proteins by C. C. Moser et al. [46], and are accurately described in 1960s by Rudolph A. Marcus who received the 1992 Nobel Prize in Chemistry "for his contributions to the theory of electron transfer reactions in chemical systems" [47, 48]. In broad terms, the ET rate between two sites increases as the edge-to-edge separation between them decreases or as the orbital overlap[6] between them increases or as the *Gibbs energy* (activation energy) of reaction becomes more well-matched.

2.3.1. CRYPTOCHROME

Magnetic field effect (MFE) is the effect of magnetic fields on the rate, products and/or their distribution of chemical reactions. Many MFEs are known on reactions occuring in solids or the interior of proteins. The mechanism of these reactions revolves around a spin-selective reaction step that is characterized by the reaction's rate constant which, in turn, describes ET process.

Fig. 2.3 shows the series of sequential electron-transfer steps that are though to produce MFEs in the cryptochrome[7] family of proteins. The distances between the electron sites favor a rapid sequential ET. The most experimentally studied MFEs on protein ET are those that occur in bacteria PRCs, after they have been chemically modified to prevent forward ET down one of the two almost symmetrical branches of cofactors in the PRC [46].

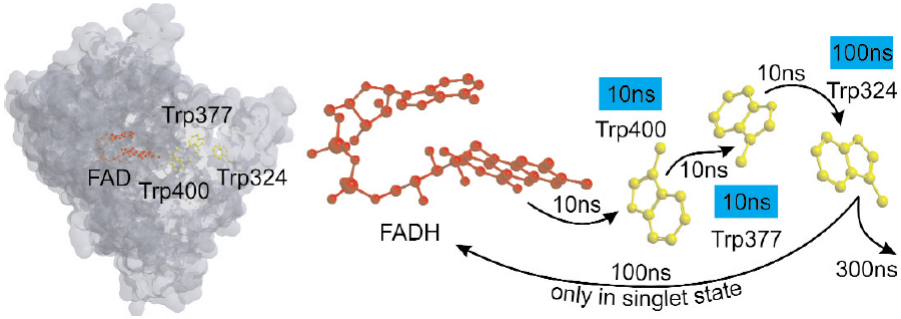

Figure 2.3: Although cryptochrome's photocycle is yet unknown, there is a suggestion that as light is absorbed, it triggers photochemical electron transfer from the flavin adenine dinucleotide (FAD) cofactor to tryptophan (amino acid) Trp400. The unpaired electron would then continue to 'hop' rapidly to Trp377, and then to Trp324. At this point, there is a competition between back-electron transfer to the flavin or further reaction leading to generation of signalling state of cryptochrome. Picture reproduced from [46].

[5] Classically, the Franck–Condon principle is the approximation that an electronic transition is most likely to occur without changes in the positions of the nuclei in the molecular entity and its environment. The resulting state is called a Franck–Condon state, and the transition involved, a vertical transition. The quantum mechanical formulation of this principle is that the intensity of a vibronic transition (simultaneous change in electronic and vibrational energy levels) is proportional to the square of the overlap integral between the vibrational wavefunctions of the two states that are involved in the transition.– IUPAC Compendium of Chemical Terminology, 2nd Edition (1997)

[6] Orbitals are stationary electronic states in which the probability of finding the electron is high. The ready visualization of the overlap of orbitals provides an intuitive and easy-to-grasp method of deciding if electron transfer will occur or not.

[7] Cryptochrome has been proposed to be responsible for the magnetic compass sensitivity of migratory birds.

2.3.2. PHOTOSYNTHETIC REACTION CENTERS

The reaction center (RC) is the key component for the primary events in the photochemical conversion of light into chemical energy in every photosynthetic organism [49, 50]. After light excitation, a charge separation that spans the cell membrane is formed in the RC in a few hundred picoseconds with a quantum yield of almost unity. The coupling of the primary electron-donor to secondary electron-donor and acceptor molecules, allows electrons and accompanying protons to be transferred to other components of the photosynthetic apparatus, ultimately to be converted into chemically rich compounds such as ATP.

The RC is an integral membrane pigment-protein complex, composed from a special dimer of pigments (P) which corresponds to the primary electron-donor, the path of the electron-transfer cascade. Since the photo-excited pigment (P^*) is a strong reducing species, it rapidly loses an electron to a nearby acceptor (A) forming a charge-separated state P^+A^-, which is a dipolar species consisting of the radical-cation P^+ and the radical-anion A^-, termed *radical-ion pair* (RIP). This is the primary process in the photosynthetic reaction center (Fig. 2.4); the photon's energy is transformed to (electro)chemical energy. Now, if the electron is back-transferred from A to P, then the stored energy is lost into heat. However, this is not the case since another fast electron transfer to a secondary acceptor molecule takes place. The growing, at each forward ET step, spatial separation between the donor and the acceptor reduces the charge-recombination rate by orders of magnitude. Hence, within a very short time the distance between the donor and the acceptor is almost the thickness of the photosynthetic membrane.

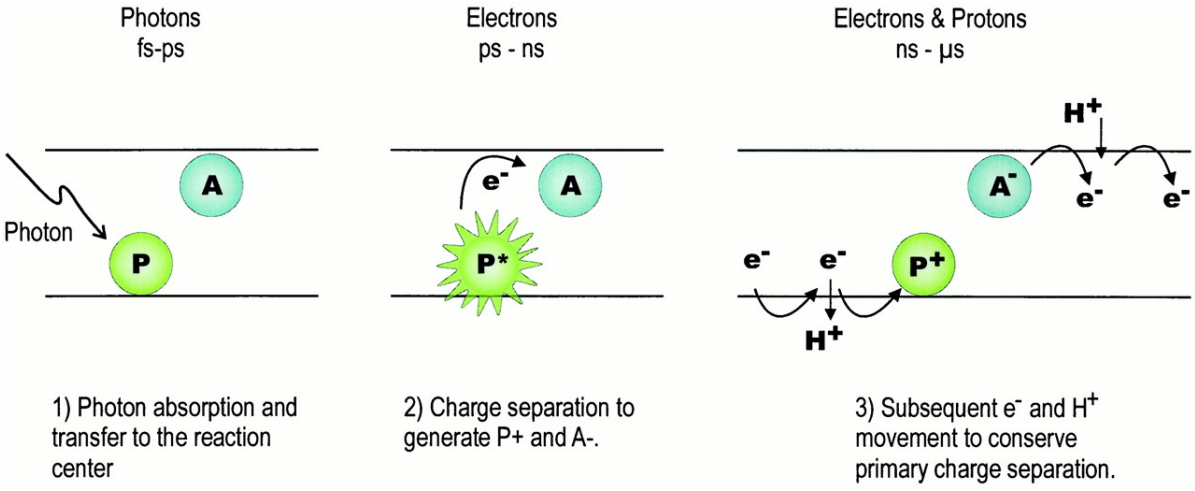

Figure 2.4: Primary reaction of photosynthesis with typical timescales involved. P and A represents the primary electron-donor and the first 'stable' acceptor, respectively. 1) Energy transfer from the antenna pigments (e.g. bacteriochlorophylls) leads to photo-excitation of P on the fs-ps timescale. 2) Electron transfer from the photo-excited P^* to A produces the charge-separated state P^+A^- on the ps-ns timescale. 3) The backward electron transfer from A^- to P^+ (charge recombination) to produce PA, and practically heat, is efficiently prevented by further forward electron transfer, which is now proton-coupled. These more complex chemical processes ultimately produce stable photosynthetic products, and happen on the ns-μs timescale. Picture reproduced from [50].

Photosynthetic reaction centers (PRCs) can be categorized into two types based upon the nature of the electron-acceptors :

I. Green-sulfur bacteria, heliobacteria and Photosystem I (PSI) belong to the iron-sulfur type.

II. Purple bacteria, green-filamentous bacteria and Photosystem II (PSII) belong to the pheophytin-quinone type.

Nowadays, we know two types of PRCs each has three classes that are summarized in (Fig.2.5).

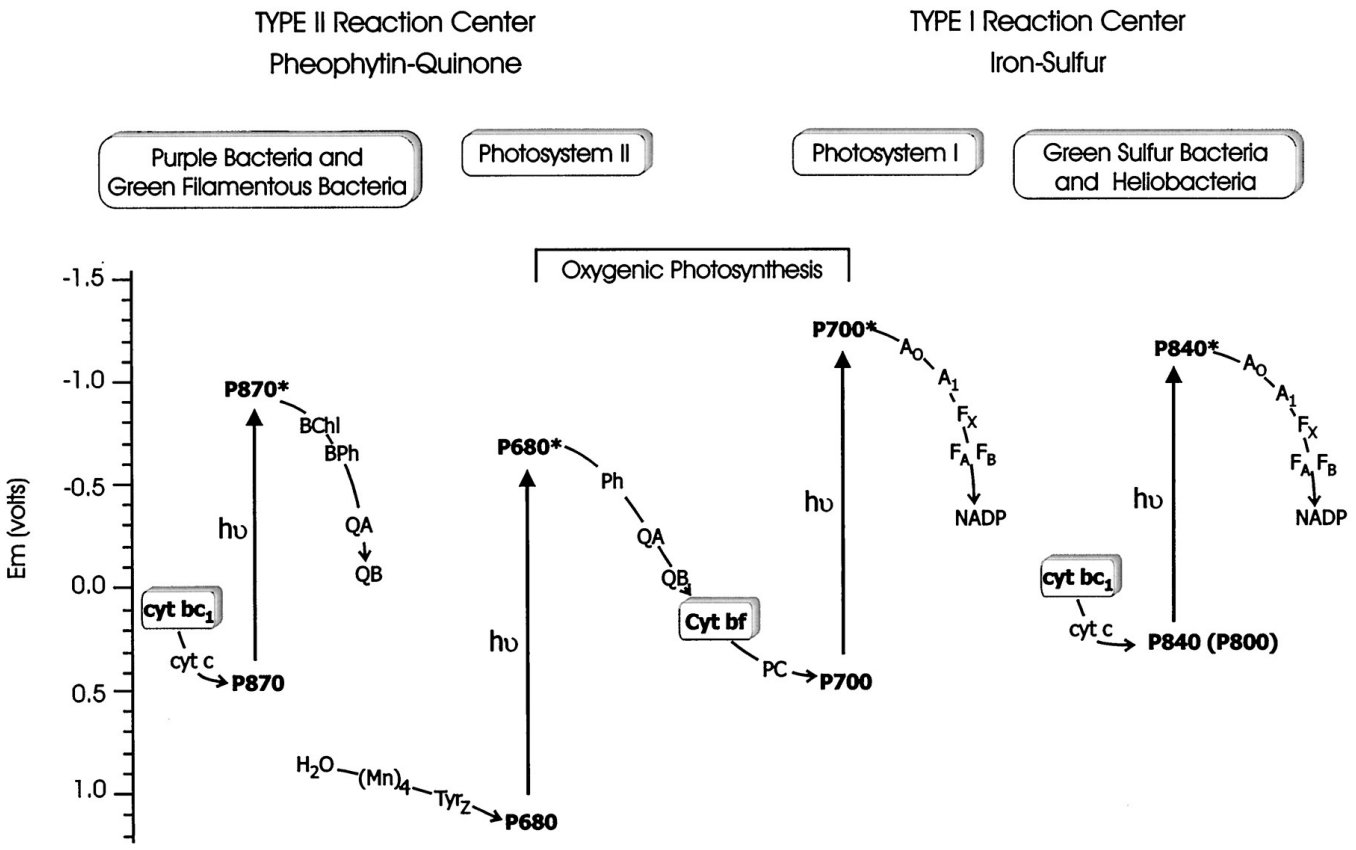

Figure 2.5: Electron-transfer pathways for the two types and six classes of PRCs. In type I PRCs (right), iron-sulfur clusters are used as the electron-acceptors. Type I is subdivided into 3 classes: PSI, green-sulfur bacteria and heliobacteria. In type II PRCs (left), quinones are used as the first 'stable' electron-acceptors. Type II is also subdivided into 3 classes: PSII, purple bacteria and green-filamentous bacteria. Intermediates in the figure have the following designations: **P** → PRC primary donor, **(B)Ph** → transient initial (bacterio)pheophytin acceptor, **QA** and **QB** → 'stable' quinone acceptors, $\mathbf{A}_0$ ($\mathbf{A}_1$) → transient initial chlorophyll (quinone) acceptor, $\mathbf{F}_X$, $\mathbf{F}_A$ and $\mathbf{F}_B$ → 'stable' iron-sulfur cluster acceptors, **NAPD** → final acceptor. The electron-donors are $\mathbf{Tyr}_z$ and a cluster of 4 manganese (**Mn**) ions for PSII, a plastocyanin molecule (**PC**) for PSI and cytochrome (**cyt**) c for the bacterial PRCs. The intermediate electron-transfer complexes, cytochrome $\mathbf{bc}_1$ and **bf**, are boxed. Picture reproduced from [50].

3

RADICAL-PAIR MECHANISM

3.1. INTRODUCTION

The Radical-Pair Mechanism (RPM) has evolved to the cornerstone of *spin chemistry*, i.e. the study of electronic and nuclear spin effects on chemical reactions. Chemical reactions which involve radical intermediates can be affected by magnetic fields that act to change their rate (kinetics), yields/products and/or their distribution. Such effects have been studied extensively and are known as Magnetic Field Effects (MFEs).

The origin of the RPM, which marks the birth of the spin chemistry, is set in the 1960s due to the observation of anomalous lineshapes and enhanced intensities in Electron Paramagnetic Resonance (EPR) and Nuclear Magnetic Resonance (NMR) signals in chemical reactions of organic molecules. These effects termed, respectively, as Chemically-Induced Dynamic Electron Polarization (CIDEP) and Chemically-Induced Dynamic Nuclear Polarization (CIDNP). G. L. Closs and L. E. Closs [51] and, independently, R. Kaptein and J. L. Oosterhoff [52] introduced the RPM as a reaction intermediate to explain these observations. Since then, spin chemistry has grown into a mature field of theoretical and experimental physical chemistry [35]. An intriguing result of early spin chemistry work was the proposal by K. Schulten and co-workers that avian magnetoreception is based on RP biochemical reactions [16, 39, 53, 54].

The RPM involves a multi-spin system of electrons and nuclei embedded in a biomolecule and undergoing a number of physical/chemical processes, such as magnetic interactions and coherent spin motion, electron transfer, spin relaxation etc., which provide, between others, the mechanistic framework for the interpretation of MFEs. Although the RPM has been known since the late 1960s, the rich quantum physical underpinnings of the mechanism have been unraveled only recently [55], and the RPM was shown to be a rich biophysical laboratory where the conceptual tools of quantum information science can be fruitfully applied. However, the fundamental quantum dynamics of RPM is, hitherto, hotly debated [55].

3.2. A BRIEF BIOGRAPHY OF A RADICAL PAIR

Radical-Pair creation. The quantum degrees of freedom of RPs are formed by a multi-spin system hosted in a biomolecule that can be either solid or liquid. These spin degrees of freedom can mathematically be described by the density matrix ρ. Upon absorption of a photon by this biochemical system, one of the two paired (covalently bound) electrons in a singlet state, $|S\rangle = 1/\sqrt{2}(|\uparrow\downarrow\rangle - |\downarrow\uparrow\rangle)$ in Dirac notation, is excited from the highest occupied to the lowest unoccupied molecular orbital (HOMO-LUMO transition), and subsequently transferred to a separate location leaving behind the other electron. So, each of the two locations possesses an unpaired electron, and hence together they form an RP. Typically, one chemical bond breaks at a time so that the radicals are created in pairs. In short, an RP is a pair of biomolecular ions created by a charge transfer from a photo-excited donor-acceptor dyad DA, schematically described by the reaction $\mathrm{DA}\xrightarrow{h\nu}\mathrm{D^*A}\xrightarrow{ET}\mathrm{D^{\bullet+}A^{\bullet-}}$, with the dot denoting an unpaired electron.

Since (i) the ground state DA and the excited state D*A molecular dyads are usually in a spin-zero/unpolarized state, (ii) the RP formation process is fast, and (iii) effects such as spin-orbit coupling can be neglected, the RP initial electronic spin-state is also a spin-zero state, particularly the spin-correlated singlet state described by $\rho_{el}(0) = |S\rangle\langle S|$. The RP initial nuclear spin-state is a thermal and practically unpolarized state, termed maximally-mixed state $\rho_{nuc}(0) = \mathbb{1}/d$, where d is the nuclear spin-multiplicity. For instance, the proton (spin-1/2 nucleus) polarization at room temperature and at magnetic fields $\sim 1T$ is about 10^{-5}, which is practically negligible. Thus, $\rho_{p^+}(0) = \mathbb{1}/2$ and the RP initial total spin-state is $\rho(0) = |S\rangle\langle S| \otimes \mathbb{1}/2$. Hence, the total angular momentum is conserved, it is a 'constant of motion' in the course of the RP creation process. We denote the singlet RP as $^{\mathrm{S}}\mathrm{D^{\bullet+}A^{\bullet-}}$.

Radical-Pair spin evolution. Now, both D and A molecules host a number of nuclear spins that interact to the respective electron spin through the *hyperfine interaction*. Neither singlet-state nor triplet-state RPs are eigenstates of the resulting magnetic Hamiltonian, $\mathscr{H}_m$, thus the RP spin-state undergoes a coherent singlet-triplet (S-T) oscillation / mixing / inter-conversion, designated by $^{\mathrm{S}}\mathrm{D^{\bullet+}A^{\bullet-}} \rightleftharpoons {}^{\mathrm{T}}\mathrm{D^{\bullet+}A^{\bullet-}}$. At the same time, the nuclear spins also precess and hence the total electron/nuclear spin system undergoes a coherent spin motion driven by hyperfine couplings, and the rest of the magnetic interactions to be detailed later.

The simplest way to understand S-T mixing is by using the classical vector model, and assuming an (unphysical) RP that comprises just two electronic spins having precession or *Larmor frequencies* different by $\delta\omega$. If the RP initial state is the singlet $|S\rangle$, after a time interval $\Delta t = \pi/\delta\omega$ the two electronic spins will develope a π phase difference and their state will convert to the triplet $|T_0\rangle$, as shown in Fig. 3.1(a) [55]. In reality, this model is encountered in the so-called Δg-mechanism operating at high magnetic fields, where an actual difference in the g-factor of the two electrons is responsible for their different Larmor frequency. Specifically, $\delta\omega = \Delta g \mu_B B/\hbar$ where μ_B is the Bohr's magneton. However, S-T inter-conversion is usually induced by the different nuclear spin environment (local 'classical nuclear magnetic field') hosted in the two radicals and hyperfine coupled to the respective electronic spin. In Fig. 3.1(b) we show key transitions of the RP spin-state caused by hyperfine (local) and Zeeman (global) interactions [56].

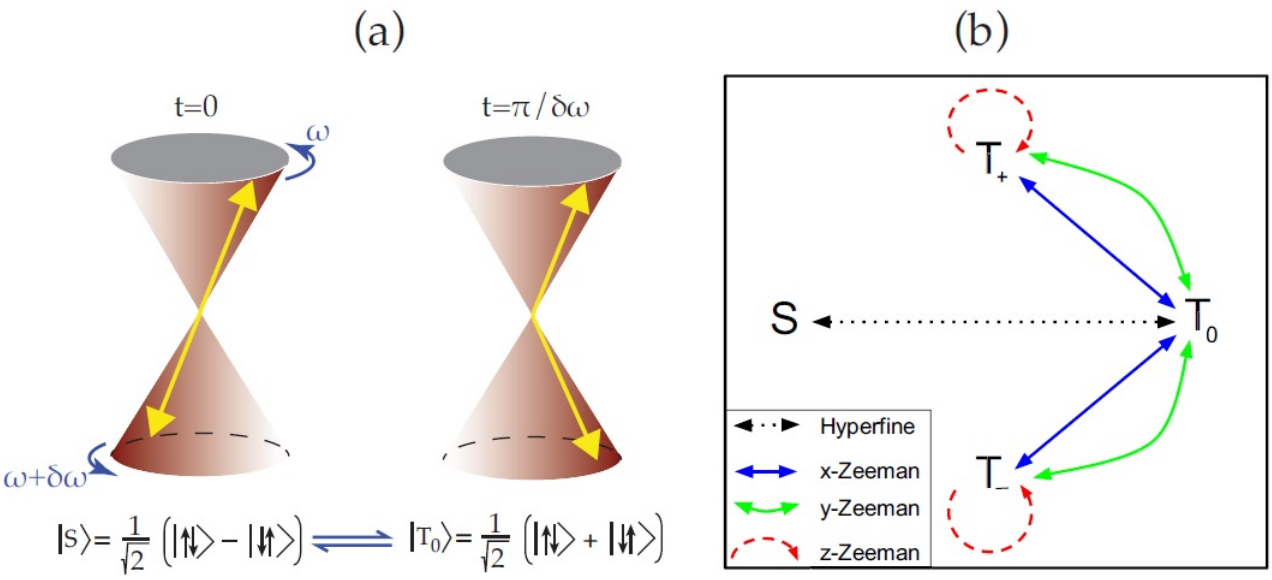

Figure 3.1: (a) Classical vector model describing the S-T mixing of the spin-state of two electrons, which is driven by their different Larmor frequencies. Reproduced from [55]. (b) Key transitions of the Radical-Pair spin-state caused by Zeeman and hyperfine interactions. Reproduced from [56].

Radical-Pair reaction. The coherent unitary evolution of the RP spin-state, which is the key feature of the RPM, has a finite lifetime. Charge recombination, i.e. backward charge transfer from A to D, terminates the coherent spin motion and leads to the formation of the neutral reaction products/yields in a spin-dependent way; angular momentum conservation at this step empowers the molecular spins and their minuscule energy[1] to determine the fate of the RP reaction. There are two neutral product species, singlet, such as the original DA molecules, and triplet, $^{\mathrm{T}}$DA, resulting, on average, from singlet RPs and triplet RPs, respectively. It turns out that the relative concentration of the reaction yields can be substantially influenced by the magnetic spin interactions entering the mixing Hamiltonian $\mathscr{H}_m$. It is noted for completeness that the reaction can close through the so-called *intersystem crossing* (ISC) $^{\mathrm{T}}$DA$\longrightarrow$DA, mediated by, e.g., spin-orbit (LS) coupling.

All the previous processes can be summarized in Fig. 3.2(a). If we neglect the photoexcitation and the initial charge transfer, then the RP reaction scheme can be further simplified into Fig. 3.2(b); the two gray boxes show that the RP reaction comprises two physically very different and concurrent processes: (i) the unitary dynamics embodied by the magnetic Hamiltonian, $\mathscr{H}_m$, driving a coherent S-T oscillation of the RP spin-state, and (ii) the non-unitary/irreversible reaction dynamics reducing spin-selectively the RP population. While the former is somehow trivial, it turns out that the latter is non-trivial at all and is still an intense scientific debate [55].

[1] Even weak magnetic fields whose interaction energies are far less than the thermal energy $k_B T$ may cause significant changes in the RP reaction yields. But this does not contradict the laws of thermodynamics, because the formation of the RP requires much more than the thermal energy. Moreover, tiny energies (weak magnetic fields) can have large effects on the RP chemical reactivity when the RP state is far from equilibrium, which is indeed the case.

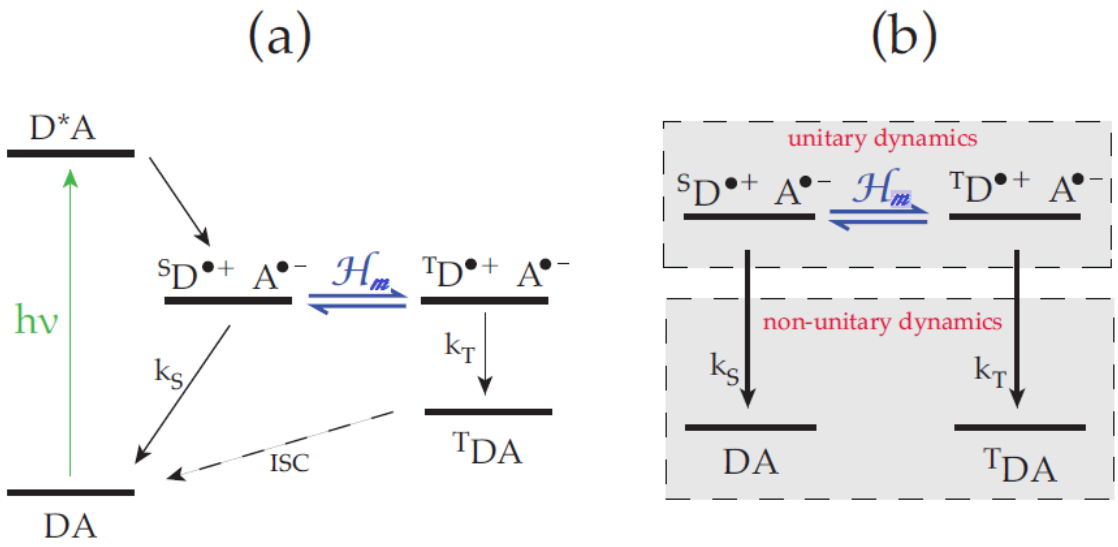

Figure 3.2: Reproduced from [55]. (a) Simplified energy level structure of Radical-Pair reaction dynamics. A donor-acceptor molecular dyad DA is photo-excited to D*A, and a subsequent charge transfer from D to A forms a singlet RP, $^{S}D^{\bullet+}A^{\bullet-}$. Intra-molecule magnetic interactions, embodied by $\mathscr{H}_m$, converts singlet RPs to triplet RPs in a coherent and unitary fashion. At the same time, charge transfer from A back to D leads to singlet (DA) and triplet (^{T}DA) neutral products in a spin-dependent way with rates k_S and k_T, respectively. The reaction cycle can be close through *intersystem crossing* (ISC) from ^{T}DA to DA. (b) Simplified version of (a) omitting the light excitation and the subsequent charge transfer. Both figures could not be taken too literally, because an RP can recombine into, e.g., a singlet DA even if its state is a coherent S-T superposition and not only a pure singlet.

Dimension of RP spin-space. A radical pair consists of two electrons and some number N of magnetic nuclei located in donor D and acceptor A molecules. Its spin-state is described by the density matrix ρ whose dimension is $d = 4 \times \Pi_{j=1}^{N}(2I_j + 1)$, where 4 is the spin-multiplicity of the two electronic spins, $\Pi_{j=1}^{N}(2I_j + 1)$ is the spin-multiplicity of the N nuclear spins, and I_j is the nuclear spin of the jth nucleus with $j = 1, 2, \ldots, N$. For example, in the aforementioned case of just one-proton nucleus the density matrix has dimension $d = 8$.

Definitions. At the RP recombination/reaction process, the conservation of angular momentum forces the decomposition of the RP spin-space into an electronic singlet and an electronic triplet subspace, defined by the projection operators (projectors) Q_S and Q_T, respectively. These are $d-$dimensional square matrices defined as

$$Q_S = \frac{1}{4}\mathbb{1}_d - \mathbf{s}_D \cdot \mathbf{s}_A$$

and

$$Q_T = \frac{3}{4}\mathbb{1}_d + \mathbf{s}_D \cdot \mathbf{s}_A \quad ,$$

where $\mathbf{s}_D$ and $\mathbf{s}_A$ are the respective spin-operators of the Donor's and Acceptor's electron. They are $d \times d$ matrices, e.g. the ith component of $\mathbf{s}_D$ would be written as $s_{Di} = s_i \otimes \mathbb{1}_2 \otimes$

$\mathbb{1}_{2I_1+1} \otimes \mathbb{1}_{2I_2+1} \otimes \cdots \otimes \mathbb{1}_{2I_N+1}$, with $i \equiv x, y, z$, where the first operator in the tensor/Kronecker product denotes Donor's electron spin, the second the Acceptor's electron spin, and the rest refer to the nuclear spins. By s_i we denote the familiar two-dimensional spin-1/2 Pauli operators, and by $\mathbb{1}_n$ the $n-$dimensional identity/unity operator. Moreover, the projectors Q_S and Q_T have the following properties: (i) $Q_m = Q_m^2$, $m \equiv S, T$, (ii) $Q_S + Q_T = \mathbb{1}_d$ (completeness), and (iii) $Q_S Q_T = Q_T Q_S = 0$ (orthogonality).

The dimension of the RP total singlet subspace is $1 \times \Pi_{j=1}^{N}(2I_j+1)$, and for the total triplet subspace it is $3 \times \Pi_{j=1}^{N}(2I_j+1)$. The electronic spin-multiplicity in the former corresponds to the spin-zero (s=0) singlet state

$$|S\rangle = \frac{1}{\sqrt{2}}(|\uparrow\downarrow\rangle - |\downarrow\uparrow\rangle) \quad ,$$

whereas the electronic spin-multiplicity in the latter corresponds to the spin-one (s=1) triplet states

$$\begin{aligned} |T_+\rangle &= |\uparrow\uparrow\rangle \quad , \\ |T_0\rangle &= \frac{1}{\sqrt{2}}(|\uparrow\downarrow\rangle + |\downarrow\uparrow\rangle) \quad , \\ |T_-\rangle &= |\downarrow\downarrow\rangle \quad , \end{aligned}$$

as expressed in the uncoupled two-qubit basis $\{|\uparrow\uparrow\rangle, |\uparrow\downarrow\rangle, |\downarrow\uparrow\rangle, |\downarrow\downarrow\rangle\}$. The triplet state has three projections along the quantization axis, which is usually defined by the magnetic field axis. There is, also, the coupled 2-qubit basis $\{|S\rangle, |T_0\rangle, |T_+\rangle, |T_-\rangle\}$. For an RP containing n spin-1/2 nuclei, the dimension of the Hilbert space for the RP's total spin is $d = 2^{n+2}$. Then, the projectors would be written as $Q_S = |S\rangle\langle S| \otimes \mathbb{1}_2^{\otimes n}$ and $Q_T = \sum_{q=0,\pm} |T_q\rangle\langle T_q| \otimes \mathbb{1}_2^{\otimes n}$.

Finally, there are the singlet k_S and triplet k_T recombination rates that are defined as follows: At $t = 0$, we prepare an RP ensemble having no magnetic interactions ($\mathscr{H}_m = 0$) in the singlet (triplet) electronic spin-state and any nuclear spin-state. If the singlet (triplet) recombination channel is open, i.e. $k_S \neq 0$ ($k_T \neq 0$), then its population (diagonal density-matrix elements) would decay exponentially at the rate k_S (k_T). In general, during a time interval dt, the singlet and triplet reaction yields will be

$$dr_S = k_S dt Tr[\rho Q_S]$$

and

$$dr_T = k_T dt Tr[\rho Q_T] \quad ,$$

respectively. If all RPs were in the singlet (triplet) state, the fraction of them recombining through the singlet (triplet) channel during dt would indeed be $k_S dt$ ($k_T dt$). Instead, if they are in a general state described by ρ, then $k_S dt$ ($k_T dt$) has to be multiplied by the respective fraction of singlet (triplet) RPs, i.e. $Tr[\rho Q_S] = \langle Q_S \rangle \equiv f_S \quad \left(Tr[\rho Q_T] = \langle Q_T \rangle \equiv f_T\right)$ known as singlet (triplet) *fidelity*.

3.3. RADICAL-PAIR MAGNETIC HAMILTONIAN

The total magnetic interactions of the radical-pair spin-system can be described by the Hamiltonian

$$\mathscr{H}_m = H_Z + H_{HF} + H_E + H_D \quad ,$$

where H_Z is the Zeeman interaction Hamiltonian, H_{HF} the hyperfine, H_E the (spin-)exchange, and H_D the dipolar ones.

Zeeman interaction

The interaction of the two unpaired electronic spins in each radical with an external (applied) magnetic field $\mathbf{B}$ may be written, in general, as

$$H_Z = -\frac{\mu_B}{\hbar}(\mathbf{s}_D \cdot \hat{\mathbf{g}}_D + \mathbf{s}_A \cdot \hat{\mathbf{g}}_A) \cdot \mathbf{B} \quad ,$$

where $\mu_B = |e|\hbar/2m_e$ is the Bohr's magneton, $\mathbf{s}_D$ ($\mathbf{s}_A$) is the electron spin-operator of the donor (acceptor), and $\hat{\mathbf{g}}_D$ ($\hat{\mathbf{g}}_A$) is the g-tensor[2] of the donor (acceptor) that accounts for complexities related to intra-molecule complicated interactions between the electrons [46]. The g-tensor is a $2^{\text{nd}}-$rank tensor (g_{ij}) defined by the 3×3 matrix

$$\hat{\mathbf{g}} = \begin{pmatrix} g_{xx} & g_{xy} & g_{xz} \\ g_{yx} & g_{yy} & g_{yz} \\ g_{zx} & g_{zy} & g_{zz} \end{pmatrix} \quad .$$

However, for small organic radicals it is reasonable to assume that the g-tensor is that of a free electron, i.e. $\hat{\mathbf{g}}_{D,A} = \text{diag}\{g, g, g\} = g\mathbb{1}_3$ where $g \approx 2$ is the electron's g-factor. In doing so,

$$H_Z = -\gamma_e(\mathbf{s}_D + \mathbf{s}_A) \cdot \mathbf{B}$$

where $\gamma_e = g\mu_B/\hbar \approx |e|/m_e$ is the gyromagnetic ratio of the free electron.

The nuclear spins located in an RP also interact with the external magnetic field, but the nuclear Zeeman interactions are negligible with respect to the electronic Zeeman interaction, because the nuclear gyromagnetic ratios are much smaller than that of the electron. For instance, a proton's Zeeman interaction is three orders of magnitude weaker, since $m_p/m_e \approx 1836$.

For an RP spin-system, the Zeeman interaction splits apart the $|T_\pm\rangle$ and $|T_0\rangle$ states, i.e it lifts the triplet's energy degeneracy, and this triplet-triplet (Zeeman) splitting is proportional to the intensity of the external magnetic field B. Moreover, transitions between them could be induced dependent on the orientation of the external magnetic field $\mathbf{B}$ (Fig. 3.1b).

[2]The g-tensor is often determined empirically from EPR spectra, whereas for molecules as large as small proteins modern density functional theory (DFT) allows reasonably accurate calculations.

Hyperfine interaction

In natural radical pairs, each radical contains a number of nuclei which generally have non-zero spin. Hence, the electronic spin in each radical is not isolated, it is embedded in a magnetic environment induced by its neighboring nuclear spins. In other words, each unpaired electronic spin is coupled to its local magnetic nuclei through the hyperfine interaction,

$$H_{HF} = \sum_i \mathbf{s}_D \cdot \hat{\mathbf{a}}_{D,i} \cdot \mathbf{I}_{D,i} + \sum_j \mathbf{s}_A \cdot \hat{\mathbf{a}}_{A,j} \cdot \mathbf{I}_{A,j}$$

where $\mathbf{I}_{D,i}$ ($\mathbf{I}_{A,j}$) is the spin-operator of the ith (jth) nucleus located in the donor (acceptor), and $\hat{\mathbf{a}}_{D,i}$ ($\hat{\mathbf{a}}_{A,j}$) is the hyperfine tensor that couples the ith (jth) nuclear spin of the donor (acceptor) to the donor's (acceptor's) electronic spin. The hyperfine tensor accounts for the geometry of this coupling, and it is expressed by the 3×3 matrix

$$\hat{\mathbf{a}} = \begin{pmatrix} a_{xx} & a_{xy} & a_{xz} \\ a_{yx} & a_{yy} & a_{yz} \\ a_{zx} & a_{zy} & a_{zz} \end{pmatrix} \quad .$$

In the *minimal RP model* we consider that the one electronic spin is devoid of hyperfine interactions, while the other interacts with just one nuclear spin located in its radical. Hence,

$$\mathrm{h}_{HF} = \mathbf{s} \cdot \hat{\mathbf{a}} \cdot \mathbf{I} \quad .$$

This simple model, also known as *'reference-and-probe' RP model*, is an approximation of multiple nuclei environments with one effective dominant hyperfine coupling component. It permits us to obtain analytic expressions and acquire, by this way, a better understanding of the underlying physics.

In solids or in oriented media, such a liquid crystal, the hyperfine interaction is anisotropic, i.e. it depends not only on the relative orientation of electronic and nuclear spin, but also on their orientations with respect to the molecular frame of the radical. Instead, in isotropic liquids any anisotropy is averaged to zero by the rapid tumbling (motion/disorder) of the radical. In this case, the hyperfine tensor becomes the isotropic hyperfine coupling constant, $\hat{\mathbf{a}} = \mathrm{diag}\{\alpha, \alpha, \alpha\} = \alpha \mathbb{1}_3$, and thus the hyperfine Hamiltonian is further simplified to

$$h_{HF} = \alpha \mathbf{s} \cdot \mathbf{I} \quad ,$$

known as *Fermi contact interaction*[3]. The hyperfine coupling constant (α) is proportional to the gyromagnetic ratio of the respective nucleus.

In an RP spin-system, the hyperfine interaction induces the coherent singlet-triplet inter-conversion. Specifically, for fields $B < 50$ mT, the S-T mixing responsible for MFEs

[3]The Fermi contact interaction is the magnetic interaction of the electronic and nuclear spin when the electron is *inside* that nucleus. It is isotropic, i.e. it depends only on the relative orientation between the electronic and nuclear spins, and its strength is proportional to the *s*-orbital character of the *singly occupied molecular orbital* (SOMO) around that nucleus [46].

is governed primarily by the hyperfine mechanism [46]. However, at higher fields the induced S-T mixing is dominated by the small differences in the g-factors of the two radicals, $\Delta g \approx 10^{-3}$, the so-called $\Delta g-$mechanism. This is because the difference of the Larmor frequencies of the two unpaired electron spins is $\Delta\omega = \frac{\Delta g \mu_B}{\hbar} B$, where $\mu_B/\hbar \approx 10$ GHz/T.

Exchange interaction

Within each radical, Coulombic forces between the electrons and nuclei determine the radical's geometry and electronic structure that, in turn, contribute to the radical's spin/magnetic Hamiltonian characterized by the hyperfine and g- tensors. The consideration that the radicals in a radical pair are separate entities is not complete, because the Coulombic interactions between the electrons and nuclei in one radical with those in the other radical must be taken into account.

When the radicals in an RP approach closely enough for inter-radical electron correlation and bonding effects to set in, the spin evolution can be described by

$$H_E = J\mathbf{s}_D \cdot \mathbf{s}_A \quad ,$$

known as (spin-)exchange interaction. The exchange coupling strength J is the energy difference between the singlet and triplet states. In spin chemistry, the exchange coupling is normally assumed to behave as $J(r) \approx J_0 e^{-r/r_0}$, where J_0 is the magnitude (positive/negative), r is the radical-radical separation, and $r_0 > 0$ is a range parameter [46, 57]. The values of the parameters vary considerably with the nature of the radicals and the intervening medium.

For RP reactions in solutions, the exchange interaction acts to prevent singlet-triplet mixing since it produces singlet-triplet energy splitting. Thus, whenever the radicals are close enough, e.g. during diffusive encounters, the exchange interaction dominates the RP's magnetic Hamiltonian, and hence no MFEs are expected.

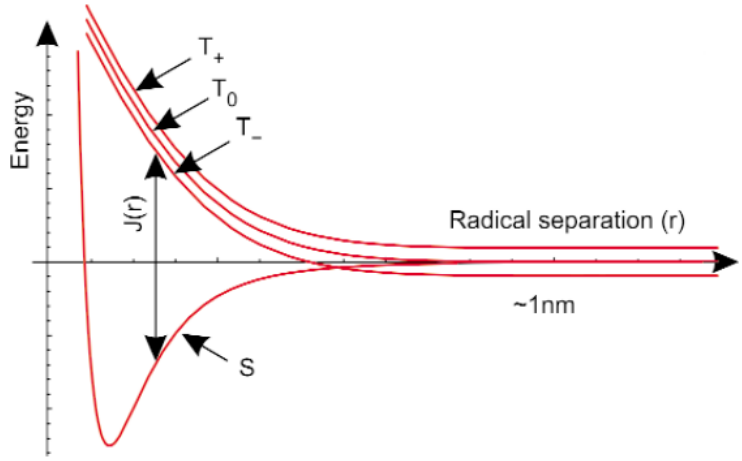

Figure 3.3: Singlet-Triplet energy splitting with respect to radical-radical distance. The T_0 and $T_\pm$ states are split apart due to the Zeeman interaction and $J(r)$ denotes the energy distance between S and T_0 states. Diagram reproduced from [46].

Dipolar interaction

Each unpaired electronic spin also experiences a magnetic field induced by the other unpaired electronic spin. This is a magnetic dipole-dipole interaction, also called dipolar coupling, that can be described by the Hamiltonian

$$H_D = \frac{\mu_0}{4\pi r^3}\left[\mathbf{m}_D \cdot \mathbf{m}_A - 3(\mathbf{m}_D \cdot \mathbf{r}_0)(\mathbf{m}_A \cdot \mathbf{r}_0)\right] \quad ,$$

where μ_0 is the magnetic constant (vacuum permeability), $\mathbf{m}_D$ ($\mathbf{m}_A$) is the magnetic dipole moment of the donor's (acceptor's) electronic spin, and $\mathbf{r} = r\mathbf{r}_0$ is the spatial vector joining the centers of these two magnetic dipoles. Since $\mathbf{m}_x = \gamma_x \mathbf{s}_x$ ($x \equiv D, A$), the dipolar Hamiltonian reads

$$H_D = \frac{\mu_0 \gamma_D \gamma_A}{4\pi r^3}\left[\mathbf{s}_D \cdot \mathbf{s}_A - 3(\mathbf{s}_D \cdot \mathbf{r}_0)(\mathbf{s}_A \cdot \mathbf{r}_0)\right] \quad ,$$

where $\gamma_x = g_x \mu_B / \hbar$ is the electron gyromagnetic ratio of the x-radical. Strictly speaking, the above Hamiltonian is only valid for point dipoles separated by $\mathbf{r}$. In real molecules, $\mathbf{r}$ is approximated by the vector between the 'centers' of the SOMOs on each radical, and then the dipolar Hamiltonian can be written as

$$H_D = \mathbf{s}_D \cdot \hat{\mathbf{D}} \cdot \mathbf{s}_A \quad ,$$

where $\hat{\mathbf{D}}$ is the dipolar tensor. At high fields, the diffusive motion of one radical around the other vanishes the dipolar interaction. However, in weak fields it turns out that the dipolar interaction suppresses the singlet-triplet mixing, unless the dipolar and exchange interactions are of similar energies; if they have similar magnitudes but opposite signs, then they mutually cancel each other [46, 57].

3.4. RADICAL-PAIR REACTION DYNAMICS

In addition to the unitary evolution of the RP spin-density matrix ρ, a non-unitary term describing the spin-selective RP reactions must also be taken into account. This biochemical spin-system is an open quantum system, and hence its density matrix does not just obey the *Schrödinger equation*, $d\rho/dt = -i[\mathscr{H}_m, \rho]/\hbar$, but more terms are needed to account for the 'open' character of RPs. Such terms are compactly written as a *'reaction super-operator'* $\mathscr{L}(\rho)$. The *Master Equation*

$$\frac{d\rho}{dt} = \underbrace{-\frac{i}{\hbar}[\mathscr{H}_m, \rho]}_{\text{unitary dynamics}} + \underbrace{\mathscr{L}(\rho)}_{\text{non-unitary dynamics}}$$

is the starting point for all theoretical calculations involving RP reactions; hence it is of fundamental importance for spin chemistry, being the basis for predicting all experimental observables.

The majority of theoretical calculations were so far performed with a phenomenological theory elaborated upon by Haberkorn [58] in 1976, termed 'traditional' master equation. The Haberkorn's reaction super-operator reads

$$\begin{aligned}\mathscr{L}(\rho) &= -\frac{k_S}{2}(Q_S\rho + \rho Q_S) - \frac{k_T}{2}(Q_T\rho + \rho Q_T) \\ &= -k_T\rho + \frac{k_T - k_S}{2}(Q_S\rho + \rho Q_S)\end{aligned}$$

where the second equation is due to $Q_S + Q_T = \mathbb{1}$. This or any master equation requires as input all the magnetic interactions entering the Hamiltonian $\mathscr{H}_m$ and the two recombination rates k_S and k_T, and it can theoretically predicts any experimental observable as output. Few customary examples are the following:

(i) The singlet and triplet reaction yields given by $Y_x = \int_0^\infty dr_x$, where $dr_x = k_x dt Tr[Q_x\rho_t]$ with $x \equiv S, T$. Given that the initial density matrix is normalized, i.e. $Tr[\rho_0] = 1$, it will be $Y_S + Y_T = 1$.

(ii) The reaction/recombination rate, given by the decay rate of the RP population, $dTr[\rho_t]/dt = -k_S Tr[Q_S\rho_t] - k_T Tr[Q_T\rho_t]$. In the special case of symmetric/spin-independent recombination, $k_S = k_T \equiv k$, the RP population decays exponentially at the rate k, that is $dTr[\rho_t]/dt = -kTr[\rho_t]$.

(iii) The magnetic field effect is about the magnetic field B-dependence of the evolved $Tr[\rho]$, defined as MFE$\equiv Tr[\rho]_B - Tr[\rho]_0$ [36].

Concluding, the particular form of $\mathscr{L}(\rho)$ is imprinted in all physically accessible observables. In the more realistic case of asymmetric/spin-dependent recombination, $k_S \neq k_T$, the reaction super-operator affects both the RP population, $Tr[\rho]$, and the spin-character of RP's density matrix ρ. Assume, for example, a balanced mixture of singlet and triplet RPs, $\rho = a|S\rangle\langle S| + b|T\rangle\langle T|$, which does not evolved unitarily, $\mathscr{H}_m = 0$, and only reacts, $\mathscr{L}(\rho) \neq 0$.

When $k_S = k_T$ the balance is not distorted, since the RPs disappear at the same rate in a spin-independent way. But if $k_S \neq k_T$, the ensemble of the surviving/unreacted RPs will become more triplet (singlet) if $k_S > k_T$ ($k_T > k_S$).

3.5. PHYSICAL MODEL OF THE RADICAL-PAIR MECHANISM

Figures 3.2(a) and 3.2(b) depict a gross picture of the RP reactions and miss important details. We show in Fig.3.4 a more detailed energy level structure, which is crucial to unravel the quantum foundations of the RPM. In our picture, i.e. our physical model about RPM, we take into account the vibrational excitations, termed *phonons*, of the neutral product molecules, the precursors of the RPs. These excited states (phonon degrees of freedom) form at large energies a quasi-continuous reservoir that is quasi-resonant with the RP magnetic energy levels. As we will demonstrate in Chapter 6, this *phonon vacumm* is the fundamental source of singlet-triplet decoherence in RP reactions, similar to the effect of photon vacuum on atomic coherences, and moreover the generator of a Lamb-shift-type energy splitting in the RP magnetic levels.

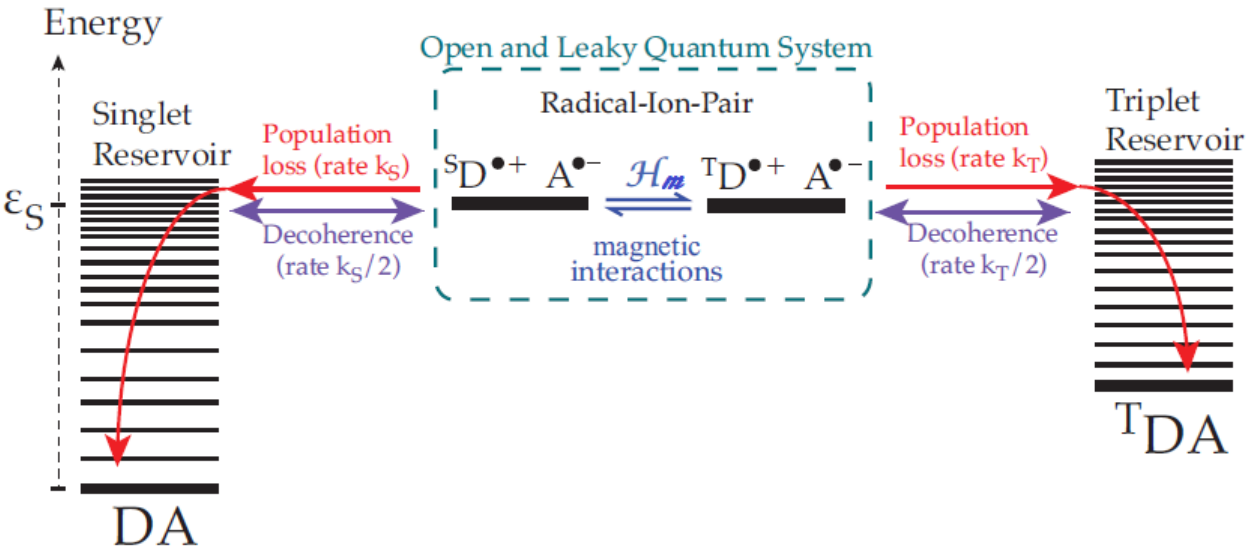

Figure 3.4: Reproduced from [55]. Radical-Pair energy levels including the singlet and triplet reservoirs, which correspond to the vibrational excitations of the RP neutral precursors. The existence of these reservoir states forces the RPs to: (i) lose population by charge recombination into the neutral ground states through *two real* and consecutive transitions, from RP to the quasi-resonant reservoir states followed by the decay of the latter to the ground state (in a picosecond timescale relevant to nuclear re-organization), and (ii) suffer, at the same time, S-T decoherence due to *virtual* transitions from RP to the reservoir states *and back*. These virtual transitions interrupt the S-T mixing induced by the RP magnetic Hamiltonian.

II

SPIN TRANSPORT DYNAMICS IN PHOTOSYNTHETIC REACTION CENTERS

" *We all monitor our world indirectly,*
eavesdropping on the environment. "

— Wojciech H. Zurek

4

DECOHERENCE

4.1. INTRODUCTION

Decoherence [59–62], though based at the heart of quantum theory developed in the first decades of the twentieth century, was pioneered by H. D. Zeh and W. J. Zurek much later (1970s-1980s) with their work on the emergence of classicality in the quantum framework. Until that time, the orthodox (Copenhagen) interpretation of quantum mechanics dominated, with its strict distinction between the macroscopic classical and the microscopic quantum worlds. This attitude engraved a boundary between the quantum and the classical, that was mainly considered as a purely philosophical problem and a non-experimental field, intangible by any physical analysis. This, however, changed when we were be able to understand within the quantum framework why the macro-world is *manifested* as classical, and that there is no need for denying quantum mechanics to hold even macroscopically. Consider, as an example, macroscopic objects which occupy well-defined positions in space; they are found in approximate position eigenstates of their center of mass, and never in superpositions of macroscopically distinct positions. The study of decoherence was originally motivated to explain these effective *super-selection* rules, and the emergence of classicality within quantum theory by taking into account the environment of a quantum system and its crucial impact on it.

The theoretical framework for the study of decoherence is the theory of *open quantum systems*, which was originally developed to incorporate the friction and thermalization effects in the quantum formulation. The theory of open quantum systems studies the effects an (uncontrollable) environment has on the system's quantum evolution. However, the intuition and approximations developed in the traditional treatments are not necessarily appropriate to yield a correct description of decoherence effects, which may take place on a timescale much shorter than typical relaxation phenomena. While the traditional treatments of open quantum systems focus on how the environmental 'bath' affects the system,

the emphasis in decoherence is more on the contrary question, namely how the system affects and disturbs environmental degrees of freedom, thereby revealing information about its state.

The experimental technological advances of the last two decades, brought the physics of decoherence in the foreground. Now, there are several experiments which reveal the gradual emergence of classical properties in a quantum system, in agreement with the predictions of decoherence theory. The popularity of decoherence is, also, because its relevance to quantum information processing (QIP). In QIP tasks, the coherence of a relatively large quantum system has to be maintained over a sufficiently long time. One of the major challenges to the observation and exploitation of quantum effects is decoherence: every quantum system is inevitably coupled to its surroundings, and hence its time evolution is corrupted by uncontrolled, 'environmental' degrees of freedom. Consequently, any initially prepared pure state will decohere, i.e. evolve into a mixed state, and thereby lose its potential for QIP tasks.

Let's now describe the basic decoherence effect in a rather general framework. In what follows we deal with *conventional*, i.e. *environmental* decoherence. We need to account for the unavoidable coupling of the quantum system to its environment. Although these environmental degrees of freedom are to be treated quantum mechanically, their state must be taken practically unobservable because of their large number or uncontrollable nature. The detailed dynamics induced by the environmental interaction will be very complicated in general, but we can get an idea of the basic effect by assuming that the interaction is sufficiently short-ranged to admit a description in terms of scattering theory. In this case, only the map between the asymptotically free states before and after the interaction needs to be discussed, thus avoiding a temporal description of the collision dynamics.

In general, the quantum state of the system is described by the density operator ρ on the Hilbert space $\mathscr{H}$. Consider that the system interacts with a single environmental degree of freedom at a time, e.g. a phonon, a polaron or a gas particle scattering off your favorite implementation of a quantum register. Moreover, assume that this environmental 'particle' is in a pure state $\rho_E = |\psi_{in}\rangle_E\langle\psi_{in}|_E$ with $|\psi_{in}\rangle_E \in \mathscr{H}_E$. The scattering operator S_{tot} maps between the *in*- and *out*-asymptotes in the total Hilbert space $\mathscr{H}_{tot} = \mathscr{H} \otimes \mathscr{H}_E$, and for sufficiently short-ranged interaction potentials we may identify those with the states before collision (bc) and after collision (ac). The initially uncorrelated system and environment turn into a joint state

$$\rho_{tot}^{(bc)} = \rho \otimes \rho_E = \rho \otimes |\psi_{in}\rangle_E\langle\psi_{in}|_E \quad ,$$

$$\rho_{tot}^{(ac)} = S_{tot}\Big[\rho \otimes |\psi_{in}\rangle_E\langle\psi_{in}|_E\Big]S_{tot}^{\dagger} \quad .$$

Additionally, consider that the interaction is *non-invasive* with respect to a certain system property, i.e there is a number of distinct system states such that the environmental scattering off these states does not cause any transitions in the system. For instance, if these distinguished states correspond to the system being localized at well-defined sites, then the

environmental particle should induce no hoping between the locations; for elastic scattering they will be the energy eigenstates. We denote the set of the orthogonal system states by $\{|m\rangle\} \in \mathscr{H}$. The non-invasiveness requirement means that S_{tot} commutes with those states, and hence it is expressed as

$$S_{tot} = \sum_m |m\rangle\langle m| \otimes S_m \quad ,$$

where S_m are scattering operators acting in the environmental Hilbert space $\mathscr{H}_E$. Inserting this into the expression of the total state after collision, we get

$$\begin{aligned} \rho_{tot}^{(ac)} &= \sum_{m,n} \langle m|\rho|n\rangle |m\rangle\langle n| \otimes S_m|\psi_{in}\rangle_E\langle\psi_{in}|_E S_n^\dagger \\ &\equiv \sum_{m,n} \rho_{mn}|m\rangle\langle n| \otimes |\psi_{out}^{(m)}\rangle_E\langle\psi_{out}^{(n)}|_E \quad , \end{aligned}$$

and by performing a partial trace[1] over the environmental state, i.e. disregarding the environment, we end up with the (reduced) *system* state after the interaction

$$\rho^{(ac)} = Tr_E[\rho_{tot}^{(ac)}] = \sum_{m,n} \rho_{mn}|m\rangle\langle n| \underbrace{\langle\psi_{in}|_E S_n^\dagger S_m|\psi_{in}\rangle_E}_{\equiv Tr[S_n^\dagger S_m \rho_E] = \langle\psi_{out}^{(n)}|\psi_{out}^{(m)}\rangle_E} \quad .$$

Since the S_m are unitary, i.e. $S_m^\dagger S_m = S_m S_m^\dagger = \mathbb{1}$, the diagonal density-matrix elements or *populations* are unaffected, $\rho_{mm}^{(ac)} = \rho_{mm}$, whereas the off-diagonal density-matrix elements or *coherences* are multiplied by the overlap of the environmental states scattered off the system states m and n, $\rho_{mn}^{(ac)} = \rho_{mn}\langle\psi_{out}^{(n)}|\psi_{out}^{(m)}\rangle_E$. The modulus of this overlap is less than unity, and hence the coherences which characterize the ability of the system state to display a superposition between $|m\rangle$ and $|n\rangle$, which is a genuine quantum property, get suppressed. The value $|\rho_{mn}|$ determines the maximum fringe visibility in a general interference experiment involving the states $|m\rangle$ and $|n\rangle$, as described by the projection on a general superposition $|\psi_{\theta,\phi}\rangle = \cos\theta|m\rangle + e^{i\phi}\sin\theta|n\rangle$. It is important to note that this loss of coherence occurs in a *special basis*, which is determined only by the scattering operator, i.e. by the type of the environmental interaction, and to a degree that is determined by the environmental state and the interaction.

The loss of ability to show quantum behavior due to the interaction with an environmental quantum degree of freedom is the basic effect of decoherence. One may view it as due to the arising *correlation* between the system with the environment. After the interaction, the joint quantum state of system and environment is no longer separable, i.e. mathematically expressed as a tensor product, and part of the coherence initially located in the system now resides in the non-local correlation between the system and the environmental particle; it is lost once the environment is disregarded (mathematically traced out). A complementary point of view argues that the interaction constitutes an information transfer from the system to the environment. The more the overlap $|\langle\psi_{out}^{(n)}|\psi_{out}^{(m)}\rangle_E|^2$ diverges from unity, the more an observer could, in principle, learn about the system state by measuring the environmental particle. Even though this measurement is never made (by

[1] The 'partial trace' is a generalization of the 'trace'. While the 'trace' is a scalar-valued function of an operator, the 'partial trace' is an operator-valued function.

a conscious observer), the complementarity principle then explains that the wave-like interference phenomenon, characterized by the coherences, vanishes as more ('which path') information discriminating the distinct, 'particle-like' system states is revealed. It is hardly surprising that an imprint is left whenever two quantum systems interact, even when 'nobody is looking', and even when the environment is 'messy' and full of excitations.

In the above demonstration of the decoherence effect, the choice of the interaction and the environmental state was rather special. Consider now arbitrary S_{tot} and ρ_E, and follow the same analysis. In the expression of the system's state after the collision, we carry out the partial trace in the eigenbasis of the environmental state, $\rho_E = \sum_l p_l |\psi_l\rangle_E \langle\psi_l|_E$, and we get

$$\begin{aligned}\rho^{(ac)} = Tr_E\left[S_{tot}[\rho\otimes\rho_E]S_{tot}^\dagger\right] &= \sum_{j,l} p_l \ {}_E\langle\psi_j|S_{tot}|\psi_l\rangle_E \ \rho \ {}_E\langle\psi_l|S_{tot}^\dagger|\psi_j\rangle_E \\ &= \sum_k W_k \rho W_k^\dagger \quad ,\end{aligned}$$

where W_k are the *Kraus operators* given by

$$W_k = \sqrt{p_{l_k}}\langle\psi_{j_k}|S_{tot}|\psi_{l_k}\rangle \quad ,$$

and satisfy

$$\sum_k W_k^\dagger W_k = \mathbb{1}$$

due to the unitarity of S_{tot}. This implies that $\sum_k W_k \rho W_k^\dagger$ is the *operator-sum representation* of a *completely positive map* $\Phi : \rho^{(bc)} \mapsto \rho^{(ac)}$. In other words, the scattering transformation has the form of the most general evolution of a quantum state which obeys the rules of quantum mechanics, usually called as *quantum channel* or *quantum operation* [2]. It is feasible to construct a scattering operator S_{tot} and an environmental state ρ_E that gives rise to the transformation, when an arbitrary quantum channel is known. However, it is usually not very helpful to model the action of a general, dissipative quantum channel as a single scattering event.

Finishing the introduction, some other characteristics and popular statements about the phenomenon of decoherence are the following: *Decoherence*

(i) can be extremely fast with respect to all other relevant timescales,
(ii) can be interpreted as an indirect measurement process, a monitoring of the system by the environment,
(iii) creates dynamically a set of preferred ('robust' or 'pointer') states that are not coherent superpositions, thus providing the microscopic mechanism for the emergence of effective super-selection rules, and
(iv) helps to understand the emergence of classicality in the quantum realm.

[2] More formally, a quantum channel is a completely positive trace-preserving map between spaces of operators. Some authors use the term 'quantum operation' to also include trace-decreasing maps, while reserving 'quantum channel' for strictly trace-preserving maps.

4.2. ENVIRONMENTAL MONITORING INTERPRETATION OF DECOHERENCE

We can relate the decoherence of a quantum system to the information it reveals to the environment. Before that, it is necessary to mention some aspects of Measurement Theory since the formulation is based on the notion of indirect measurements.

4.2.1. ELEMENTS OF GENERAL MEASUREMENT THEORY

Projective Measurements

A projective measurement, also known as *von-Neumann measurement*, is the most common type of quantum measurement encountered in standard quantum mechanics. A projective operator, briefly projector, $|a\rangle\langle a| \equiv P_a = P_a^2 = P_a^\dagger$ is attributed to each possible outcome a of an idealized measurement apparatus. The probability of the outcome a is obtained by the *Born rule*

$$\Pi(a|\rho) = Tr[\rho P_a] = \langle a|\rho|a\rangle \quad ,$$

and after the measurement of a the state of the quantum system is given by the normalized projection

$$\mathscr{M} : \rho \mapsto \rho' \equiv \mathscr{M}(\rho|a) = \frac{P_a \rho P_a}{Tr[\rho P_a]} \quad .$$

The basic requirement that the projectors form a resolution of the identity operator, $\sum_a P_a = \mathbb{1}$, in other words they satisfy the completeness relation, ensures that the corresponding probability distribution $\Pi(a|\rho)$ is normalized to unity.

If the measured system property (system observable) corresponds to a self-adjoint (Hermitian) operator $A = A^\dagger$, its expectation value is given by

$$\langle A\rangle = Tr[A\rho] \quad .$$

Moreover, if A has a continuous spectrum, i.e. a set of eigenvalues taking continuous values, and P_a are the projectors into its eigenspace, then the outcomes are characterized by intervals of a real parameter, and the sum $\sum_a P_a = \mathbb{1}$ should be replaced by a projector-valued Stieltjes integral $\int dP(a) = \mathbb{1}$, or equivalently by a Lebesgue integral over a *projector-valued measure* (PVM).

Projective measurements are not the most general type of measurements compatible with the rules of quantum mechanics. For instance, non-destructive measurements of a quantum system are usually not of the projective kind.

Generalized Measurements

In the most general case, a positive and Hermitian operator $G_a = G_a^\dagger > 0$ is attributed to each outcome a. The set of operators corresponding to all possible outcomes must satisfy the completeness relation, $\sum_a G_a = \mathbb{1}$. Particularly, we refer to a *positive operator-valued measure* (POVM) in the case of a continuous outcome parameter, $\int dG(a) = \mathbb{1}$, and the probability (or the probability density in the continuous case) of outcome a reads $\Pi(a|\rho) = Tr[\rho G_a]$. The effect of a generalized measurement on the system state is described by a non-linear transformation

$$\mathscr{M} : \rho \mapsto \rho' \equiv \mathscr{M}(\rho|a) = \frac{\sum_k O_{a,k} \rho O_{a,k}^\dagger}{Tr[\rho G_a]} \quad ,$$

that involves a *norm-decreasing completely positive map* in the numerator, and the normalization which is subject to the *consistency requirement*

$$\sum_k O_{a,k}^\dagger O_{a,k} = G_a \quad .$$

The operators $O_{a,k}$ are called 'measurement operators' and they characterize the measurement process completely. The operators G_a are sometimes called 'effects' or 'measurement elements'. It is noted that different measurement operators can lead to the same measurement element.

A simple class of generalized measurements are the *unsharp* measurements, where a number of projectors are lumped together with probabilistic weights in order to account for the finite resolution of a measurement device, or for classical noise in its signal processing. However, generalized measurement schemes may also perform tasks which are seemingly impossible with a projective measurement, such as error-free discrimination of two non-orthogonal states.

Efficient Measurements

As efficient, is defined a generalized measurement for $k = 1$, i.e.

$$\mathscr{M}(\rho|a) = \frac{O_a \rho O_a^\dagger}{Tr[\rho O_a^\dagger O_a]} \quad .$$

This implies that pure states are mapped to pure states. In a sense, there are measurements where no classical noise (uncertainty) is introduced during the measurement process. Efficient measurement operators have the form

$$O_a = U_a \sqrt{G_a} \quad ,$$

where U_a is an unitary operator. In doing so, the state's transformation due to an efficient measurement can be decomposed as

$$\mathscr{M}(\rho|a) = \underbrace{U_a}_{\text{back-action}} \underbrace{\frac{\sqrt{G_a}\rho\sqrt{G_a}}{Tr[\rho G_a]}}_{\text{raw measurement}} \underbrace{U_a^\dagger}_{\text{back-action}} \quad ,$$

where the positive operators $\sqrt{G_a}$ 'squeeze' the state along the measured property and expand it along the complementary one, while the back-action operators U_a 'kick' the state by transforming it in a reversible manner, in principle, provided that the outcome a is known. It is noted that the projective measurements $\mathcal{M}(\rho|a) = \frac{P_a \rho P_a}{Tr[\rho P_a^2]}$ are a subclass of back-action-free efficient measurements.

4.2.2. INDIRECT MEASUREMENTS

By performing an indirect measurement on a system, we try to acquire information about its state by disturbing it as little as possible. This is achieved as follows: Firstly, a well-prepared microscopic quantum probe is let to interact with the system. Then, this probe is measured by projection, i.e. destructively. In doing so, we can reveal information about the properties of the system by avoiding its direct contact with a macroscopic measurement device.

Let the prepared state of the probe to be described by the density matrix ρ_{probe}, and P_a being the projectors corresponding to the various outcomes of the probe measurement. The probability of measuring a is determined by the (reduced) state of the probe after interaction, i.e.

$$\Pi(a|\rho_{sys}) = Tr[P_a \rho'_{probe}] = Tr\Big[P_a Tr_{sys}[\rho'_{tot}]\Big] = Tr\Big[P_a Tr_{sys}[S_{tot}\rho_{tot}S_{tot}^\dagger]\Big] \quad ,$$

where the operator S_{tot} describes the system-probe interaction. By pulling out the system partial trace and instead extending the projectors to $\mathcal{H}_{tot} = \mathcal{H}_{sys} \otimes \mathcal{H}_{probe}$, and then using the cyclic permutability of operators under the trace, we get

$$\Pi(a|\rho_{sys}) = Tr\Big[S_{tot}^\dagger(\mathbb{1} \otimes P_a)S_{tot}(\rho_{sys} \otimes \rho_{probe})\Big] = Tr\big[G_a(\rho_{sys} \otimes \mathbb{1})\big] \quad .$$

The measurement elements are microscopically defined as

$$G_a = S_{tot}^\dagger(\mathbb{1} \otimes P_a)S_{tot}(\mathbb{1} \otimes \rho_{probe}) > 0 \quad ,$$

and they satisfy the completeness relation $\sum_a G_a = \mathbb{1}$. Since the probe is subjected on a projective measurement, the new system state can be conditionally specified on the click at a of the probe detector

$$\begin{aligned}
\mathcal{M}(\rho_{sys}|a) &= Tr_{probe}[\mathcal{M}_{tot}(\rho_{tot}|a)] \\
&= Tr_{probe}\Big[\frac{P_a \rho'_{tot} P_a^\dagger}{Tr[P_a \rho'_{tot} P_a^\dagger]}\Big] \\
&= Tr_{probe}\Big[\frac{(\mathbb{1} \otimes P_a) \cdot S_{tot}(\rho_{sys} \otimes \rho_{probe})S_{tot}^\dagger \cdot (\mathbb{1} \otimes P_a)}{Tr\big[(\mathbb{1} \otimes P_a) \cdot S_{tot}(\rho_{sys} \otimes \rho_{probe})S_{tot}^\dagger \cdot (\mathbb{1} \otimes P_a)\big]}\Big] \\
&= \frac{Tr_{probe}\Big[(\mathbb{1} \otimes P_a) \cdot S_{tot}(\rho_{sys} \otimes \sum_k w_k|\psi_k\rangle\langle\psi_k|)S_{tot}^\dagger \cdot (\mathbb{1} \otimes P_a)\Big]}{Tr\big[S_{tot}^\dagger \cdot (\mathbb{1} \otimes P_a) \cdot S_{tot}(\mathbb{1} \otimes \rho_{probe}) \cdot (\rho_{sys} \otimes \mathbb{1})\big]} \\
&= \sum_k \frac{O_{a,k}\rho_{sys}O_{a,k}^\dagger}{Tr\big[G_a(\rho_{sys} \otimes \mathbb{1})\big]} \quad .
\end{aligned}$$

A microscopic description also of the measurement operators is obtained by taking $P_a = |a\rangle\langle a|$, that is

$$O_{a,k} = \sqrt{w_k}\langle a|S_{tot}|\psi_k\rangle \quad .$$

This shows that an indirect measurement is efficient if the probe is initially in a pure state ($k = 1$), i.e. if there is no unnecessary (classical) uncertainty/noise introduced in the measurement process, except for the fundamental/unavoidable quantum noise imposed by the uncertainty relations on ρ_{probe}.

When an indirect measurement has taken place but its outcome a is unknown, one has to resort to a *Bayesian* (probabilistic) description of the new system, which is given by the sum over all possible outcomes weighted by their respective probabilities:

$$\rho'_{sys} = \sum_a \Pi(a|\rho_{sys})\mathcal{M}(\rho_{sys}|a) = \sum_{a,k} O_{a,k}\rho_{sys}O^\dagger_{a,k} \quad .$$

This form is similar to the general one of Kraus operators, where the basic effect of decoherence has been described (see Sec. 4.1). Therefore, the decoherence process can be legitimately viewed as a consequence of the information transfer from the system to the environment, and the complementarity principle can then be invoked to understand which particular system properties lose their quantum behavior, namely those complementary to the ones revealed to the environment. This is the 'monitoring interpretation' of the decoherence process (Fig. 4.1).

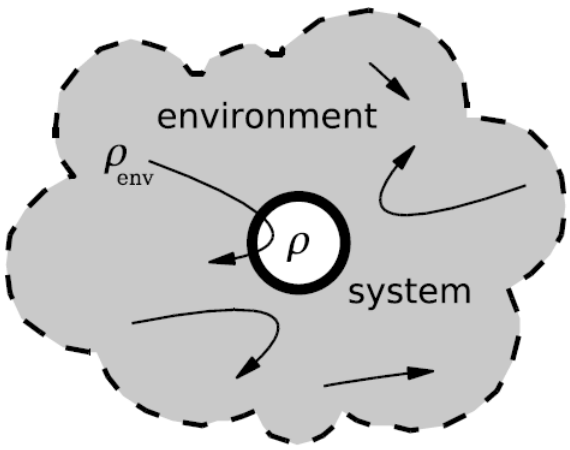

Figure 4.1: In the environmental monitoring approach of the process of decoherence, the system is taken to interact at most with one environmental (quasi-)particle at a time, so the three-body collisions are excluded. Moreover, in agreement with the *Markov assumption*, it is assumed that the environmental particles disperse their correlation with the system before scattering again. In doing so, the environmental decoherence can be understood as due to the information transfer from the system to the environment occurring in a sequence of *indirect measurements*. In accordance with this, the environment is monitoring the system continuously by sending probe particles which scatter off the system at random times. Thus, the system-environment interaction can reasonably be described in terms of individual interaction events or 'collisions'. The Markov assumption is then easily incorporated by disregarding the change of the environmental state after each collision. Picture reproduced from [61].

5

MARKOVIAN DYNAMICS OF OPEN QUANTUM SYSTEMS

5.1. INTRODUCTION

In the Schrödinger picture and for general mixed states, isolated/closed systems evolve according to the *von Neumann equation*

$$\frac{d\rho(t)}{dt} = -\frac{i}{\hbar}[H, \rho(t)]$$

which is the quantum generalization of the classical stochastic *Liouville equation*. A similar differential equation for the reduced dynamics of an 'open' quantum system which interacts with its surroundings is, also, desirable. By extending our description to include the environment $\mathscr{H}_E$ and its coupling to the system, the total state in $\mathscr{H}_{tot} = \mathscr{H} \otimes \mathscr{H}_E$ undergoes unitary/reversible evolution in time. The partial trace over the environment gives the evolved system state, and its 'equation of motion' reads

$$\frac{d\rho(t)}{dt} = \frac{d}{dt} Tr_E\{U_{tot}(t)\rho_{tot}(0)U_{tot}^{\dagger}(t)\} = -\frac{i}{\hbar} Tr_E\{[H_{tot}, \rho_{tot}(t)]\} \quad ,$$

which is exact but not closed, and therefore not particularly helpful as it stands. However, it can be used as the starting point to derive approximate time-evolution equations for ρ, in particular, if it is permissible to take the initial system state to be uncorrelated with the environment, i.e. $\rho_{tot}(0) = \rho(0) \otimes \rho_E(0)$.

These equations are often non-local in time, though in agreement with causality, the change of the system state at each instant in time depends only on the state evolution in the past. In this case, the evolution equation is called a *generalized master equation* which can be specified in terms of super-operator functionals, i.e. linear operators which take ρ with its past time evolution until time t and map it to the differential change of the operator at that time,

$$\frac{d\rho_t}{dt} = \mathscr{K}[\{\rho_\tau : \tau < t\}] \quad .$$

The dependence on the system's past can be interpreted as follows : The environment has a memory, since it affects the system in a way which depends on the history of the system-environment interaction. On a coarse-grained timescale that is large compared to the inter-environmental correlation times (environment self-correlation times), these memory effects might become irrelevant. In such a case, a proper master equation might be appropriate, where the infinitesimal change in ρ depends only on the instantaneous / present system state through a Liouville super-operator $\mathscr{L}$,

$$\frac{d\rho_t}{dt} = \mathscr{L}\rho_t \quad .$$

Master equations of this type are called *Markovian*, reminiscent to the differential Chapman-Kolmogorov equation for a classical Markov process. The fact that a number of approximations are involved in their derivation makes unclear whether the corresponding time evolution respects important properties of a quantum state, such as positivity $\langle\psi|\rho(t)|\psi\rangle \geq 0$. We will see in Section 5.3 that these constraints restrict the possible form of $\mathscr{L}$ rather strongly.

5.2. QUANTUM DYNAMICAL SEMIGROUPS

A rigorous formulation of the Markovian assumption in quantum theory is permissible by the notion of a quantum dynamical semigroup. In order to introduce it, one first needs a number of concepts from the theory of open quantum systems.

5.2.1. DYNAMICAL MAPS

A dynamical map is an element of a one-parameter family of trace-preserving, convex linear and completely positive maps (CPM)

$$\mathscr{D}_t : \rho_0 \mapsto \rho_t, \quad t \geq 0$$

satisfying $\mathscr{D}_0 = \mathbb{I}$, where $\mathbb{I}$ is the identity map, and it yields the most general description of a time evolution that maps an arbitrary initial state ρ_0 to valid states at later times. The normalization of the state is guaranteed by the trace preservation, $Tr\{\rho_t\} = 1$, while the convex linearity, $\mathscr{D}_t\Big(q\rho_0 + (1-q)\rho_0'\Big) = q\mathscr{D}_t(\rho_0) + (1-q)\mathscr{D}_t(\rho_0')\ \forall q \in [0,1]$, ensures that the transformation of mixed states is consistent with the classical notion of ignorance. The final requirement of *complete positivity* is stronger than mere positivity of $\mathscr{D}_t(\rho_0)$; all the tensor product extensions of $\mathscr{D}_t$ to spaces of higher dimension, defined with the identity map $\mathbb{I}_{ex}$, are positive, $\mathscr{D}_t \otimes \mathbb{I}_{ex} > 0$, i.e. the image of any positive operator in the higher dimensional space is again a positive operator. This guarantees that the system state remains positive even if it is the reduced part of a non-separable state evolving in a higher dimensional space.

5.2.2. KRAUS REPRESENTATION

Any dynamical map $\mathscr{D}_t$ admits an *operator-sum representation* of the form

$$\mathscr{D}_t(\rho) = \sum_{k=1}^{N} W_k(t)\rho W_k^\dagger(t) \quad ,$$

where W_k are the Kraus operators. In the case of a *trace-preserving*, convex linear, CPM they satisfy the completeness relation

$$\sum_{k=1}^{N} W_k^\dagger(t) W_k(t) = \mathbb{1} \quad .$$

It is noted that for a *trace-decreasing*, convex linear, CPM the completeness condition is replaced with $\sum_k W_k^\dagger(t)W_k(t) < \mathbb{1}$, that is the operator $\mathbb{1} - \sum_k W_k^\dagger(t)W_k(t)$ must be positive. Also, the number N of Kraus operators $W_k(t)$ is limited by $N \leq dim(\mathscr{H})^2$, with $\mathscr{H}$ denoting the Hilbert space of the system, and it is confined to a countable set in the case of an infinite-dimensional, separable Hilbert space. However, their choice is not unique.

5.2.3. SEMIGROUP ASSUMPTION

At this point, one can assume that the set/family of dynamical maps $\{\mathscr{D}_t : t \geq 0\}$ on the space of density matrices ρ forms a continuous *dynamical semigroup*

$$\mathscr{D}_{t_2}(\mathscr{D}_{t_1}(\rho)) = \mathscr{D}_{t_1+t_2}(\rho) \quad \forall\ t_1, t_2 \geq 0 \quad ,$$

where $\mathscr{D}_0 = \mathbb{I}$ (the inverse element $\mathscr{D}^{-1}$, required for a group structure, is missing for general, irreversible CPMs). This is a rather strong statement which is certainly violated for truly microscopic times. However, it is not unreasonable for a coarse-grained timescale that is long compared to the time it takes for the environment to 'forget' the past interactions with the system due to the dispersion of correlations into the many environmental degrees of freedom (Markovian assumption).

For a given dynamical semigroup $\mathscr{D}_t$ there exists, under rather weak conditions, a super-operator $\mathscr{L}$ that satisfies

$$\mathscr{D}_t = e^{\mathscr{L}t}, \quad t > 0$$

i.e. the Lindblad super-operator $\mathscr{L}$ is the generator of the quantum dynamical semigroup $\mathscr{D}_t$. In this case, $\mathscr{D}_t(\rho)$ is the formal solution of the Markovian master equation $d\rho/dt = \mathscr{L}\rho$.

The generator can be obtained by

$$\mathscr{L}\rho = \lim_{\Delta t \to 0} \frac{\mathscr{D}_{\Delta t}(\rho) - \mathscr{D}_0(\rho)}{\Delta t}$$

which is a linear super-operator due to the linearity of $\mathscr{D}_t$. The semigroup can be recovered as

$$\mathscr{D}_{t_1+t_2}(\rho) = e^{\mathscr{L}t_2}\mathscr{D}_{t_1}(\rho) \quad .$$

5.3. MICROSCOPIC DERIVATION – WEAK-COUPLING LIMIT

The following first-principle derivation of the Master Equation describing the dynamics of an open quantum system, which is weakly coupled to its environment/reservoir/bath, shortly *Lindblad Master Equation*, is based on [61](p.255-259), [63](p.130-136) and [64](p.155-167). The Lindblad Master Equation is a special and more simplified form of the general Born-Markov Master Equation, which plays a key role for the study of open quantum systems and decoherence.

A simplified model that describes the dynamics of a microscopic-quantum system S which is coupled to the environment E, is given by the total Hamiltonian

$$H = \underbrace{H_S + H_E}_{\equiv H_0} + H_{SE} \quad ,$$

with H_S and H_E being the free/unperturbed Hamiltonian of the system and the environment, respectively. Considering *weak* system-environment coupling, i.e. $||H_{SE}|| << ||H_0||$, a perturbative treatment of the interaction Hamiltonian is permissible. In other words, we can approximate the system-environment interaction using *perturbation theory*.

According to *Born approximation* which states that H_{SE} is sufficiently small, we can factorize the total state both initially, $\rho(0) = \rho_S(0) \otimes \rho_E$, and subsequently in those terms which involve H_{SE} up to *second order*, i.e.

- Assumption 1 : $\rho(t) \simeq \rho_S(t) \otimes \rho_E \quad , \quad t > 0 \quad \text{up to} \quad \mathcal{O}(H_{SE}^2) \quad .$ (5.1)

Here we assume that the environment is approximately at equilibrium[1], that is $\frac{d\rho_E}{dt} = \frac{1}{i\hbar}[H_E, \rho_E] \simeq 0$, and thus ρ_E is stationary (homogeneous in time or time-independent). The rationale of this approach is that the environment is assumed to be much larger than the system, so its variation due to the coupling with the system is small. Thus, it is justified to assume that $\rho_E(t) \simeq \rho_E(0) = \rho_E$.

For the reason that the master equation of an open quantum system is most easily derived in the interaction/Dirac picture, a picture into which both quantum states and operators are time-dependent, we use a tilde (~) to denote the interaction picture.

The Schrödinger-von Neumann equation (or the 'quantum Liouville' equation) for the total system, i.e. system plus environment, in the interaction picture reads

$$\begin{aligned} \frac{d\tilde{\rho}(t)}{dt} &= \frac{1}{i\hbar}[\tilde{H}_{SE}(t), \tilde{\rho}(t)] \\ &= \frac{1}{i\hbar}[\tilde{H}_{SE}(t), \rho(0)] - \frac{1}{\hbar^2}\int_0^t d\xi [\tilde{H}_{SE}(t), [\tilde{H}_{SE}(\xi), \tilde{\rho}(\xi)]] \end{aligned} \tag{5.2}$$

[1] It is important to mention that this does not mean that there are no system-induced excitations in the environment. The Markovian approximation, that we will consider afterwards, provides a description on a coarse-grained timescale and the assumption is that the environmental excitations decay over times which are not resolved. Put differently, the 'memory' of the environment about the system is negligible, in the sense that any self-correlations within the environment created by the coupling to the system, decay rapidly with respect to the characteristic timescale over which the system's state changes appreciably.

which is still exact. To derive this, i.e. the second equation, we insert into the first differential equation its integral equation version $\tilde{\rho}(t) = \rho(0) + \frac{1}{i\hbar}\int_0^t d\xi[\tilde{H}_{SE}(\xi), \tilde{\rho}(\xi)]$. We also note that

$$\tilde{H}_{SE}(t) = e^{iH_0 t/\hbar} H_{SE} e^{-iH_0 t/\hbar} \qquad \text{and}$$

$$\tilde{\rho}(t) = e^{iH_0 t/\hbar}\rho(t)e^{-iH_0 t/\hbar} = e^{iH_0 t/\hbar}e^{-iHt/\hbar}\rho(0)e^{iHt/\hbar}e^{-iH_0 t/\hbar} = e^{-iH_{SE}t/\hbar}\rho(0)e^{iH_{SE}t/\hbar} \quad .$$

The general $\tilde{H}_{SE}$ can be decomposed in a basis of Hilbert-Schmidt operators of the product Hilbert space, taking the form

$$\tilde{H}_{SE}(t) = \sum_k \tilde{A}_k(t) \otimes \tilde{B}_k(t) \tag{5.3}$$

with $\tilde{A}_k$ and $\tilde{B}_k$ being Hermitians. The intuitive physical interpretation of this diagonal decomposition is that the operators $\tilde{A}_k$ correspond to the physical quantities of the system that are continuously 'monitored' by the environment [64].

At this point, we use the Born approximation in the double commutator of (5.2), and consequently the exact Schrödinger-von Neumann equation (5.2) obtains the approximative form of a *second order perturbation expansion*. Thereafter, we substitute (5.3) into the second order perturbation expansion and then we perform the partial trace over the environment, since the environment is at equilibrium and hence we are only interested in the dynamics of the system. In doing so, after some algebra we get

$$\begin{aligned}\frac{d\tilde{\rho}_S(t)}{dt} &= Tr_E\Big[\frac{d\tilde{\rho}(t)}{dt}\Big] \\ &\simeq \frac{1}{i\hbar}\sum_k \langle \tilde{B}_k(t)\rangle_{\rho_E}[\tilde{A}_k(t), \rho_S(0)] \\ &\quad - \frac{1}{\hbar^2}\sum_{kl}\Big\{\int_0^t d\xi \underbrace{\langle \tilde{B}_k(t)\tilde{B}_l(\xi)\rangle_{\rho_E}}_{=C_{kl}(t-\xi)}\Big(\tilde{A}_k(t)\tilde{A}_l(\xi)\tilde{\rho}_S(\xi) - \tilde{A}_l(\xi)\tilde{\rho}_S(\xi)\tilde{A}_k(t)\Big) + h.c.\Big\}\end{aligned} \tag{5.4}$$

where $h.c.$ means the hermitian conjugate (complex conjugate transpose) expression and $C_{kl}(t-\xi)$ are the (complex) *bath self-correlation functions* which, broadly speaking, quantify to what degree the environment retains information over time about its interaction with the system. Let us explain this further: The Hermitian operators $\tilde{B}_k$ are considered as observables 'measured' on the environment by the system-environment interaction. So, the bath *self*-correlation functions tell us to what extend the result of such a 'measurement' of a particular $\tilde{B}_k$ is correlated with the result of a 'measurement' of the *same* observable performed at a later time. Moreover, these functions depend only on the time difference $\tau \equiv t-\xi$ between these two identical 'measurements' since ρ_E is stationary, they are determined by the environmental state alone $C_{kl}(\tau) = \langle e^{iH_E\tau}B_k e^{-iH_E\tau}B_l\rangle_{\rho_E} \equiv Tr[e^{iH_E\tau}B_k e^{-iH_E\tau}B_l\rho_E]$, and they are typically appreciable only in the vicinity of $\tau = 0$, because of their rapid decay compared to the timescale set by the system's evolution.

The latter 'equation of motion' of the (reduced) system density matrix has the closed form of a *generalized master equation* non-local in time, that is non-Markovian. Viewing the second-order term as a superoperator functional which depends essentially on $t-\xi$, we can rewrite it in the closed form

$$\frac{d\tilde{\rho}_S(t)}{dt} \simeq \frac{1}{i\hbar}\sum_k \langle \tilde{B}_k(t)\rangle_{\rho_E}[\tilde{A}_k(t),\rho_S(0)] + \int_0^t d\xi\ \mathscr{K}(t-\xi)\tilde{\rho}_S(\xi) \quad . \tag{5.5}$$

Furthermore, one can always reformulated H_E such that $\langle \tilde{B}_k(t)\rangle_{\rho_E} = 0$. Thus, the first-order term may be ignored leading to

$$\frac{d\tilde{\rho}_S(t)}{dt} \simeq \int_0^t d\xi\ \mathscr{K}(t-\xi)\tilde{\rho}_S(\xi) \quad . \tag{5.6}$$

The above equation can be interpreted as follows: The infinitesimal change of ρ_S depends on the history of the system-environment interaction or, in other words, it depends on the state evolution in the past. An interpretation of this dependence on the system's past is that the environment has a memory, it does 'keep track of his history' since it affects the system in a way which depends on the history of the system-environment interaction. For this reason $\mathscr{K}(t-\xi)$ corresponds to a *superoperator memory kernel*.

Since the memory kernel is sharply peaked around $\tau \equiv t-\xi = 0$, it is reasonable to consider the *Born-Markov approximation* :

- Assumption 2 : $$\int_0^t d\xi\ \mathscr{K}(t-\xi)\tilde{\rho}_S(\xi) \simeq \left[\int_0^t d\xi\ \mathscr{K}(t-\xi)\right]\tilde{\rho}_S(t) \simeq \int_0^\infty d\xi\ \mathscr{K}(\xi)\tilde{\rho}_S(t) \tag{5.7}$$

Firstly, we replace the retarded-time density operator $\tilde{\rho}_S(\xi)$ with the current-time density operator $\tilde{\rho}_S(t)$, since the latter varies insignificantly during the typical time-interval τ_B over which the bath self-correlation functions $C_{kl}(t-\xi)$ vanish. In doing so, the resulting master equation is the *Redfield equation* (the middle term above is the right-hand side of it) which is local in time but not Markovian, because the integrated superoperator is still time-dependent.

The last term is the result of the replacement of the integration variable ξ with $t-\xi$ and the reasonable change of the upper integration limit $t \to \infty$; the change of the integral variable affects, obviously, only the superoperator $\mathscr{K}$ which now becomes time-independent. The aforementioned substitution is allowed if the memory kernel goes to zero sufficiently fast for $\xi >> \tau_B$, where τ_B is a characteristic timescale of the environment, called bath correlation time over which any dynamically established quantum correlations between its parts are destroyed. Therefore, the Markovian assumption is justified when the timescale τ_R over which the system changes significantly, called relaxation time, is large with respect to the timescale τ_B over which the bath correlation functions vanish. In other words, $\tau_B << \tau_R$ is

the physical condition for the Born-Markov approximation.

By this way, we arrive at a *Markovian master equation* which is local in time, i.e. it depends only on the *present* state of the system

$$\begin{aligned}\frac{d\tilde{\rho}_S(t)}{dt} &\simeq \int_0^\infty d\xi\, \mathcal{K}(\xi)\tilde{\rho}_S(t) \\ &= \frac{1}{\hbar^2}\sum_{kl}\Big\{\int_0^\infty d\xi \underbrace{\langle \tilde{B}_k(\xi)B_l(0)\rangle_{\rho_E}}_{=C_{kl}(\xi)}\Big(\tilde{A}_l(t-\xi)\tilde{\rho}_S(t)\tilde{A}_k(t) - \tilde{A}_k(t)\tilde{A}_l(t-\xi)\tilde{\rho}_S(t)\Big) + h.c.\Big\}\end{aligned} \tag{5.8}$$

In a description of the system's equation of motion on the basis of a Markovian master equation, the dynamical behaviour over times of the order of τ_B is not resolved, and in this sense the evolution is described on a coarse-grained time-axis. The Born-Markov approximation is reasonable, because damping destroys memory of the past. In such a case, a proper master equation might be appropriate, where the infinitesimal change of ρ_S depends only on the *instantaneous* system state through a time-independent superoperator. Such an equation, is the Markovian master equation which is characterized by the *Liouville* superoperator $\mathscr{L} : d_t\rho(t) = \mathscr{L}\rho(t)$. Obviously, in our case $\mathscr{L} = \int_0^\infty d\xi\, \mathcal{K}(\xi)$.

Now, the master equation that governs the evolution of a non-leaky system must be trace-preserving, i.e. without population loss, and completely positive for any initial condition, since the rates that determine the dynamics must be positive and $\langle\psi|\rho_S(t)|\psi\rangle \geq 0$ in order to be interpreted as occupation probabilities. However, the Markovian master equation (5.8) is not guaranteed to be completely positive. A completely positive master equation can be obtained by the *'secular' approximation*, which is applicable if the system's unperturbed Hamiltonian H_S has a discrete, non-degenerate set of energy eigenvalues (spectrum). Then, the system's operators A_k can be decomposed in the system's energy eigenbasis (since it is complete and orthonormal) or, in other words, the system's operators A_k in the interaction Hamiltonian H_{SE} can be decomposed into eigenoperators of H_S.

Combining the contributions with equal energy differences, i.e. with fixed frequency ω, the system's operators are defined as

$$A_k(\omega) = \sum_{E'-E=\hbar\omega} \langle E|A_k|E'\rangle |E\rangle\langle E'| \tag{5.9}$$

where E and $|E\rangle$ are the eigenvalues and eigenstates of H_S, respectively. Some useful relations based on the above definition are the following:

$$[H_S, A_k(\omega)] = -\omega A_k(\omega) \tag{5.10}$$

$$[H_S, A_k^\dagger(\omega)] = \omega A_k^\dagger(\omega) \tag{5.11}$$

$$e^{iH_St}A_k(\omega)e^{-iH_St} = e^{-i\omega t}A_k(\omega) \tag{5.12}$$

$$e^{iH_St}A_k^\dagger(\omega)e^{-iH_St} = e^{i\omega t}A_k^\dagger(\omega) \tag{5.13}$$

$$[H_S, A_k^\dagger(\omega)A_l(\omega)] = 0 \tag{5.14}$$

$$A_k^\dagger(\omega) = A_k(-\omega) \tag{5.15}$$

If we sum (5.9) over all energy differences and employ the completeness relation, then the system's operator can be written as

$$A_k = \sum_{\omega} A_k(\omega) \quad . \tag{5.16}$$

However, in our master equation (5.8) we have the system's operators as a function of time in the interaction picture. So, by performing a discrete Fourier transform (DFT) from ω-space to t-space, the time-dependence of these operators in the interaction picture is, now, particularly simple :

$$\tilde{A}_k(t) = \sum_{\omega} e^{-i\omega t} A_k(\omega) \quad . \tag{5.17}$$

Substituting this decomposition into the master equation (5.8), we get

$$\frac{d\tilde{\rho}_S(t)}{dt} = \sum_{kl}\sum_{\omega\omega'} e^{i\Delta\omega t} \underbrace{\frac{1}{\hbar^2}\int_0^{\infty} d\xi\; e^{i\omega'\xi} \overbrace{Tr_E[\tilde{B}_k(\xi)B_l(0)\rho_E]}^{=\langle \tilde{B}_k(\xi)B_l(0)\rangle_{\rho_E}=C_{kl}(\xi)}}_{\equiv\Gamma_{kl}(\omega')} \times$$
$$\times \left(A_l(\omega')\tilde{\rho}_S(t)A_k^{\dagger}(\omega) - A_k^{\dagger}(\omega)A_l(\omega')\tilde{\rho}_S(t) \right) + h.c. \tag{5.18}$$

where we have made use of (5.15), $\Delta\omega = \omega - \omega'$ is the detuning, and $\Gamma_{kl}(\omega)$ is the one-sided Fourier transform of the bath correlation function $C_{kl}(\xi)$. Essentially, the 'secular' approximation consists of replacing the generator of the interaction picture master equation by its time-average.

For times t, e.g. the relaxation time of the system τ_R, which are sufficiently larger than the typical timescale of the inherent evolution of the system τ_S given by the smallest system's energy spacings/splittings/gaps, i.e $t >> \tau_S \sim 1/|\omega - \omega'|$, it is reasonable to expect that only the secular terms for which $\omega = \omega'$, i.e. the resonances, contribute appreciably into the sum of (5.18). All the other non-secular terms are averaged out by the rapidly oscillating phase factor, $\exp(i\infty) \simeq 0$, or, in other words, vanish due destructive interference.

This is the, commonly encountered in quantum optics, *rotating wave approximation (RWA)*

- Assumption 3 : $$\sum_{\omega\omega'} e^{i(\omega-\omega')t} f(\omega,\omega') \simeq \sum_{\omega} f(\omega,\omega) \tag{5.19}$$

due to which the master equation (5.18) becomes

$$\frac{d\tilde{\rho}_S(t)}{dt} = \sum_{kl}\sum_{\omega} \underbrace{\frac{1}{\hbar^2}\int_0^{\infty} d\xi\; e^{i\omega\xi}\langle \tilde{B}_k(\xi)B_l(0)\rangle_{\rho_E}}_{\equiv\Gamma_{kl}(\omega)} \left(A_l(\omega)\tilde{\rho}_S(t)A_k^{\dagger}(\omega) - A_k^{\dagger}(\omega)A_l(\omega)\tilde{\rho}_S(t) \right) + h.c. \quad , \tag{5.20}$$

where $\Gamma_{kl}(\omega)$ is a complex matrix element which has dimensions of frequency. It is useful to rewrite it as

$$\Gamma_{kl}(\omega) = \frac{1}{2}\gamma_{kl}(\omega) + iS_{kl}(\omega) \quad , \tag{5.21}$$

where $\gamma_{kl}(\omega)$ is positive[2] and given by the full Fourier transform of the bath correlation function,

$$\gamma_{kl}(\omega) = \Gamma_{kl}(\omega) + \Gamma^*_{lk}(\omega) = \frac{1}{\hbar^2}\int_{-\infty}^{\infty} d\xi\ e^{i\omega\xi}\ \langle \tilde{B}_k(\xi)B_l(0)\rangle_{\rho_E} \tag{5.22}$$

and $S_{kl}(\omega)$ is Hermitian defined by

$$S_{kl}(\omega) = \frac{1}{2i}\left(\Gamma_{kl}(\omega) - \Gamma^*_{lk}(\omega)\right) \quad . \tag{5.23}$$

Using the identities $Tr[O^\dagger] = (Tr[O])^*$ and $Tr[ABC] = Tr[CAB] = Tr[BCA]$, we have:

$$\Gamma^*_{lk}(\omega) = \frac{1}{\hbar^2}\int_0^{\infty} d\xi\ e^{-i\omega\xi}\ \left(Tr_E[\tilde{B}_l(\xi)B_k(0)\rho_E]\right)^* \overbrace{=}^{\xi\to-\xi'} \frac{1}{\hbar^2}\int_{-\infty}^{0} d\xi'\ e^{i\omega\xi'}\ Tr_E[\rho_E B_k(0)\tilde{B}_l(-\xi')] \tag{5.24}$$

$$\overbrace{=}^{\xi'\to\xi} \frac{1}{\hbar^2}\int_{-\infty}^{0} d\xi\ e^{i\omega\xi}\ Tr_E[\rho_E B_k(0)\tilde{B}_l(-\xi)] = \frac{1}{\hbar^2}\int_{-\infty}^{0} d\xi\ e^{i\omega\xi}\ Tr_E[\rho_E B_k(0)e^{-iH_E\xi}B_l(0)e^{iH_E\xi}] \tag{5.25}$$

$$= \frac{1}{\hbar^2}\int_{-\infty}^{0} d\xi\ e^{i\omega\xi}\ Tr_E\left[\rho_E\left(e^{iH_E\xi}B_k(0)e^{-iH_E\xi}\right)B_l(0)\right] = \frac{1}{\hbar^2}\int_{-\infty}^{0} d\xi\ e^{i\omega\xi}\ Tr_E[\tilde{B}_k(\xi)B_l(0)\rho_E] \quad , \tag{5.26}$$

which proves (5.22).

At this point it is useful to write the hermitian conjugate (*h.c.*) term in (5.20). Then, we have

$$\begin{aligned}\frac{d\tilde{\rho}_S(t)}{dt} &= \sum_{kl\omega}\Gamma_{kl}(\omega)\left(A_l(\omega)\tilde{\rho}_S(t)A^\dagger_k(\omega) - A^\dagger_k(\omega)A_l(\omega)\tilde{\rho}_S(t)\right)\\ &\quad + \sum_{kl\omega}\Gamma^*_{lk}(\omega)\left(A_l(\omega)\tilde{\rho}_S(t)A^\dagger_k(\omega) - A^\dagger_k(\omega)A_l(\omega)\tilde{\rho}_S(t)\right)^\dagger\\ &= \sum_{kl\omega}\Gamma_{kl}(\omega)\left(A_l(\omega)\tilde{\rho}_S(t)A^\dagger_k(\omega) - A^\dagger_k(\omega)A_l(\omega)\tilde{\rho}_S(t)\right)\\ &\quad + \sum_{kl\omega}\Gamma^*_{lk}(\omega)\left(A_k(\omega)\tilde{\rho}_S(t)A^\dagger_l(\omega) - \tilde{\rho}_S(t)A^\dagger_l(\omega)A_k(\omega)\right) \quad ,\end{aligned} \tag{5.27}$$

[2]These matrix elements, as we will see soon, are constants that determine the dynamics, and specifically play the role of relaxation rates for the different decay modes of the open quantum system. Hence, they must be positive to ensure that the master equation is trace-preserving and completely positive. The positivity of this matrix $\gamma(\omega) = (\gamma_{kl}(\omega))$ is proved according to the Bochner's theorem, which states that the Fourier transform of a function which is of positive type is, also, positive.

where

$$\Gamma^*_{lk}(\omega) = \frac{1}{2}\gamma^*_{lk}(\omega) - iS^*_{lk}(\omega) = \frac{1}{2}\gamma_{lk}(\omega) - iS_{lk}(\omega) \quad . \tag{5.28}$$

Substituting (5.21) and (5.28) into (5.27) and performing some algebra, we end up with the master equation of the *first Lindblad form* (first standard form for a generator of a quantum dynamical semigroup),

$$\begin{aligned}\frac{d\tilde{\rho}_S(t)}{dt} =& \frac{1}{i\hbar}[H_{\text{Lamb}}, \tilde{\rho}_S(t)] \\ &+ \sum_{klo} \gamma_{kl}(\omega)\Big(A_l(\omega)\tilde{\rho}_S(t)A^\dagger_k(\omega) - \frac{1}{2}A^\dagger_k(\omega)A_l(\omega)\tilde{\rho}_S(t) - \frac{1}{2}\tilde{\rho}_S(t)A^\dagger_k(\omega)A_l(\omega)\Big)\end{aligned} \tag{5.29}$$

where the coefficients γ_{kl} have dimensions of frequency, and constitute a positive matrix as it is proved according to the Bochner's theorem. Diagonalizing this (coefficient) matrix by an appropriate unitary transformation, the master equation (5.29) can be brought into the *second Lindblad form* or *diagonal form* $\sum_m r_m\Big(L_m\tilde{\rho}_S(t)L^\dagger_m - \frac{1}{2}L^\dagger_m L_m\tilde{\rho}_S(t) - \frac{1}{2}\tilde{\rho}_S(t)L^\dagger_m L_m\Big)$, which is the most general form for a generator of a quantum dynamical semigroup, and the dimensionless operators L_m are called *Lindblad* or *jump* operators.

In the first unitary term of (5.29), there is the Hermitian operator

$$H_{\text{Lamb}} = \hbar\sum_{klo} S_{kl}(\omega)A^\dagger_k(\omega)A_l(\omega) \quad , \tag{5.30}$$

which is not equal to the self-Hamiltonian of the system, but it incorporates effective unitary dynamics arising from the system-environment interaction. Specifically, it describes a *renormalization* of the system's energy levels due to the (weak) coupling with the environment, the so-called *Lamb shift*. Since there is no energy exchange between system and environment, the commutation relation $[H_S, H_{\text{Lamb}}] = 0$ must be satisfied. Hence, the first term of this master equation describes effective unitary evolution.

The second term of (5.29) is non-unitary, and it corresponds to the incoherent part of the system's evolution that describes the damping/dephasing/decoherence of the system due to its coupling with the environment. It is the dissipator of the master equation

$$\mathscr{D}\tilde{\rho}_S(t) = \sum_{klo} \gamma_{kl}(\omega)\Big(A_l(\omega)\tilde{\rho}_S(t)A^\dagger_k(\omega) - \frac{1}{2}A^\dagger_k(\omega)A_l(\omega)\tilde{\rho}_S(t) - \frac{1}{2}\tilde{\rho}_S(t)A^\dagger_k(\omega)A_l(\omega)\Big) \tag{5.31}$$

which is known as Lindblad term, and the matrix coefficients $\gamma_{kl}(\omega)$ are the rate constants that determine these deleterious dynamics, known as decoherence rates.

Transformation back to the Schrödinger picture

Finally, the interaction-picture master equation (5.29) can be transformed back to the Schrödinger picture by the following general recipe.

Since

$$\tilde{\rho}_S(t) = e^{iH_S t/\hbar}\rho_S(t)e^{-iH_S t/\hbar} \quad , \tag{5.32}$$

it is straightforward to show that

$$\frac{d\tilde{\rho}_S(t)}{dt} = \frac{i}{\hbar}[H_S, \tilde{\rho}_S(t)] + e^{iH_S t/\hbar}\frac{d\rho_S(t)}{dt}e^{-iH_S t/\hbar} \quad . \tag{5.33}$$

Inserting (5.32) into the commutator of (5.33), the latter reads

$$\frac{d\rho_S(t)}{dt} = -\frac{i}{\hbar}[H_S, \rho_S(t)] + e^{-iH_S t/\hbar}\frac{d\tilde{\rho}_S(t)}{dt}e^{iH_S t/\hbar} \quad , \tag{5.34}$$

where we multiplied both sides from the left by $e^{-iH_S t/\hbar}$ and from the right by $e^{iH_S t/\hbar}$.

Then, we insert (5.29) into the above equation, and utilizing the properties (5.10)-(5.14), after some algebra we end up with the Schrödinger-picture master equation

$$\begin{aligned}\frac{d\rho_S(t)}{dt} = &-\frac{i}{\hbar}[H_S + H_{\text{Lamb}}, \rho_S(t)] \\ &+ \sum_{kl\omega}\gamma_{kl}(\omega)\Big(A_l(\omega)\rho_S(t)A_k^\dagger(\omega) - \frac{1}{2}A_k^\dagger(\omega)A_l(\omega)\rho_S(t) - \frac{1}{2}\rho_S(t)A_k^\dagger(\omega)A_l(\omega)\Big) \quad .\end{aligned} \tag{5.35}$$

" *No progress was made for 20 years. Then a development came, initiated by Lamb's discovery and explanation of the Lamb shift, which fundamentally changed the character of theoretical physics.* "

— Paul M. Dirac

6

LAMB SHIFT IN RADICAL-ION PAIRS PRODUCES A SINGLET-TRIPLET ENERGY SPLITTING IN PHOTOSYNTHETIC REACTION CENTERS

6.1. INTRODUCTION

Radical-ion pairs (RPs) [35] are biomolecules recently shown [26, 27, 31, 65–70] to exhibit a host of non-trivial quantum effects, providing a strong link between biology and quantum information science, thus further driving the emerging field of quantum biology [2, 23, 28–30, 32, 34, 71–73]. Radical-ion-pair reactions are thought to underlie the avian magnetic compass [38, 39, 54, 74, 75], however the primary interest in them stems from their central role in photosynthesis [76, 77]. The photon energy absorbed by the chlorophyll antennae is transformed to an electronic excitation finally reaching the photosynthetic reaction center (PRC), and resulting in the transmembrane charge separation essential for biochemical energy production. This charge separation is the end result of a cascade of electron transfers through a series of RPs. So the fundamental understanding of PRC dynamics and hence the efficiency of photosynthesis is intimately linked to the understanding of RP reactions.

A new approach for describing spin-selective RP reactions was recently introduced [26, 27, 71] based on quantum measurement theory. In particular, we showed that spin-selective RP reactions can be understood as an intra-molecule quantum measurement of the RP's electron spin-state. This intra-molecule quantum measurement leads to spin decoherence, in particular to singlet-triplet (S-T) dephasing. Now, it is well-known that decoherence is one facet of an open quantum system's interaction with its environment. Another is, in principle, a shift in the unperturbed energy levels of the system, generically known as *Lamb*

shift [61, 63, 78, 79], first measured by W. E. Lamb and R. C. Retherford in 1947 as an upward energy shift of about 1 GHz on $2\,^2S_{1/2}$ level relative to $2\,^2P_{1/2}$ level of atomic hydrogen ($2S_{1/2}-2P_{1/2}$ splitting). This discovery was the harbinger of the development of modern quantum electrodynamics and awarded with the Nobel Prize in 1955.

We will here show that the intra-molecule quantum dynamics of RPs result in a Lamb shift of their magnetic energy levels, that is the physical energy levels of the RP are shifted relative to the levels of a 'bare' RP, which is an imaginary RP without the decohering vibrational states. It will be shown that, in general, singlet and triplet RP states are shifted by a different amount, resulting in an S-T energy splitting, which is physically indistinguishable from an exchange interaction.

Radical-ion pairs are biomolecular ions with two unpaired electrons and any number of magnetic nuclei, created by a charge transfer from a photo-excited donor-acceptor molecular dyad DA. It is spin dynamics that are of interest in RP reactions, the spin-space consisting of the electron and nuclear spins. RPs are usually created from singlet neutral precursors, so their initial state is the singlet electronic spin-state denoted by ${}^{S}D^{\bullet+}A^{\bullet-}$, where the two dots signify the two unpaired electrons in the donor (+) and the acceptor (−) molecular ions. Intra-molecule magnetic interactions, dominated by hyperfine couplings of the RP's electrons to the RP's nuclei, lead to a coherent singlet-triplet mixing of the RP spin-state, ${}^{S}D^{\bullet+}A^{\bullet-} \longleftrightarrow {}^{T}D^{\bullet+}A^{\bullet-}$. While mixing, RP population is lost spin-selectively due to charge recombination taking place at a random instant in time and leading to the neutral reaction products. In the following, we do not at all consider recombination reactions, but focus on the state evolution of radical pairs until the time they recombine.

According to our approach [26], shown in Fig. 3.4, the vibrational excitations of the neutral product molecules form a decohering reservoir for the RP's spin evolution. That is, the coupling of the RP's spin degrees of freedom to the vibrational modes is responsible not only for charge recombination, but it also produces random jumps from the RP state to the reservoir states and back, interrupting the coherent S-T mixing driven by the RP's magnetic Hamiltonian $\mathscr{H}_m$ and leading to S-T dephasing [80]. The same intra-molecule coupling to the vibrational reservoir has yet another consequence : the physical RP Hamiltonian will be slightly different, shifted from the 'bare' Hamiltonian $\mathscr{H}_m$ by the Lamb-shift correction $\delta\mathscr{H}_{Lamb}$, which we are now going to calculate.

6.2. SYSTEM-RESERVOIR INTERACTION

Consider for the moment just the singlet reservoir, consisting of states with energy ε_i (Fig. 6.1a). These are described by fermionic creation and annihilation operators $a_i^\dagger$ and a_i, respectively, and the reservoir Hamiltonian is $\mathscr{H}_{res} = \sum_i \varepsilon_i a_i^\dagger a_i$. The fact that we treat a vibrational reservoir with fermionic operators might appear questionable. The reason is that we wish to describe a single occupation of just one of the reservoir states. That is, when the acceptor's electron is transferred back to the donor, just one among the quasi-continuous manifold of reservoir states is occupied, and hence this notation is useful to account for this process. This will be evident in the following after we introduce the system-reservoir

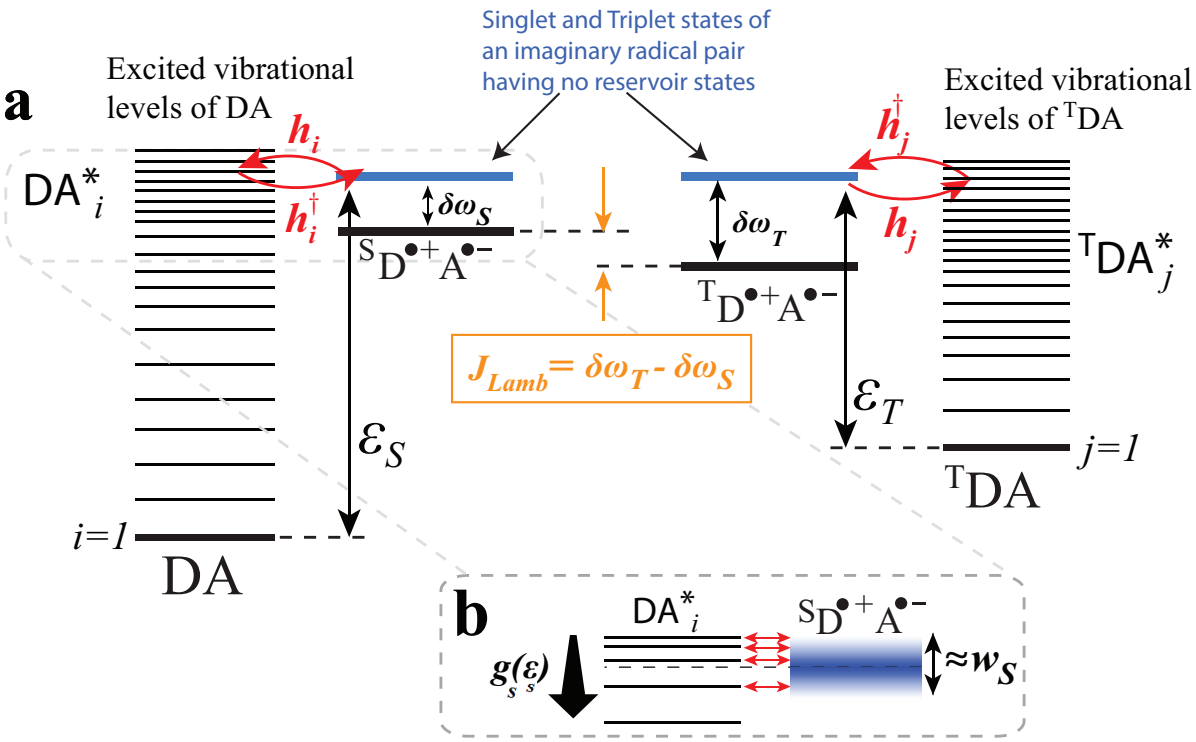

Figure 6.1: **(a)** Radical-ion pair with singlet (S) and triplet (T) reservoir states. These are the vibrational excitations of the singlet, DA, and triplet, ^{T}DA, neutral ground states which form the RP recombination-reaction products. In a 'bare' (unphysical) RP without any reservoir states, the S and T involved in S-T mixing through the magnetic Hamiltonian $\mathscr{H}_m$ would be degenerate (blue levels). The presence of reservoir states and the virtual transitions they cause from the RP to them (Hamiltonians h_i and h_j) and back (Hamiltonians $h_i^\dagger$ and $h_j^\dagger$) do not only dump the S-T coherence, but they also shift the x-RP states downwards by $\delta\omega_x = k_x w_x/\varepsilon_{0x}$, with $x \equiv S, T$. The resulting S-T energy splitting is $J_{Lamb} = \delta\omega_T - \delta\omega_S$. **(b)** The Lamb shift is due to the asymmetry of the Franck-Condon-averaged density of states $g_x(\varepsilon_x)$ around the finite-lifetime-broadened energy of the x-RP.

coupling Hamiltonian in Section 6.2.1.

If $\mathscr{H}_m$ denotes all magnetic interactions within the radical pair (Zeeman, hyperfine, exchange, dipolar etc.), the RP unperturbed Hamiltonian is $\mathscr{H}_{RP} = c^\dagger c(\varepsilon_S + \mathscr{H}_m)$, where ε_S is the energy gap of the radical pair from the neutral precursor (DA) ground state. The operator c describes the occupation of the acceptor's electron cite, i.e. $c^\dagger c = \mathbb{1}$ means the electron is localized at the acceptor, and $c^\dagger c = 0$ means that the electron has moved back to the donor and hence the RP does not exist ($\mathscr{H}_{RP} = 0$). The sole role of the c operator is to ensure energy conservation for the transitions from the RP state to a reservoir state lying ε_S above the ground state.

6.2.1. SYSTEM-RESERVOIR COUPLING

The spin degrees of freedom of the RP represent the open system under consideration. Since the coupling of the RP to the vibrational reservoir states of the neutral product molecule is spin-selective, the amplitude for the transition to one of the singlet reservoir

states, ${}^{S}D^{\bullet+}A^{\bullet-} \longrightarrow DA_i^*$, is proportional to the singlet character of the RP state. Thus, the RP-reservoir interaction/coupling Hamiltonian reads $\mathcal{V} = \sum_i (h_i + h_i^\dagger)$, where $h_i = u_i a_i^\dagger c Q_S$. This coupling is assumed to be weak, and hence it is treated as a perturbation. The operator Q_S projects the RP spin-state onto the electron-singlet subspace, while the raising operator $a_i^\dagger$ produces a single occupation of the i-th reservoir level. The transition amplitude u_i will be detailed later. The hermitian conjugate $h_i^\dagger$ describes the reverse process, $DA_i^* \longrightarrow {}^{S}D^{\bullet+}A^{\bullet-}$. As has been explained in [26], a *virtual* transition ${}^{S}D^{\bullet+}A^{\bullet-} \longrightarrow DA_i^*$ driven by h_i, followed by the reverse transition $DA_i^* \longrightarrow {}^{S}D^{\bullet+}A^{\bullet-}$ driven by $h_i^\dagger$, produces within *2nd-order perturbation theory* the fundamental S-T decoherence of RPs. We will now show that these virtual transitions also shift the RP energy levels.

6.2.2. TOTAL HAMILTONIAN AND INITIAL STATE

The radical pairs are created at $t = 0$ in the singlet electron state with a practically zero nuclear spin-polarization, equivalently a maximally-mixed nuclear spin-state, hence the initial RP density matrix is $\rho(0) = Q_S / Tr[Q_S]$. The dimension of the RP's density matrix is $d = 4\Pi_{j=1}^{n}(2I_j + 1)$, where 4 is the spin-multiplicity of the two electrons and the rest is the nuclear spin-multiplicity of n magnetic nuclei with spin $I_1, I_2, \ldots, I_n$. The singlet and the triplet projection operators $Q_S = (1/4)\mathbb{1} - \mathbf{s}_1 \cdot \mathbf{s}_2$ and $Q_T = (3/4)\mathbb{1} + \mathbf{s}_1 \cdot \mathbf{s}_2$ are d-dimensional matrices. The initial density matrix $\rho(0) = Q_S / Tr[Q_S]$ is properly normalized ($Tr[\rho(0)] = 1$), and it describes a singlet electronic spin-state ($Tr[\rho(0) Q_S] = 1$) with completely unpolarized nuclear spins, i.e. $Tr[\rho(0) I_{\beta,j}] = 0$ for components $\beta \equiv x, y, z$ of the j-th nuclear spin.

The reservoir states are initially empty (and in the Markovian approximation remain empty throughout the considered evolution), hence the total state of the RP and reservoir is initially $\sigma(0) = \rho(0) \otimes \rho_E(0)$, where $\rho_E(0) = |0\rangle\langle 0|^{\otimes N}$, with N being the number of singlet reservoir states with energy up to ε_S.

The unperturbed Hamiltonian of the total system, i.e. RP plus reservoir, is $\mathcal{H}_0 = c^\dagger c(\varepsilon_S + \mathcal{H}_m) + \mathcal{H}_{res}$, while the interaction Hamiltonian $\mathcal{V}$ is the perturbation, $||\mathcal{V}|| \ll ||\mathcal{H}_0||$. The magnetic Hamiltonian $\mathcal{H}_m$ could have been completely omitted and brought back in at the end of the calculation, as its contribution is the simple unitary evolution $d\rho/dt = -i[\mathcal{H}_m, \rho]$. In [26] the magnetic Hamiltonian was treated as part of the perturbation, again leading to the same result of the ordinary unitary evolution. This is because $\mathcal{H}_m$ effects the state evolution to first order in dt, and indeed if we treat it as a perturbation we retrieve the term $d\rho/dt = -i[\mathcal{H}_m, \rho]$ within $1^{\text{st}}-$order perturbation theory. Decoherence and Lamb shift are derived within $2^{\text{nd}}-$order perturbation theory, but interestingly, they also effect reaction dynamics to first order in dt.

Finally, the perturbation $\mathcal{V}$ can be written as a linear combination of system⊗reservoir operators known as Hilbert-Schmidt decomposition, i.e. $\mathcal{V} = \sum_i S_i \otimes E_i + h.c.$, where $S_i = cQ_S$ independent of i, $E_i = u_i a_i^\dagger$, and $h.c.$ denotes the hermitian conjugate term.

6.2.3. INTERACTION PICTURE DENSITY MATRIX EVOLUTION

In the interaction picture, the quantum states are evolved under the interaction Hamiltonian, whereas the quantum-mechanical operators are evolved under the total unperturbed Hamiltonian. So the perturbation in the interaction picture reads

$$\begin{aligned}\tilde{\mathcal{V}}(t) &= e^{i\mathcal{H}_0 t}\mathcal{V}e^{-i\mathcal{H}_0 t}\\ &= \sum_i u_i \tilde{c}(t)\tilde{Q}_S(t)\otimes\tilde{a}_i^\dagger(t) + h.c.\\ &= \sum_i u_i e^{i(\varepsilon_i-\varepsilon_S)t} c\tilde{Q}_S(t)\otimes a_i^\dagger + h.c. \quad ,\end{aligned}$$

where $\tilde{Q}_S(t) = e^{ic^\dagger c\mathcal{H}_m t}Q_S e^{-ic^\dagger c\mathcal{H}_m t} = e^{i\mathcal{H}_m t}Q_S e^{-i\mathcal{H}_m t}$, since the magnetic interactions $\mathcal{H}_m$ premise that the RP already exists and thus $c^\dagger c = \mathbb{1}$, and because in general $[\mathcal{H}_m, Q_S] \neq 0$, i.e. the electronic singlet state is not an eigenstate of $\mathcal{H}_m$. Moreover, we used the fact that $\tilde{E}_i(t) = e^{i\mathcal{H}_{res}t}E_i e^{-i\mathcal{H}_{res}t} = u_i e^{i\varepsilon_i t}a_i^\dagger$ and $\tilde{c}(t) = e^{i\varepsilon_S t c^\dagger c}ce^{-i\varepsilon_S t c^\dagger c} = e^{-i\varepsilon_S t}c$, since for the fermionic ladder operators $f \equiv c, a$ it holds that: $f^2 = (f^\dagger)^2 = 0$, $(f^\dagger f)^n = f^\dagger f,\ n = 1,2,3,\ldots$ and $\{f, f^\dagger\} = f^\dagger f + ff^\dagger = \mathbb{1}$.

The still exact equation of motion for $\tilde{\sigma}(t)$ is (see Eq. 5.2)

$$\frac{d\tilde{\sigma}(t)}{dt} = -i[\tilde{\mathcal{V}}(t), \sigma(0)] - \int_0^t d\tau [\tilde{\mathcal{V}}(t), [\tilde{\mathcal{V}}(\tau), \tilde{\sigma}(\tau)]] \quad ,$$

where we set $\hbar = 1$. Taking the partial trace over the reservoir degrees of freedom and then performing the Born-Markov approximation (see the derivation of Eq. 5.8 in Section 5.3), we arrive at a Markovian master equation for the RP density matrix ρ in the interaction picture,

$$\frac{d\tilde{\rho}(t)}{dt} = \sum_{ij}\int_0^\infty d\tau \langle E_i(0)\tilde{E}_j^\dagger(\tau)\rangle e^{-i\varepsilon_S\tau}\Big(\tilde{Q}_S(t)\tilde{\rho}(t)\tilde{Q}_S^\dagger(t-\tau) - \tilde{\rho}(t)\tilde{Q}_S^\dagger(t-\tau)\tilde{Q}_S(t)\Big) + h.c. \quad (6.1)$$

where (i) we also traced out the c degrees of freedom, as we are interested in the time evolution of the RP state for which $\langle c^\dagger c\rangle = 1$, (ii) we ignored the first-order term via a reformulation of $\mathcal{H}_{res}$ such that $\langle\tilde{E}_i(t)\rangle = \langle\tilde{E}_i^\dagger(t)\rangle = 0$, and (iii) $\langle A\rangle$ is the expectation value of the reservoir operator A in the state $\rho_E(0)$. In particular, it is $\langle\tilde{a}_i^\dagger(\tau)a_j(0)\rangle = 0$ since the singlet reservoir states are empty, and $\langle a_i(0)\tilde{a}_j^\dagger(\tau)\rangle = \delta_{ij}e^{i\varepsilon_j\tau}$.

Finally, if the eigenvalues and eigenstates of $\mathcal{H}_m$ are denoted by e_l and $|e_l\rangle$, respectively, then $Q_S = \sum_{lm}|lm)$, where $|lm) = \langle e_l|Q_S|e_m\rangle|e_l\rangle\langle e_m|$, hence in the interaction picture it will be $\tilde{Q}_S(t) = \sum_{lm}e^{-i\omega_{lm}t}|lm)$, where $\omega_{lm} = e_m - e_l$. Inserting this into (6.1), we find that

$$\frac{d\tilde{\rho}(t)}{dt} = \sum_i\sum_{lm,pq}\Gamma^i_{lm,pq}\Big(|lm)\tilde{\rho}(t)(pq| - \tilde{\rho}(t)(pq|lm)\Big) + h.c. \quad ,$$

where

$$\Gamma^i_{lm,pq} = |u_i|^2 e^{-i(\omega_{lm}-\omega_{pq})t}\int_0^\infty d\tau e^{i(\varepsilon_i-\varepsilon_S-\omega_{pq})\tau} \quad .$$

6.2.4. MASTER EQUATION FOR UNREACTED RADICAL PAIRS

To go back to the Schrödinger picture, we set $\tilde{\rho}(t) = e^{i\mathscr{H}_m t}\rho(t)e^{-i\mathscr{H}_m t}$ in the left-hand side (LHS) of the previous master equation, and then multiply both sides from the left by $e^{-i\mathscr{H}_m t}$ and from the right by $e^{i\mathscr{H}_m t}$. The LHS will lead to $d\rho/dt + i[\mathscr{H}_m, \rho]$. To evaluate the RHS we note that :

(**i**) since $[\mathscr{H}_m, |lm)] = -\omega_{lm}|lm)$ and $[\mathscr{H}_m, (lm|] = \omega_{lm}(lm|$, we have $e^{-i\mathscr{H}_m t}|lm)\tilde{\rho}(pq|e^{i\mathscr{H}_m t} = e^{i(\omega_{lm}-\omega_{pq})t}|lm)\rho(pq|$,

(**ii**) since $[\mathscr{H}_m, (pq|lm)] = [\mathscr{H}_m, (pq|]\cdot|lm) - (pq|\cdot[\mathscr{H}_m, |lm)] = (\omega_{pq} - \omega_{lm})\cdot(pq|lm)$, and $\sum_{lm,pq}(pq|lm) = Q_S^2 = Q_S$ because Q_S is a projector, it easily follows that $\sum_{lm,pq} e^{-i\mathscr{H}_m t}\tilde{\rho}(pq|lm)e^{i\mathscr{H}_m t} = e^{i(\omega_{lm}-\omega_{pq})t}\rho Q_S$, and

(**iii**) in the integral over τ in the expression for $\Gamma^i_{lm,pq}$ we omit $\omega_{pq}\tau$ in the phasor, since $\omega_{pq} \ll \varepsilon_i - \varepsilon_S$. Let us explain this: obviously $\varepsilon_S \gg \omega_{pq}$, where ω_{pq} is a typical frequency scale of $\mathscr{H}_m$, since $\varepsilon_S \approx 1$ eV $\approx 10^{14}$ Hz is of electrostatic origin, whereas $\omega_{pq} \approx 10^7$ Hz is determined by typical hyperfine couplings of about 10 Gauss. The frequency ω_{pq} is also much smaller than $\varepsilon_i - \varepsilon_S$, since the latter is on the order of the detuning $\Delta = \varepsilon - \varepsilon_S$, which is on the order of the singlet recombination rate $k_S \approx 10^9$ s^{-1} or even higher.

In doing so, the master equation becomes

$$\frac{d\rho(t)}{dt} + i[\mathscr{H}_m, \rho(t)] = \Gamma\big(Q_S\rho(t)Q_S - \rho(t)Q_S\big) + h.c. \quad , \tag{6.2}$$

where $\Gamma = \sum_j \Gamma_j$ and $\Gamma_j = |u_j|^2 \int_0^\infty d\tau e^{i(\varepsilon_j - \varepsilon_S)\tau}$.

The tunneling amplitude u_j is composed of an electronic matrix element, v_j, and a nuclear vibrational overlap integral, χ_j, between the wavefunctions of the j-th reservoir state and the state of the RP, $u_j = v_j\chi_j$ [81]. We consider the former to be independent of j in the vicinity of ϵ_S, i.e. $v_j = v$, and introduce the *Franck-Condon-averaged density of states* $g_S(\varepsilon) = |\chi(\varepsilon)|^2 d(\varepsilon)$, which takes into account both $\chi(\varepsilon)$, the nuclear wavefunction overlap integral, and $d(\varepsilon)$, the density of vibrational states at the energy ε. The discrete sum $\sum_j \Gamma_j$ is thus approximated by the integral $|v|^2 \int d\varepsilon g_S(\varepsilon) \int_0^\infty d\tau e^{i(\varepsilon-\varepsilon_S)\tau}$. Introducing the detuning $\Delta = \varepsilon - \varepsilon_S$, the complex coefficient becomes

$$\Gamma = |v|^2 \int d\Delta\ g_S(\Delta + \varepsilon_S) \int_0^\infty d\tau e^{i\Delta\tau} \quad .$$

Noting then the well-known relation for the Fourier transform of the *Heaviside* (unit step) function $H(t) = {}^{1,\ t\geq 0}_{0,\ t<0}$,

$$\int_{-\infty}^{\infty} e^{-i\omega t} H(t) dt = \int_0^\infty e^{-i\omega t} dt = \pi\delta(\omega) - i\mathbb{P}\frac{1}{\omega} \quad ,$$

we find

$$\Gamma \equiv \gamma_R - i\gamma_I = |v|^2 \int d\Delta \Big(\pi\delta(\Delta) - i\mathbb{P}\frac{1}{\Delta}\Big) g_S(\Delta + \varepsilon_S) \quad . \tag{6.3}$$

6.3. LAMB SHIFT IN RADICAL-ION PAIRS IS PHYSICALLY EQUIVALENT TO A SPIN-EXCHANGE INTERACTION

When the real part of (6.3) is inserted into (6.2), we will arrive at the Lindblad description of S-T decoherence already discussed in [26]. Using the imaginary part of (6.3) in (6.2) leads to the Lamb shift Hamiltonian. Before proceeding to the latter, we note that the real part of (6.3), considering the well-known property of the Dirac delta function $\int dx\delta(x)f(x) = f(0)$, is $\gamma_R = \pi|v|^2 g_S(\varepsilon_S)$ and is nothing else than the half singlet recombination rate, $k_S/2$. Indeed, recombination of RPs proceeds within $1^{\text{st}}-$order perturbation theory by a *real* transition to a reservoir state, followed by another real transition (decay) of the reservoir state to the ground state of the neutral product DA. The latter happens very fast, e.g. at picoseconds, so the rate limiting process is the former. Using *Fermi's golden rule*, we immediately find that the recombination rate will be $k_S = 2\pi|\langle f|\mathcal{V}|i\rangle|^2 d(\varepsilon_S) = 2\pi|v|^2 g_S(\varepsilon_S) = 2\gamma_R$, where as initial state $|i\rangle$ we chose a pure singlet state of the RP, e.g. $|S\Uparrow\rangle$, and as a final state $|f\rangle$ one among the near-resonant and quasi-continuum reservoir states described by the density of states $d(\varepsilon_S)$.

In order to find the imaginary part $\gamma_I = |v|^2 \int d\Delta\, \mathbb{P}(1/\Delta) g_S(\Delta+\varepsilon_S)$, we expand $g_S(\Delta+\varepsilon_S) \approx g_S(\varepsilon_S) + g'_S(\varepsilon_S)\Delta$. The Δ-integration range is determined by the RP's energy uncertainty. Since the singlet RP has a finite lifetime τ_S, its energy level will be broadened by $w_S \approx 1/\tau_S$ according to the Heisenberg's energy-time 'uncertainty'. Since $\mathbb{P}(1/\Delta)$ is an odd function of Δ, only the second term of the integral $\gamma_I \approx |v|^2 g_S(\varepsilon_S)\int d\Delta\, \mathbb{P}(1/\Delta) + |v|^2 g'_S(\varepsilon_S)\int d\Delta\, \mathbb{P}(1/\Delta)\Delta$ will survive, and the result will be $\gamma_I = |v|^2 g'_S(\varepsilon_S) w_S$. Putting everything together (also using the hermitian conjugate term in (6.2)) and repeating the above calculation for the triplet reservoir states, we find that the density matrix of the unreacted/non-recombining RPs evolves according to

$$\frac{d\rho(t)}{dt} = -i[\mathcal{H}_m + \delta\mathcal{H}_{Lamb}, \rho(t)] + \mathcal{L}\rho(t) \quad .$$

This equation is known from quantum optics as a 'null' measurement and describes the null measurement of RP recombination products. The Lamb shift Hamiltonian reads

$$\delta\mathcal{H}_{Lamb} = \delta\omega_S Q_S + \delta\omega_T Q_T \quad , \tag{6.4}$$

with

$$\delta\omega_x = \frac{1}{2\pi}\frac{g'_x(\varepsilon_x)}{g_x(\varepsilon_x)} k_x w_x \quad , \quad x \equiv S, T \quad . \tag{6.5}$$

For completeness, we reiterate that

$$\begin{aligned}\mathcal{L}\rho(t) &= -\frac{k_S}{2}\Big(Q_S\rho(t) + \rho(t)Q_S - 2Q_S\rho(t)Q_S\Big) - \frac{k_T}{2}\Big(Q_T\rho(t) + \rho(t)Q_T - 2Q_T\rho(t)Q_T\Big) \\ &= -\frac{k_S + k_T}{2}\Big(Q_S\rho(t) + \rho(t)Q_S - 2Q_S\rho(t)Q_S\Big)\end{aligned}$$

is the aforementioned S-T dephasing Lindblad term, the foundamental source of S-T decoherence [26].

The physical interpretation of $\delta\mathscr{H}_{Lamb}$ is based on these two points :

(**i**) the RP singlet and triplet energy levels acquire a broadening w_S and w_T, respectively, due to their finite lifetime, and

(**ii**) the Franck-Condon-averaged density of states $g(\varepsilon)$ (for simplicity we will henceforth omit the S or T index of the function g and its argument ε) has a steep ε-dependence, in fact $dg(\varepsilon)/d\varepsilon < 0$ [82, 83]. Hence, when the RP makes a *virtual* transition to a reservoir level, it momentarily acquires an energy which is smaller, on average, than the 'bare' RP energy. The physical energy levels of the singlet and triplet RP are thus shifted downwards by $\delta\omega_S$ and $\delta\omega_T$, respectively, compared to the 'bare' RP having no reservoir states (see Fig. 6.1).

In the general case when $\delta\omega_S \neq \delta\omega_T$, the Lamb shift will lead to an S-T *energy splitting*, as if there was an exchange coupling of the form $J\mathbf{s}_1 \cdot \mathbf{s}_2$, which is known to produce an S-T energy splitting of J, specifically the triplet being higher in energy for $J > 0$. In other words, the *differential Lamb shift* of singlet and triplet RP states, which is inherent in the RP due to the interaction with its intra-molecule vibrational reservoir, would physically look as an exchange interaction having $J_{Lamb} = \delta\omega_T - \delta\omega_S$. Put differently, if an exchange interaction with coupling J actually exists in the RP, then the physically observed S-T energy splitting will not be J, but $J' = J + J_{Lamb}$.

The sign of J_{Lamb} is determined by the sign of $\delta\omega_T$ and $\delta\omega_S$ and their relative size. Since $g'(\varepsilon) < 0$, it is $\delta\omega_S = -|\delta\omega_S| < 0$ and $\delta\omega_T = -|\delta\omega_T| < 0$. Therefore the sign of J_{Lamb} will be the sign of $|\delta\omega_S| - |\delta\omega_T|$. How large is $|J_{Lamb}|$ in realistic cases? To this end, we have to first evaluate the typical value of $g'(\varepsilon)/g(\varepsilon)$. It is known that $g(\varepsilon)$ can be locally approximated [82, 83] by an exponential, $g(\varepsilon) \propto e^{-\varepsilon/\varepsilon_0}$, where $\varepsilon_0 \approx$ 200-700 cm$^{-1} \approx 10^{13}$ Hz, hence $|g'(\varepsilon)/g(\varepsilon)| \approx 1/\varepsilon_0 \approx 0.1$ ps. Thus, apart from the constants of order unity, the absolute shifts will be of order

$$|\delta\omega| \approx \frac{kw}{\varepsilon_0} \quad . \tag{6.6}$$

For isolated RPs, the singlet and triplet lifetimes are determined by the spin-selective charge-recombination rates, i.e. $w = k$, hence $|\delta\omega| \approx k^2/\varepsilon_0$. For a typical recombination rate of $k \approx 10^9$ s^{-1} it follows that $|\delta\omega| \approx 10^5$ s^{-1}, which, expressed in magnetic-field units, is $|\delta\omega| \approx 5$ mGauss, that is two order of magnitudes smaller than the geomagnetic field. The splitting J_{Lamb}, which will result if $k_S \neq k_T$ and/or $\varepsilon_{0S} \neq \varepsilon_{0T}$ will be of the same order. Although small, such splittings can produce interesting low-field level-crossing effects to be addressed elsewhere.

6.4. RADICAL-ION-PAIR LAMB SHIFT IN PHOTOSYNTHETIC REACTION CENTERS

The considered effect becomes much larger for RPs participating in the charge-separation pathway in PRCs as shown in Fig. 6.2. PRCs exhibit a cascade of electron-transfer steps until the stable charge-separated state is produced. In each of those steps a different RP is formed and its inverse lifetimes w_S and w_T are also influenced, and in cases dominated by the electron-transfer rates to the following step. For example, the lifetime of the singlet RP, ${}^{S}P^{\bullet+}A_0^{\bullet-}A_1$ shown in Fig. 6.2, is not dominated by the singlet or triplet recombination time of about 10 ns and 1 ns, respectively, but by the electron transfer to the next-stage RP, ${}^{S}P^{\bullet+}A_0A_1^{\bullet-}$, taking place in about $w^{-1} \approx 50$ ps. In this case, there will be two different shifts, one stemming from reservoir states of the singlet and triplet neutral products PA_0A_1 and ${}^{T}PA_0A_1$, respectively, and one stemming from the reservoir states of the next-stage RP, ${}^{S}P^{\bullet+}A_0A_1^{\bullet-}$. For the former it will be $|\delta\omega_x| \approx k_x w/\varepsilon_0$, where we took $\varepsilon_{0S} \approx \varepsilon_{0T} \approx \varepsilon_0 \approx 10$ THz. Since $k_T \gg k_S$, it will be $|\delta\omega_T| \gg |\delta\omega_S|$ and $J_{Lamb} \approx -|\delta\omega_T| \approx -0.1$ Gauss. For the latter the shifts will be on the order of $\delta\omega \approx -w^2/\varepsilon_0 \approx -2$ Gauss, which is a significant shift (about 4 times the geomagnetic field). Since the electron-transfer rate to the next-stage RP is *not* spin-dependent ($w_S = w_T = w$), it would appear that both the singlet and triplet RPs would be shifted by $\delta\omega$. However, the interplay of these shifts with PRC dynamics is more involved and will be explored elsewhere.

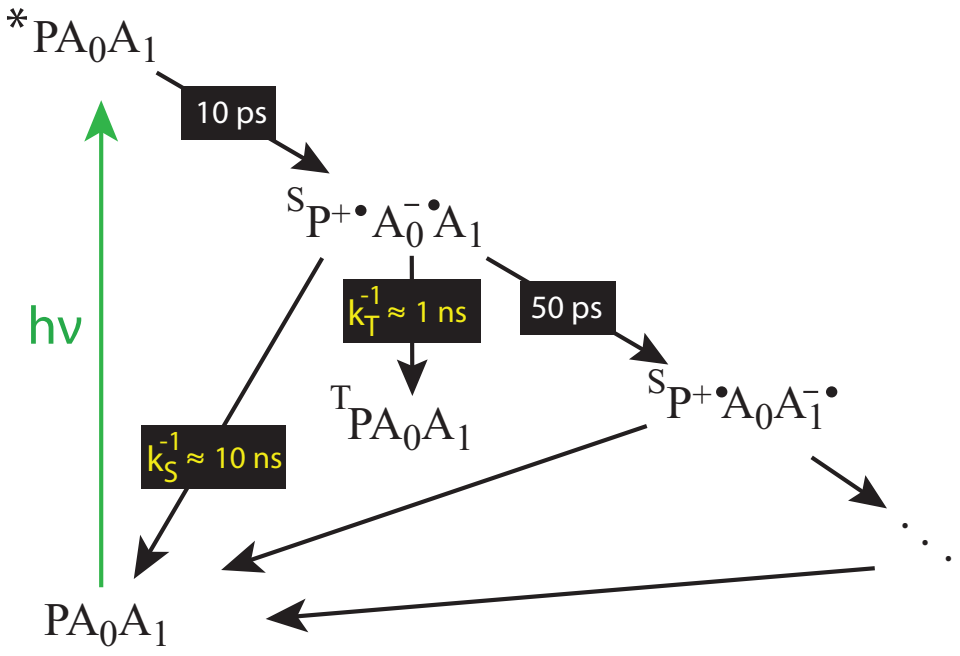

Figure 6.2: First stages of charge separation in the photosynthetic reaction center (PRC) of Photosystem I [84]. The goal of the PRC is to efficiently create the final charge-separated state (after the dots in the lower part of the figure) starting from the photo-excited ${}^{*}PA_0A_1$ and going through a series of electron transfers to intermediate radical-ion pairs. P (primary donor) and A_0 (transient initial acceptor) are chlorophyll molecules and A_1 (transient initial acceptor) is phylloquinone. The lifetime of the intermediate radical-ion pair ${}^{S}P^{\bullet+}A_0^{\bullet-}A_1$ is not dominated by the recombination rates k_S and k_T, but by the much faster electron transfer (50 ps timescale) to the following charge-separated state ${}^{S}P^{\bullet+}A_0A_1^{\bullet-}$.

6.5. DISCUSSION-CONCLUSIONS

We finally comment on our perturbative derivation of the Lamb shift Hamiltonian. In the application of the Lamb shift expression (6.5) in PRCs, we used as input the short RP lifetime $w^{-1} \approx 50$ ps, so the use of $\mathcal{V}$ as a perturbation might appear questionable. In other words, the relevant rate $w \approx 10^{10}$ Hz related to the perturbation $\mathcal{V}$ is much larger than the typical frequency scale $\omega \approx 10^7$ Hz of the unperturbed magnetic Hamiltonian $\mathscr{H}_m$. To alleviate such a concern, we first note that there is a similar example in NMR [85], where spin-lattice relaxation theory is equally applicable at low magnetic fields, where the typical Larmor frequency is smaller than the relaxation rate. We secondly note that the calculated magnitude of the shift is of the same order as $||\mathscr{H}_m||$, so at least the use of perturbation theory produces a consistent result. Finally, the actual reason why our perturbative treatment does not pose a problem is that the high reaction rate w strongly depends on the high density of states of the reservoir, i.e. each individual term in the expansion $\mathcal{V} = \sum_i S_i \otimes E_i$ can indeed be considered and treated as a perturbation, while the final rates depend on the combined action of all those terms. Indeed, one of the main starting assumptions of all calculations, such as the one presented in [82] (see, e.g., Eq. (II.1) of [82]), is that the number of reservoir states within the lifetime-broadened width w of the RP is much larger than one. This is expected since the energy gap ε_S relevant for the reservoir density of states is about two orders of magnitude higher than the typical vibrational frequency.

Concluding, we have analyzed the complete effect of the continuous quantum measurement taking place in RPs as a result of their coupling to the intra-molecule vibrational reservoir. Besides the spin decoherence that was described in our earlier work, we here considered the shift this quantum measurement brings about to the RP energy levels. This shift can have non-negligible values in photosynthetic reaction centers. Since this shift is equivalent to an exchange interaction, which is known to suppress singlet-triplet mixing and thus directly affect RP spin dynamics, it will be interesting to examine the effect of such shifts in the dynamics of PRCs.

III

Quantum Metrology in Radical-Pair Magnetometers

7

QUANTUM METROLOGY & PARAMETER ESTIMATION

7.1. INTRODUCTION

The estimation of parameters characterizing dynamical processes is a central problem in science and technology. It is an essential part of the scientific analysis of experimental data playing an important role at a very basic level, which involves, for instance, the measurement of fundamental constants of Nature, or yet the evaluation of : the duration of some interaction, the value of a coupling constant, a transition frequency in atomic spectroscopy, a phase shift in optical interferometry etc.

Detailed techniques for parameter estimation are dated back to the work of Fisher [86], Cramér [87], and Rao [88] that allowed the characterization of the achievable limits in the precision of estimation. In classical parameter estimation, the estimation error scales as $1/\sqrt{\nu}$, where ν is the number of experiments (experimental repetitions/rounds of measurements). The estimation error also depends on the number N of resources employed in each experiment, e.g. the number of probes or the probing energy, and for independent/uncorrelated/non-entangled probes it scales as $1/\sqrt{\nu N}$. This is the so-called *standard quantum limit* (SQL), a consequence of the central-limit theorem, that characterizes the precision limit of quantum measurements in the presence of the shot-noise. Quantum strategies, using 'quantum tricks' such as entangled or squeezed states which correspond to distinctive resources of quantum mechanics, may improve the estimation precision, for noiseless processes, by an extra factor $1/\sqrt{N}$, leading to the so-called *Heisenberg limit*. This is a more fundamental imprecision of quantum measurements that originates from the Heisenberg uncertainty principle due to the probabilistic nature of quantum measurements, implying an improvement of $1/\sqrt{N}$ over the SQL. An important question is if and when this improvement can be achieved in the case of noisy processes [89].

The basic steps for parameter estimation are presented in Fig. 7.1. A probe, prepared in a known initial configuration, is sent through the parameter-dependent process to be investigated, and then the final parameter-dependent configuration of the probe is measured

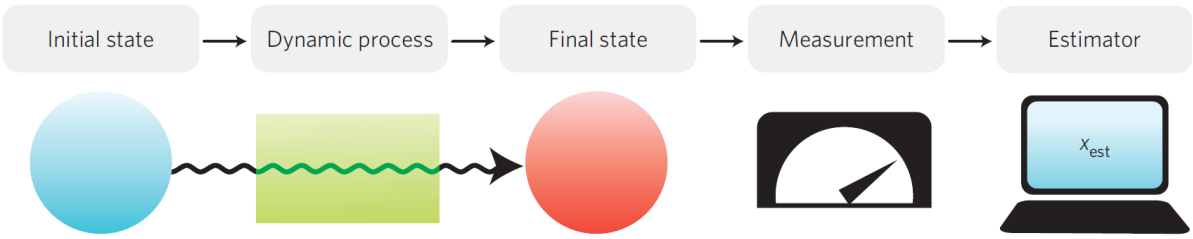

Figure 7.1: General setup for parameter estimation: (1) preparation of the probe in a known initial state, (2) evolution of the probe through a parameter-dependent dynamical process, which in general could be unitary or noisy, (3) measurement of the final parameterized probe, (4) the outcome of this measurement is used to estimate the value of the parameter through an estimation strategy (estimator). Picture reproduced from [90].

(using a measurement strategy). Since the measurement results depend on the parameter, they can be used as sample data to estimate the value of the parameter (through an estimation strategy).

Realistic experimental data are never ideal/perfect, since they have statistical uncertainties due to external perturbations, intrinsic fluctuations, or imperfect detectors. Therefore, it is not possible to unambiguously associate an experimental result (through an estimation) with the true value of the parameter under consideration. The error in an estimation may be quantified by the square root of the statistical average of the square of the difference between the estimated and the true value of the parameter, briefly *root-mean-square error* (RMSE). This error is lower bounded by the so-called *Cramér-Rao bound/limit*, which characterizes how well a parameter can be estimated from a probability distribution and it is inversely proportional to $\sqrt{\nu}$. In single-parameter estimation, the Cramér-Rao bound is expressed in terms of a quantity known as *Fisher Information*[1], to be defined later: the larger the Fisher information, the more accurate can the estimation be.

The Fisher information may be considered as a measure of the maximum amount of information that can be extracted from experiments about the true value of an unknown parameter. This quantifier of information depends on properties of the probe, the parameter-dependent process, and the measurement of the probe used to investigate the process. An important aim of metrology is to calculate the Fisher Information, to find ways to maximize it, and to find protocols that allow for better estimation.

Quantum Metrology [91–94] is rooted in the theory of quantum estimation that was pioneered by Helstrom [95] and Holevo [96], who proposed the parameter-based uncertainty relation. Thus, quantum metrology also deals with parameter estimation, but takes into account the quantum character of the systems and processes involved. The estimation error is again limited by the Cramér-Rao bound [97, 98], expressed in terms of the Fisher Information, which now considers also the constraints imposed by quantum physics, such as its intrinsic probabilistic nature, the dependence of the result on the measurement scheme, and the more restricted set of possible measurements. The complexity of quantum metrol-

[1]Ronald A. Fisher (1890–1962) was an English statistician and biologist whose work is not well-known to physicists. He is renowned in the fields of genetics, statistics, and eugenics. Among his pivotal contributions to these fields (Fisher, 1959) are the maximum likelihood estimate, the analysis of variance, and a quality metric of parameter estimation procedure now called 'Fisher information'.

ogy comes from the many different choices of the measurement strategies or POVMs allowed by quantum mechanics; different measurement schemes result in different precisions of the estimation results. Hence, one of the main purposes of quantum metrology is to increase the estimation precision by optimizing the measurement basis or POVM.

The so-called *Quantum Fisher Information* (QFI) is defined by maximizing the Fisher information over all possible measurement strategies allowed by quantum mechanics [97]. It characterizes the maximum amount of information that can be extracted from quantum experiments about an unknown parameter using the best (and ideal) measurement device. It establishes the best precision that can be attained with a given quantum probe.

Further maximization of the QFI over all initial states of the probe leads to the ultimate precision in quantum parameter estimation. For isolated systems, useful analytic results allow the calculation of this ultimate bound. Quantum strategies, involving nonclassical characteristics of the probes, like entanglement and squeezing, lead to much better bounds, as compared with standard approaches that do not profit from these properties [91]. Consider, as an example, the determination of a phase as a function of the photon number N in optical interferometry. It scales as $1/\sqrt{N}$ for non-entangled photons, whereas N-photon entangled states result in a scaling proportional to $1/N$, i.e. a better resolution for the same amount of resources.

The quantum theory of parameter estimation allows a useful complementation of the Heisenberg inequalities, associated with Hermitian operators and their canonical conjugates. Quantum metrology leads to inequalities involving parameters and operators, instead of just operators, thus allowing a precise formulation of, e.g., the phase-number uncertainty relation.

Given the importance of precision measurement in different fields of physics and engineering, the QFI has attracted great scientific interest. This stimulated the emergence of quantum metrology, which has been applied to different quantum systems to raise the precision of measurements, and to provide a route to overcome practical limits in sensing devices. Therefore, many applications of quantum metrology have been found, including quantum frequency standards, optical phase estimation, atomic clocks, atomic interferometers, quantum imaging, and quantum-enhanced position and clock synchronization. The QFI has also been studied in open systems, along with growing research on protocols assisted by error correction, or yet quantum feedback [99].

To finish the introduction, in quantum metrology an even greater range of applications arise from the ability to not just understand, but to engineer coherence and correlations at the quantum level. In the past few years, quite dramatic progress has been seen in applying these ideas into biological systems, where sensitivity and resolution constraints restrict applications both in fundamental biophysics and in medicine. For a review of the application of quantum metrology in biology, we refer the interested reader to [100].

7.2. PARAMETER ESTIMATION: CRAMÉR-RAO BOUND

The general parameter estimation scheme depicted in Fig. 7.1, opts to estimate the value of a parameter x from a set of data that depend on the parameter. Since there are different estimation strategies (estimators), e.g. method of moments, maximum likelihood estimation (MLE) etc., which lead to different estimation precisions, a convinient merit quantifier of the performance of an estimator is the RMSE,

$$\mathscr{E} \equiv \sqrt{\langle (x_{est} - x_{true})^2 \rangle} \tag{7.1}$$

where x_{est} is the estimated value of the parameter for a possible measurement result, x_{true} is the true value of the parameter, and the brackets denote the statistical average taken over all measurement results.

For unbiased estimators, i.e. $\langle x_{est} \rangle_x = x_{true}$, Cramér and Rao found that

$$\mathscr{E} \geq \frac{1}{\sqrt{\nu F(x_{true})}} \tag{7.2}$$

where $F(x)$ is the Fisher information about the parameter x. For a continuum set of measurement results, the Fisher information is given by

$$F(x) \equiv \int d\chi\, p(\chi|x) \Big(\partial_x ln[p(\chi|x)]\Big)^2 = \int d\chi \frac{1}{p(\chi|x)} \Big(\partial_x p(\chi|x)\Big)^2 \tag{7.3}$$

where $p(\chi|x)d\chi$ is the probability of finding the measurement outcome between χ and $\chi + d\chi$, and $\partial_x \equiv \partial/\partial x$. In statistics, the quantity $\partial_x ln[p(\chi|x)]$ is known as the *score* or *informant*, that is the gradient of the (natural) logarithm of the likelihood function (the log-likelihood) with respect to some parameter. The score indicates how sensitive is a likelihood function to its parameter. Hence, one can safely say that the Fisher information is the variance of the score. For a discrete set of data, we have

$$F(x) \equiv \sum_k p_k(x) \Big(\partial_x ln[p_k(x)]\Big)^2 \tag{7.4}$$

where $p_k(x)$ is the probability of getting an experimental result k given that the parameter is x.

At this point, we are going to derive the Cramér-Rao bound (7.2) which is a cornerstone of the parameter estimation theory. The aim is the estimation of a real, single or multivariate, continuous or discrete parameter x. Particularly, we consider a single continuous parameter, and ν identical and independent experiments.

Let $\chi_1, \chi_2, \ldots, \chi_\nu$ be a set of the ν measurement outcomes which obey the probability density function $p(\chi|x)$, called the 'likelihood law', to have the outcome χ given that the parameter is x. More intuitively, the $p(\chi|x)$ describes the fluctuations in data values χ in the presence of the parameter value x. We estimate x by using a certain estimator

$$x_{est} = x_{est}(\chi_1, \chi_2, \ldots, \chi_\nu) \tag{7.5}$$

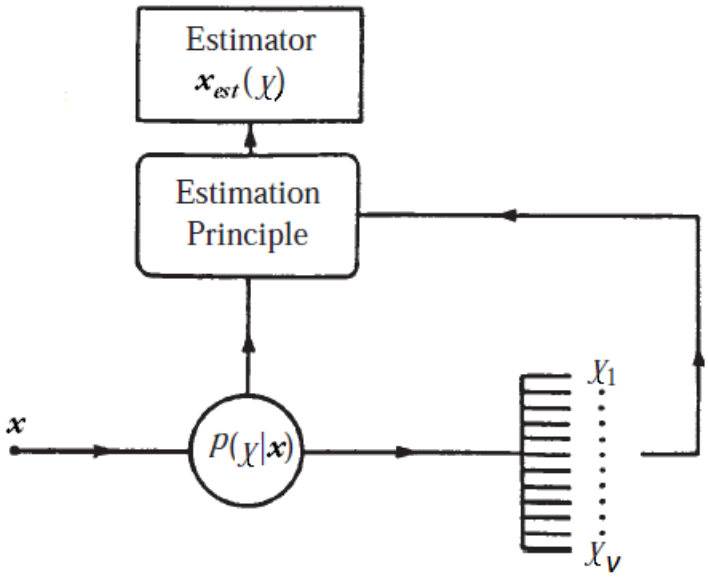

Figure 7.2: The parameter estimation problem of classical statistics. An unknown but fixed parameter value x causes intrinsic data $\{\chi_1,\ldots,\chi_\nu\}$ through random sampling of a likelihood law $P(\chi|x)$. Then, the likelihood law and the data are used to form the estimator $x_{est}(\chi)$ via an estimation principle. The scheme is a modified version of Fig.1.1 in [101].

which is constructed from the set of the ν measurement data with an appropriate algorithm (Fig. 7.2). It is noted that the estimator x_{est} does not depend on the unknown parameter x.

We then define the deviation $\Delta x_{est} \equiv x_{est} - \langle x_{est}\rangle_x$, where the index x implies that the average value of the estimation (averaged estimate) depends on x, which satisfies the following identity

$$\int d\chi_1 \ldots d\chi_\nu P(\chi_1,\ldots,\chi_\nu|x)\Delta x_{est} = 0 \tag{7.6}$$

where $P(\chi_1,\ldots,\chi_\nu|x) = p(\chi_1|x)\ldots p(\chi_\nu|x)$ is the joint probability density that ν independent measurements of the parameter x lead to the outcomes $\chi_1,\ldots,\chi_\nu$. Due to normalization, it must satisfies $\int d\chi_1 \ldots d\chi_\nu P(\chi_1,\ldots,\chi_\nu|x) = 1$. Since

$$\int d\chi_1 \ldots d\chi_\nu P(\chi_1,\ldots,\chi_\nu|x) x_{est} = \langle x_{est}\rangle_x \quad , \tag{7.7}$$

the equation (7.6) is obviously valid.

Taking the derivative of both sides of (7.6) with respect to x, we have

$$\frac{d\langle x_{est}\rangle_x}{dx} = \int d\chi_1 \ldots d\chi_\nu \Big(\sum_{n=1}^{\nu} \frac{p(\chi_1|x)\ldots p(\chi_\nu|x)}{p(\chi_n|x)} \partial_x p(\chi_n|x) \Big) \Delta x_{est}(\chi_1,\ldots,\chi_\nu) \tag{7.8}$$

$$= \int d\chi_1 \ldots d\chi_\nu p(\chi_1|x)\ldots p(\chi_\nu|x) \Big(\sum_{n=1}^{\nu} \partial_x ln[p(\chi_n|x)] \Big) \Delta x_{est}(\chi_1,\ldots,\chi_\nu) \tag{7.9}$$

$$= \int d\chi_1 \ldots d\chi_\nu P(\chi_1,\ldots,\chi_\nu|x) \Big(\sum_{n=1}^{\nu} \partial_x ln[p(\chi_n|x)] \Big) \Delta x_{est}(\chi_1,\ldots,\chi_\nu) \tag{7.10}$$

where the right-hand side (RHS) of (7.10) can be regarded as a scalar product between the vectors $\{\partial_x ln[p(\chi_1|x)],\ldots,\partial_x ln[p(\chi_\nu|x)]\}$ and $\{\Delta x_{est},\ldots,\Delta x_{est}\}$, with the joint probability $P(\chi_1,\ldots,\chi_\nu|x)$ to be the measure. Applying the *Schwarz inequality* to this scalar product, we get

$$\Big(\frac{d\langle x_{est}\rangle_x}{dx}\Big)^2 \leq \langle(\Delta x_{est})^2\rangle \int d\chi_1\ldots d\chi_\nu p(\chi_1|x)\ldots p(\chi_\nu|x)\Big(\sum_{n=1}^{\nu}\partial_x ln[p(\chi_n|x)]\Big)^2 \tag{7.11}$$

which reduces to

$$\Big(\frac{d\langle x_{est}\rangle_x}{dx}\Big)^2 \leq \langle(\Delta x_{est})^2\rangle \int d\chi_1\ldots d\chi_\nu p(\chi_1|x)\ldots p(\chi_\nu|x)\sum_{n=1}^{\nu}\Big(\partial_x ln[p(\chi_n|x)]\Big)^2 \tag{7.12}$$

$$= \langle(\Delta x_{est})^2\rangle \sum_{n=1}^{\nu}\int d\chi_1\ldots d\chi_\nu p(\chi_1|x)\ldots p(\chi_\nu|x)\Big(\partial_x ln[p(\chi_n|x)]\Big)^2 \tag{7.13}$$

since the cross terms in the squared sum in the integrand of (7.11) vanish due to the fact that $\int d\chi_j p(\chi_j|x)\partial_x ln[p(\chi_j|x)] = \int d\chi_j \partial_x p(\chi_j|x) = \partial_x \int d\chi_j p(\chi_j|x) = 0$.

Inequality (7.13) can be further simplified to

$$\Big(\frac{d\langle x_{est}\rangle_x}{dx}\Big)^2 \leq \langle(\Delta x_{est})^2\rangle \sum_{n=1}^{\nu}\int d\chi_n p(\chi_n|x)\Big(\partial_x ln[p(\chi_n|x)]\Big)^2 \tag{7.14}$$

$$= \langle(\Delta x_{est})^2\rangle \sum_{n=1}^{\nu} F(x) \tag{7.15}$$

$$= \langle(\Delta x_{est})^2\rangle \nu F(x) \quad \Rightarrow \tag{7.16}$$

$$\frac{\langle(\Delta x_{est})^2\rangle}{(d\langle x_{est}\rangle_x/dx)^2} \geq \frac{1}{\nu F(x)} \tag{7.17}$$

since in (7.13) it is $\int d\chi_j p(\chi_j|x) = 1$ for $j = 1,\ldots,n-1,n+1,\ldots,\nu$, and the Fisher information $F(x)$ does not depend on ν. The inequality (7.17) is still somewhat distant from (7.2), because Δx_{est} is the deviation of the estimator from the average value of the estimation, and not from the real value of the parameter as we want.

Braunstein and Caves [97] introduced the *estimation error*

$$\delta x \equiv \frac{x_{est}}{|d\langle x_{est}\rangle_x/dx|} - x \quad , \tag{7.18}$$

which takes into account both the estimator's systematic bias away from the parameter, and the (local) difference in units between the estimator and the parameter through the denominator $|d\langle x_{est}\rangle_x/dx|$. In other words, the denominator corrects the units and punishes wild guesses about the true value of the unknown parameter [89]. The quantity (7.18) is one of the most important benchmarks of an estimation strategy.

We next square and average both sides of (7.18). After some algebra, we find that

$$\langle(\delta x)^2\rangle = \frac{\langle(\Delta x_{est})^2\rangle}{(d\langle x_{est}\rangle_x/dx)^2} + \langle\delta x\rangle^2 \tag{7.19}$$

and taking into account the inequality (7.17), we end up with

$$\langle(\delta x)^2\rangle \geq \frac{1}{\nu F(x)} + \langle\delta x\rangle^2 \quad . \tag{7.20}$$

The second term on the RHS of the above inequality characterizes the bias of the estimator. When $\langle\delta x\rangle$ is non-zero, the (units-corrected) estimator has a systematic bias away from the parameter. In the case of unbiased estimator, i.e. $\langle x_{est}\rangle_x = x$, then $\langle\delta x\rangle = 0$. Moreover, $d\langle x_{est}\rangle_x / dx = 1$ and, therefore, the inequality (7.20) becomes

$$\langle(\delta x)^2\rangle = \langle(\Delta x_{est})^2\rangle = \langle(x_{est} - x)^2\rangle \geq \frac{1}{\nu F(x)} \quad . \tag{7.21}$$

For $x = x_{true}$ and taking the square root of the above inequality, we get the Cramér-Rao bound for unbiased estimators (7.2). The optimal estimator leads to the achievability/tightness/saturation of the Cramér-Rao inequality, i.e. the inequality becomes equality. Such an estimator is the aforementioned MLE which is unbiased and efficient. This case is addressed by the *Fisher's theorem* : For $\nu \to \infty$, the Cramér-Rao bound can be saturated asymptotically via the MLE strategy and the estimation result is unbiased, that is

$$\sqrt{\langle(\delta x)^2\rangle} = \mathscr{E} = \frac{1}{\sqrt{\nu F(x_{true})}} \quad . \tag{7.22}$$

Because of this property, MLE has been widely adopted in parameter estimation protocols.

7.3. QUANTUM PARAMETER ESTIMATION

Braunstein and Caves [97] provided an important contribution to the generalization of the problem of parameter estimation in the quantum framework, namely the association of the estimation accuracy to the fundamental concept of the distinguishability between two quantum states. Their approach maps the problem of state distinguishability onto that of precision determination of a parameter.

Consider an example from optical interferometry, in particular the Mach-Zehnder interferometer schematically depicted in Fig. 7.3. It consists of a beam splitter, two sets of mirrors and, between them, a sample which introduces a phase shift θ in one of the arms of the interferometer; in our case the upper one. This displacement θ is estimated from the measurement outcome.

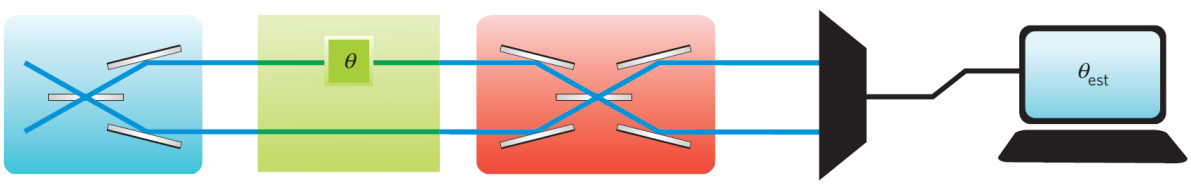

Figure 7.3: Mach-Zehnder interferometer setup for estimating a phase shift θ. Picture reproduced from [90].

When uncorrelated, i.e. non-entangled, photons (e.g. in a coherent state) are sent through the interferometer, the θ-estimation precision is shot-noise-limited, obtaining the SQL scaling

$$\delta\theta \sim \frac{1}{\sqrt{\nu\langle\mathcal{N}\rangle}} \quad , \tag{7.23}$$

where $\langle\mathcal{N}\rangle$ is the average number of photons in the field. The interpretation of (7.23) is relatively easy if the phase is probed with coherent states. Suppose that there is no phase shift when a coherent state is sent through an arm of the interferometer, and then there is a phase fluctuation $\delta\theta$, after which a second coherent state is sent through the same arm. Thus, the second coherent state will acquire a phase shift $\delta\theta$ compared to the first one. If the second coherent state, $|ae^{i\delta\theta}\rangle$, is distinguishable from the first one, $|a\rangle$, the detection of this phase variation will be feasible. Instead, the detection may be impossible when the two states overlap strongly, i.e. $|\langle a|ae^{i\delta\theta}\rangle|^2 \simeq 1$, thus they become indistinguishable. Hence, the detection of the phase displacement $\delta\theta$ is equivalent to the discrimination between the quantum states $|a\rangle$ and $|ae^{i\delta\theta}\rangle$.

For small $\delta\theta$, the overlap/fidelity between the two states can be approximated by [89]

$$|\langle a|ae^{i\delta\theta}\rangle|^2 = e^{-|a(1-e^{i\delta\theta})|^2} \approx e^{-\langle\mathcal{N}\rangle(\delta\theta)^2} \quad , \tag{7.24}$$

which is small when $\langle\mathcal{N}\rangle(\delta\theta)^2 \sim 1$, in agreement with (7.23). However, the RHS of (7.23) is not an absolute lower bound. Smaller uncertainties result when correlated/entangled states replace the uncorrelated ('classical') ones.

For instance, assume that we send through the interferometer the so-called NOON state, $|\psi_0\rangle = \frac{|N,0\rangle+|0,N\rangle}{\sqrt{2}}$, which is an N-body entangled state ($N \geq 2$) describing a coherent superposition of two states, each has N photons in one of the arms of the interferometer and none in the other; e.g., the state $|N,0\rangle$ has N photons in the upper arm and zero photons in the lower one. If there is a phase fluctuation $\delta\theta$ in the upper arm, the state with N photons in this arm will acquire a phase factor $e^{iN\delta\theta}$, since the phase displacement is proportional to the photon number in the arm. In doing so, the final NOON state will be $|\psi_{\delta\theta}\rangle = \frac{e^{iN\delta\theta}|N,0\rangle+|0,N\rangle}{\sqrt{2}}$.

According to the previous, the orthogonality between the initial $|\psi_0\rangle$ and final $|\psi_{\delta\theta}\rangle$ NOON states makes possible the determination of the phase shift $\delta\theta$. Thus, we want to find the displacement $\delta\theta$ that vanishes the overlap between the initial and final states, which in turn defines the resolution of the experiment. We have that

$$\left|\langle\psi_{\delta\theta}|\psi_0\rangle\right|^2 = \left|\frac{e^{iN\delta\theta}+1}{2}\right|^2 = \left|e^{iN\delta\theta/2}\left(\frac{e^{iN\delta\theta/2}+e^{-iN\delta\theta/2}}{2}\right)\right|^2 = \cos^2(N\delta\theta/2) \tag{7.25}$$

and for $N\delta\theta = \pi$, it is equal to zero. Therefore, $\delta\theta \sim 1/N$ indicating that the phase sensing is higher for a given number N of photons (resources), when there are in an entangled rather than a non-entangled state. The resulting enhancement is a factor of $\sqrt{N}$, that is a quadratic improvement over (7.23).

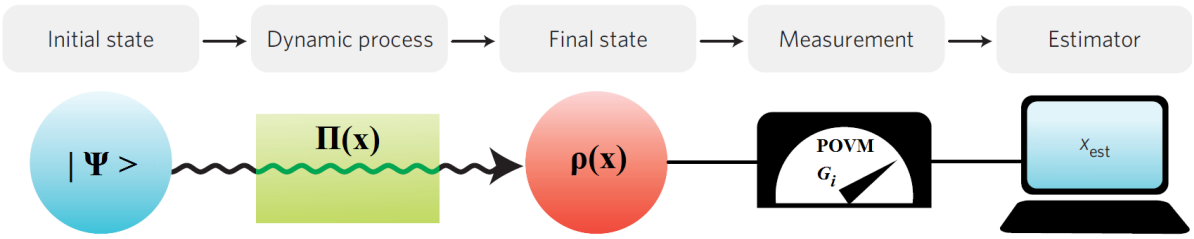

Figure 7.4: General setup for Quantum Parameter Estimation. The probe is prepared in an initial known state $|\Psi\rangle$ and then is sent through a parameter-dependent physical process (quantum channel), which may be described by a set of Kraus operators $\Pi(x)$. The output state is, in general, a parameterized density operator $\rho(x)$. The estimated value of the parameter embedded in the physical process, x_{est}, is obtained from the results of the measurements made on the final probe $\rho(x)$.

The previous treatment of the problem of quantum parameter estimation was rather special. We now investigate it from a more general perspective, shown in Fig. 7.4.

Consider an initial pure (i.e. known) state $|\Psi\rangle$ and a trace-preserving physical process that depends on a parameter x. We call this dynamical process a quantum channel, which in general is described by a set of Kraus operators $\Pi(x)$ that depend on the parameter to be estimated. The initial state is sent through this channel and it becomes, in general, a density matrix $\rho(x)$ which carries information about the parameter x embedded in the physical process. Measurement on $\rho(x)$ follows, the result of which is then used to estimate the value of the parameter x.

When the x-dependent dynamical process is unitary, i.e. noiseless, the evolved state of the probe before measurement is given by

$$\rho(x) = U(x)\rho(0)U^{\dagger}(x) \quad , \tag{7.26}$$

with $\rho(0) = |\Psi\rangle\langle\Psi|$, whereas for noisy (non-unitary) process it may be written as

$$\rho(x) = \sum_j \Pi_j(x)\rho(0)\Pi_j^{\dagger}(x) \quad , \tag{7.27}$$

which may be regarded as the integral version of the master equation of the system. Moreover, the Kraus operators satisfy the condition $\sum_j \Pi_j(x)\Pi_j^{\dagger}(x) = \mathbb{1}$.

Next, we have to choose an appropriate measurement, which quantum-mechanically is associated with a set of non-negative Hermitian operators G_i, known as POVMs. Because the G_i do not correspond necessarily to orthogonal measurements, they are a generalization of the von-Neumann projection operators. POVMs should satisfy the completeness relation $\sum_i G_i = \mathbb{1}$, and they are such that the probability of getting a discrete measurement outcome i if the value of the parameter is x, is given by $p_i(x) = Tr[\rho(x)G_i]$. For a continuous set of measurement outcomes, we have to replace the index i with a continuous

(random) variable χ, so that the completeness relation is now $\int d\chi G(\chi) = \mathbb{1}$, and the probability density reads $p(\chi|x) = Tr[\rho(x)G(\chi)]$.

We, then, associate an estimation $x_{est}(i)$ with each measurement result i that corresponds to an operator G_i, and finally we evaluate the performance of the estimation by the means of (7.18). For unbiased estimators, it results in $\sqrt{\langle(\delta x)^2\rangle} = \sqrt{\langle(x_{est} - x)^2\rangle}$ as before.

Although the classical and quantum parameter estimation schemes are very similar, we stress that their noteworthy difference is the following : the probability of measurement outcomes, $p_i(x)$ or $p(\chi|x)$, in the quantum case depends on both the choice of the measurements or POVMs performed on the system, and the density matrix of the system undergoing the dynamical process. In other words, the Fisher information defined in (7.3), in the quantum case is written as

$$F(x) = F(x;\{G(\chi)\}) = \int d\chi p(\chi|x)\Big(\partial_x ln[p(\chi|x)]\Big)^2 = \int d\chi \frac{\Big(\partial_x p(\chi|x)\Big)^2}{p(\chi|x)} \tag{7.28}$$

with the probability density to be $p(\chi|x) = Tr[\rho(x)G(\chi)]$.

As stated before, the attainability of the Cramér-Rao bound

$$\sqrt{\langle(\delta x)^2\rangle} \geq \frac{1}{\sqrt{\nu F(x;\{G(\chi)\})}} \tag{7.29}$$

premises an optimization over estimators for a given quantum measurement. In quantum mechanics, the measurement strategy matters, so one has to also optimize the procedure over all quantum measurements. This leads to the *quantum Fisher information* (QFI)

$$\mathscr{F}(x) \equiv \max_{\{G(\chi)\}} F(x;\{G(\chi)\}) \quad , \tag{7.30}$$

and the quantum Cramér-Rao bound reads

$$\sqrt{\langle(\delta x)^2\rangle} \geq \frac{1}{\sqrt{\nu\mathscr{F}(x)}} \quad . \tag{7.31}$$

Thus, in the quantum case we can take advantage of the freedom to choose the experimental setup to minimize the RHS of (7.29), and hence optimize the estimation precision.

7.4. QUANTUM FISHER INFORMATION

An important aim of Quantum Metrology is to increase the estimation precision by finding the optimal measurement basis/POVM. Braunstein and Caves [97] obtained the optimal Fisher information over all POVMs for a given parameter-dependent quantum state $\rho(x)$, which is called quantum Fisher information (QFI), through the logarithmic derivative $L(x)$:

$$\mathscr{F}(x) = Tr\{L^{\dagger}(x)\rho(x)L(x)\} \quad . \tag{7.32}$$

The most common definition of $L(x)$ is the *symmetric logarithmic derivative* (SLD), $\partial_x\rho(x) = [L(x)\rho(x) + \rho(x)L(x)]/2$, hence $L(x) = L^{\dagger}(x)$. In doing so, the QFI can be simplified to

$$\mathscr{F}(x) = Tr\{\rho(x)L^2(x)\} = Tr\{(\partial_x\rho(x))L(x)\} \quad . \tag{7.33}$$

Since it is a local quantity which dependents on $\rho(x)$ and its first derivative $\partial_x\rho(x)$, it can be intuitively and physically interpreted as the 'velocity' at which the density matrix moves for a given parameter value [102].

The SLD can be explicitly expressed in the eigenbasis of the parameterized density matrix, $\rho(x) = \sum_i r_i|r_i\rangle\langle r_i|$, as

$$L(x) = 2\sum_{i,j}\frac{\langle r_i|\partial_x\rho(x)|r_j\rangle}{r_i + r_j}|r_i\rangle\langle r_j| \tag{7.34}$$

where the $|r_i\rangle$ are the eigenstates of $\rho(x)$, and the r_i are the corresponding eigenvalues. Inserting (7.34) into (7.33) and performing some algebra, we get

$$\mathscr{F}(x) = \sum_{i,r_i>0}\frac{(\partial_x r_i)^2}{r_i} \quad + \quad 2\sum_{i,j,r_i+r_j>0}\frac{(r_i - r_j)^2}{r_i + r_j}|\langle r_i|\partial_x r_j\rangle|^2 \quad . \tag{7.35}$$

The first term in the RHS of (7.35) is just the classical Fisher information, whereas the second term can be considered as the quantum contribution [99].

Usually, it is not an easy task to express the QFI in the form of the density matrix for a general system. However, as has already been mentioned in [99], an explicit expression of the QFI in terms of a two-dimensional density matrix has been derived :

$$\mathscr{F}(x) = Tr\{(\partial_x\rho(x))^2\} + \frac{Tr\{(\rho(x)\partial_x\rho(x))^2\}}{det[\rho(x)]} \quad . \tag{7.36}$$

Moreover, the QFI is related to the *Bures distance* $\mathscr{D}$ as

$$\mathscr{D}^2\big[\rho(x),\rho(x+dx)\big]=\frac{\mathscr{F}(x)dx^2}{4} \quad . \tag{7.37}$$

The Bures distance $\mathscr{D}[A,B]$ measures the distance between the two quantum states A and B, and is defined as [97, 99]

$$\mathscr{D}[A,B]=\sqrt{2\big(1-f[A,B]\big)} \quad , \tag{7.38}$$

where $f[A,B]=Tr\Big\{\sqrt{\sqrt{A}B\sqrt{A}}\Big\}$ is the fidelity which measures the 'closeness' of A and B.

Let us now turn to the case of pure states and unitary (noiseless) parameter-dependent processes, which lead to exact expressions for the QFI.

Braunstein and Caves [97] showed that the QFI is proportional to the variance of an operator $h(x)$, which is related to the unitary time-evolution operator (propagator) as

$$h(x)=i\big(\partial_x U(x)\big)U^\dagger(x) \quad . \tag{7.39}$$

The operator $h(x)$ is the generator of the transformation associated with the parameter x. In order to illuminate this, consider a system whose Hamiltonian is $H(x)$, its initial state is ρ, and that we want to estimate the parameter x. When the system is evolved under the action of the Hamiltonian, its state becomes $\rho(x)=U(x)\rho U^\dagger(x)$, where $U(x)=e^{-iH(x)t/\hbar}$. The sensitivity of $\rho(x)$ to the parameter x can be characterized by the generator $h(x)$ of local parameter translation from $\rho(x)$ to $\rho(x+dx)$, with dx be the infinitesimal change of x.

In detail [103], if x is changed to $x+dx$, then $\rho(x)$ is updated to $\rho(x+dx)=U(x+dx)\rho U^\dagger(x+dx)$. Because $U(x+dx)\approx U(x)+\partial_x U(x)dx$, the translation from $\rho(x)$ to $\rho(x+dx)$ can be written as

$$\begin{aligned}
\rho(x+dx) &\approx \big(U(x)+\partial_x U(x)dx\big)\ \ \rho\ \ \big(U(x)+\partial_x U(x)dx\big)^\dagger \\
&= \big(U(x)+\partial_x U(x)dx\big)\ \ \mathbb{1}\rho\mathbb{1}\ \ \big(U^\dagger(x)+\partial_x U^\dagger(x)dx\big) \\
&= \big(U(x)+\partial_x U(x)dx\big)\ \ \big(U^\dagger(x)U(x)\rho U^\dagger(x)U(x)\big)\ \ \big(U^\dagger(x)+\partial_x U^\dagger(x)dx\big) \\
&= \big[\mathbb{1}+\big(\partial_x U(x)\big)U^\dagger(x)dx\big]\ \ U(x)\rho U^\dagger(x)\ \ \big[\mathbb{1}+U(x)\big(\partial_x U^\dagger(x)\big)dx\big] \\
&\approx e^{-ih(x)dx}\ \ \rho(x)\ \ e^{ih^\dagger(x)dx} \quad ,
\end{aligned} \tag{7.40}$$

and therefore the operator $h(x)$ is indeed an x-generator.

According to [97, 98], when the initial state of the probe is a pure state $|\psi_0\rangle$, the QFI is given by

$$\mathscr{F}(x)=4\langle\psi_0|\big(\Delta h(x)\big)^2|\psi_0\rangle=4\langle\big(\Delta h(x)\big)^2\rangle_0 \quad , \tag{7.41}$$

where

$$\langle\big(\Delta h(x)\big)^2\rangle_0=\langle\big(h(x)-\langle h(x)\rangle_0\big)^2\rangle_0 \tag{7.42}$$

is the average variance of $h(x)$ with respect to the initial state of the probe. Hence, in this case the inequality (7.31) reads

$$\sqrt{\langle(\delta x)^2\rangle} \geq \frac{1}{2\sqrt{\nu\langle\big(\Delta h(x)\big)^2\rangle_0}} \quad , \tag{7.43}$$

which was named a 'generalized uncertainty relation' in [98]. As opposed to the usual uncertainty relations in quantum mechanics, it does not relate the variances of two (conjugate) operators, but instead the variances of a parameter and an operator. It is, in other words, a parameter-based uncertainty relation.

In order to minimize the RHS of (7.43), i.e. to optimally improve the estimation precision, we first have to identify the generator of the transformation related to the parameter and then we must find the state which maximizes the variance of this generator. Giovannetti et al. [92] found that the variance of $h(x)$ is maximized when the input state of the probe is $|\psi_0\rangle = \frac{1}{\sqrt{2}}\Big(|\lambda_{max}\big(h(x)\big)\rangle + e^{i\phi}|\lambda_{min}\big(h(x)\big)\rangle\Big)$, where $e^{i\phi}$ is an arbitrary phase factor (phasor). This yields the *maximum quantum Fisher information*

$$\mathscr{F}_{max}(x) = \Big[\lambda_{max}\big(h(x)\big) - \lambda_{min}\big(h(x)\big)\Big]^2 \quad , \tag{7.44}$$

where λ_{max} and λ_{min} are, respectively, the maximum and minimum eigenvalues of $h(x)$. Hence, the key to the QFI is the derivation of the generator $h(x)$. By this way, the optimal x-estimation precision reads

$$\sqrt{\langle(\delta x)^2\rangle} = \frac{1}{\sqrt{\nu}\Big[\lambda_{max}\big(h(x)\big) - \lambda_{min}\big(h(x)\big)\Big]} \quad . \tag{7.45}$$

7.5. QUANTUM CRAMÉR-RAO BOUND UNCERTAINTY RELATION: A FEW EXAMPLES

Position and Momentum

Consider a system that is spatially displaced by X, and we want to estimate this displacement. It is known that such displacements are generated by the momentum operator $\mathscr{P} = -i\hbar\partial_X$ of the system. Put differently, the state $|\psi(X)\rangle$ is related to $|\psi_0\rangle$ by the unitary transformation

$$|\psi(X)\rangle = U(X)|\psi_0\rangle = e^{-iX\mathscr{P}/\hbar}|\psi_0\rangle \quad . \tag{7.46}$$

Using (7.39), we find that the X-generator is given by

$$h(X) = h = \frac{\mathscr{P}}{\hbar} \quad . \tag{7.47}$$

Insertion of (7.47) into (7.41) yields the following expression for the QFI

$$\mathscr{F}(X) = \frac{4\langle(\Delta\mathscr{P})^2\rangle_0}{\hbar^2} \quad , \tag{7.48}$$

which, in turn, leads to the following (unbiased) Cramér-Rao uncertainty relation

$$\sqrt{\langle(\delta X)^2\rangle} \geq \frac{\hbar}{2\sqrt{\nu\langle(\Delta\mathscr{P})^2\rangle_0}} \quad . \tag{7.49}$$

This is different from the usual Heisenberg position-momentum uncertainty relation $\Delta\mathscr{X}\Delta\mathscr{P} \geq \hbar/2$. Here, X is a parameter, not an operator, and the number ν of experimental repetitions is not found in the standard Heisenberg relation. The inequality (7.49) corresponds to a 'generalized uncertainty relation' [98].

Time and Energy

The parameter we want to estimate may be a time duration. For instance, we consider a system that evolves in time unitarily under the action of its (unperturbed) Hamiltonian $\mathscr{H}$, which is assumed to be time-independent. After a time lapse T, the state of the system becomes

$$|\psi(T)\rangle = U(T)|\psi_0\rangle = e^{-iT\mathscr{H}/\hbar}|\psi_0\rangle \quad . \tag{7.50}$$

We again apply (7.39) to find that

$$h(T) = h = \frac{\mathscr{H}}{\hbar} \quad , \tag{7.51}$$

hence the Hamiltonian of the system is the generator of its temporal translations (time evolution), and the Cramér-Rao uncertainty relation is

$$\sqrt{\langle(\delta T)^2\rangle}\sqrt{\langle(\Delta\mathscr{H})^2\rangle_0} \geq \frac{\hbar}{2\sqrt{\nu}} \quad . \tag{7.52}$$

The quantity $\langle(\delta T)^2\rangle$ is the square deviation of the estimator T_{est} from the actual elapsed time T averaged over all measurement results, and the $\langle(\delta\mathscr{H})^2\rangle_0$ is the energy dispersion along the initial state of the system. Thus, the brackets in the former denote a classical statistical average, whereas in the latter they denote a quantum-mechanical expectation value.

The inequality (7.52) could not be interpreted as a standard Heisenberg uncertainty relation, since in ordinary quantum mechanics there is no hermitian operator associated with time. Instead, it is an example of the so-called 'generalized Heisenberg relation' [97], an inequality which relates the energy dispersion to the uncertainty in the elapsed time, which is a parameter.

Photon number and Phase

Let us now examine the optical interferometer shown in Fig. 7.3 from a different perspective.

We want to find the relation between the uncertainty of the phase of the harmonic oscillator and the variance of the number operator. It is known that the number operator $\mathcal{N} = a^\dagger a$ is the generator of shifts in the phase θ of the oscillator. Indeed, when we apply on the input state $|\psi_0\rangle$ the unitary operator $U(\theta) = e^{-i\theta\mathcal{N}}$, we get at the output the state $|\psi(\theta)\rangle = e^{-i\theta\mathcal{N}}|\psi_0\rangle$, which it has been rotated (or phase-shifted) by θ in the phase space of the harmonic oscillator. From (7.39), we find that

$$h(\theta) = h = \mathcal{N} \quad , \tag{7.53}$$

which, through (7.41), leads to

$$\mathscr{F}(\theta) = 4\langle(\Delta\mathcal{N})^2\rangle_0 \quad . \tag{7.54}$$

In the case of the optical interferometer in Fig. 7.3, this means that the QFI is proportional to the *variance* in the number of photons in the upper arm of the interferometer, with respect to the initial state of the photons.

For coherent states obeying the Poissonian distribution, we get the shot noise limit or SQL scaling for the uncertainty in the phase θ, since $\langle(\Delta\mathcal{N})^2\rangle = \langle\mathcal{N}\rangle$, where $\langle\mathcal{N}\rangle$ is the *average* number of photons in the upper arm. Indeed, for $\nu = 1$ experiment, the θ-estimation error using coherent photons is given by the Cramér-Rao inequality

$$\delta\theta \geq \frac{1}{2\sqrt{\langle\mathcal{N}\rangle_0}} \quad . \tag{7.55}$$

In order to further improve the θ-estimation precision, we should maximize the QFI in (7.54). Equivalently, we have to find the initial state of the photons which maximizes the variance of $\mathcal{N}$. As has been stated in [89], the NOON state $|\psi_0\rangle = \frac{1}{\sqrt{2}}\big(|N,0\rangle + |0,N\rangle\big)$ yields the maximum variance $\langle(\Delta\mathcal{N})^2\rangle_0 = N^2/4$, which in turn leads to

$$\delta\theta \geq \frac{1}{N} \quad , \tag{7.56}$$

that is the Heisenberg limit scaling with the number N of resources.

Again, we conclude that the NOON states are more sensitive to phase shifts than the coherent states, offering a better precision for the same amount of resources.

" The secret of change is to focus all of your energy, not on fighting the old, but on building the new. "

— Socrates

8

QUANTUM-LIMITED BIOCHEMICAL MAGNETOMETERS DESIGNED USING THE FISHER INFORMATION AND QUANTUM REACTION CONTROL

8.1. INTRODUCTION

The quantum dynamics of the radical-pair mechanism [16, 35], underlying the avian magnetic compass [38, 39, 54, 104] and spin transport in photosynthetic reaction centers [76, 77, 105–108], have recently attracted the attention of the quantum physics community [23, 28, 30, 32, 56, 72, 73], since it was shown [26, 27, 55, 66, 67, 109, 110] that radical pairs offer an ideal system to study quantum coherence effects and explore quantum information processing in a complex biochemical setting.

Radical-pair reactions consist of a coherent spin motion in a multi-spin system embedded in a biomolecule, interrupted by an electron transfer that results in the spin-dependent charge recombination of the radical-ion pair and the termination of the reaction. It is known that the coherent spin motion as well as the measurable reaction yields in radical-pair reactions are also influenced by the external magnetic field through the unpaired electrons' Zeeman interaction. Hence, radical-pair reactions are no different than other quantum systems used to measure a classical parameter, as for example are the well-developed atomic magnetometers [111] using e.g. alkali vapors [112–117] or nitrogen vacancy centers [118–120]. Central in these studies have been the fundamental measurement precision limits set by the quantum dynamics of the system under consideration.

We here establish a venue for studying quantum metrology in a biological context [100]. We introduce the full machinery of quantum parameter estimation [89–92, 97, 121, 122] in

order (i) to establish the *exact* value of δB, the fundamental magnetic sensitivity of the reaction, and (ii) design an optimal molecular system approaching this fundamental limit. To this end we consider the quantum Fisher information obtained from the radical-pair reaction and the resulting Cramér-Rao bound. We then treat the intra-molecule hyperfine couplings as free design parameters, and obtain their optimum value by maximizing the quantum Fisher information. This leads to the fundamental limit δB, which we explicitly derive for any radical pair. Knowing the absolute quantum limit on δB, we address the well-known measurement of reaction yields and show it is sub-optimal. We then modify a recently proposed method of reaction control [123], introducing a quantum circuit analysis of the controlled reaction, and reducing δB by a factor of 3 compared to [123].

The outline of this work is the following. In Sec. 8.2 we briefly introduce the dynamics of radical-pair reactions, and in Sec. 8.3 the basic tools of quantum metrology, in particular the analytic form of the parameter-generator, a useful tool recently introduced [103]. In Sec. 8.4, the eigenvalues of this operator are then used to find the maximum quantum Fisher information and the resulting bounds on δB for radical-pair reactions. In Sec. 8.5 we discuss a common observable in radical-pair reactions, the reaction yield, in the context of magnetic sensitivity. We demonstrate that the resulting maximum possible sensitivity is an order of magnitude smaller than the absolute quantum limit. In Sec. 8.6 we present the optimum measurement scheme that can realize the optimum quantum limit on δB. Since this scheme does not appear to be chemically realistic, a natural question is whether some sort of quantum reaction control can improve the magnetic sensitivity of reaction yields. This is indeed the case as shown in Sec. 8.7, where we take advantage of the spin-exchange interaction naturally occurring in radical pairs, and known from quantum metrology work to simulate a controlled-NOT gate. The spin-exchange interaction effects a state-preparation and readout before and after the actual magnetometric state evolution, respectively, reminding one of Ramsey interferometry. Together with the reaction control method of [123], which is a factor of 6 away from the absolute quantum limit, our measurement scheme is shown to approach this limit within a factor of 2.

8.2. RADICAL-PAIR MECHANISM

Radical pairs (RPs) are the cornerstone system of spin chemistry, the field of physical chemistry and photochemistry dealing with the effect of electron and nuclear spins on chemical reactions. The radical-pair mechanism was introduced by Closs and Closs [51] and by Kaptein and Oosterhoff [52] as a reaction intermediate explaining anomalously large EPR and NMR signals observed in organic molecule reactions in the 1960s. The quantum degrees of freedom of radical-ion pairs are formed by a multi-spin system embedded in a biomolecule. The multi-spin system is composed of the two unpaired electrons of the two radical ions and a usually large number of nuclei. Their coherent spin motion is driven by intramolecule magnetic interactions, such as hyperfine couplings between each radical's magnetic nuclei and the respective unpaired electron. The magnetic field effects resulting from such interactions in this spin-dependent biochemical reaction have been extensively explored theoretically and experimentally [36, 46, 124–126].

In particular, a charge transfer following the photoexcitation of a donor-acceptor dyad DA leads to the radical pair (also called charge-separated state) $D^{\bullet+}A^{\bullet-}$, where the two dots represent the two unpaired electron spins of the two radicals. The initial spin state of the two unpaired electrons of the radical pair is usually a singlet, denoted by ${}^{S}D^{\bullet+}A^{\bullet-}$. Now, both D and A contain a number of magnetic nuclei which hyperfine-couple to the respective electron. Neither singlet-state nor triplet-state RPs are eigenstates of the magnetic Hamiltonian, $\mathscr{H}_B$; hence the initial formation of ${}^{S}D^{\bullet+}A^{\bullet-}$ is followed by singlet-triplet (S-T) mixing, i.e. a coherent oscillation of the spin state of the electrons, designated by ${}^{S}D^{\bullet+}A^{\bullet-} \leftrightharpoons {}^{T}D^{\bullet+}A^{\bullet-}$. Concomitantly, nuclear spins also precess, and hence the total electron and nuclear spin system undergoes a coherent spin motion driven by $\mathscr{H}_B$. As will be detailed later, the subscript B in $\mathscr{H}_B$ is a reminder that the Hamiltonian depends parametrically on the magnetic field B to be estimated.

This coherent spin motion has a finite lifetime. Charge recombination, i.e. charge transfer from A back to D, terminates the reaction and leads to the formation of the neutral reaction products, conserving during the process the electronic spin-angular momentum. That is, there are two kinds of neutral products, singlet (the original DA molecules) and triplet, ${}^{T}DA$. The percentage of the initial radical-pair population ending up in the singlet (triplet) neutral product defines the singlet (triplet) reaction yield. Singlet and triplet recombination takes place at the rate k_S and k_T, respectively. Both rates are in principle known parameters of the specific molecular system under consideration, as of course are the hyperfine couplings entering $\mathscr{H}_B$. The whole process is schematically depicted in Fig.8.1(a).

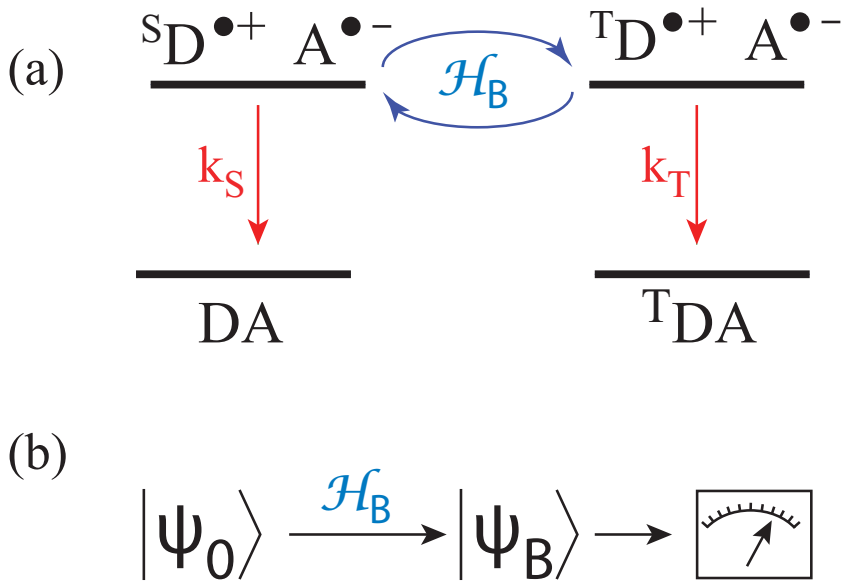

Figure 8.1: (a) Radical-pair reaction dynamics. A charge transfer following the photoexcitation (not shown here) of a donor-acceptor dyad DA produces a singlet state radical pair ${}^{S}D^{\bullet+}A^{\bullet-}$, which is coherently converted to the triplet radical pair, ${}^{T}D^{\bullet+}A^{\bullet-}$, due to intramolecule magnetic interactions embodied in the spin Hamiltonian $\mathscr{H}_B$. Simultaneously, spin-selective charge recombination leads to singlet (DA) and triplet neutral products (${}^{T}DA$). (b) Quantum metrology aspect of the radical-pair reaction, where an initial spin state is transformed into a final spin state, which depends on the magnetic field B through the spin Hamiltonian. The measurement of the final state conveys information about B.

The schematic of Fig.8.1(a) should not be taken too literally, as it suggests that only pure singlet (triplet) radical pairs can recombine to the singlet (triplet) neutral reaction products. This is not the case, like it is not the case for a two-level atom that only an excited-state atom can decay to the ground state. As in atoms having ground-excited state coherence, radical pairs can be in coherent superpositions of singlet and triplet states, continuously evolving by $\mathscr{H}_B$. A major aspect of our previous work has been to understand the physics of this coherence, its fundamental dissipation properties, and the role thereof in establishing the fundamental master equation, $d\rho/dt$, accounting for the radical-pair reaction's quantum dynamics. This issue is still hotly debated [127, 128].

8.2.1. THIS WORK

This work, however, is decoupled from this debate, as we consider only the Hamiltonian contribution to the quantum metrology aspect of the reaction. The non-trivial quantum dynamics previously alluded to mainly appear in the case of unequal recombination rates, $k_S \neq k_T$. Here we consider the simple exponential model, where $k_S = k_T \equiv k$, and we further neglect the presence of S-T decoherence [55], which is unavoidable even in the case $k_S = k_T$.

The rationale of this approach is that it allows a step-wise understanding of the quantum metrology aspect of radical-pair reactions, starting from the most evident features stemming from the coherent spin motion, and progressing to more complex properties of the system, which is an open and leaky quantum system. Earlier works [23, 28] attempted to explore some metrological aspects of these reactions, however using the traditional (called Haberkorn's) master equation and considering phenomenological sources of decoherence. Our understanding is (i) that Haberkorn's master equation scrambles the quantum dynamics of the system and is a phenomenological description valid only in the regime of strong spin relaxation, and (ii) consideration of decoherence and its role in this new kind of biochemical quantum metrology is a non-trivial task, intertwined with the understanding of the fundamental master equation.

Therefore we opt to first establish the fundamental limits to the magnetic sensitivity of radical-pair reactions in the simple case of equal recombination rates and a purely coherent spin motion. Thus, the only effect of the finite radical pair's lifetime $\tau = 1/k$ relevant to this work is that the radical-pair population decays exponentially as $e^{-t/\tau}$. Hence the sensitivity limit δB[1] will be shown to be directly dependent on τ. This is not unexpected, since measurement time is a central resource in quantum metrology.

In other words, we here explore the equivalence of Fig.8.1(a) with Fig.8.1(b), which describes the usual scheme of quantum estimation of a classical parameter such as a magnetic field. An initial state $|\psi_0\rangle$ evolves under the unitary action of the Hamiltonian $\mathscr{H}_B$ into $|\psi_B\rangle$. Measuring the final state conveys information about B. In radical-pair reactions, an initial spin state (comprising the spin of the two electrons and the present nuclei)

[1] To caution for a possible semantic confusion, we note that high (low) magnetic sensitivity means small (large) uncertainty δB in the estimate of B.

evolves under $\mathscr{H}_B$, and the recombination process effects the measurement in the singlet-triplet basis, i.e. the measurement stage is naturally built into the radical-pair mechanism.

We here treat radical-pair reactions as scalar magnetometers, and conclusively address the following questions: **(A)** What is the fundamental quantum limit, δB, to the precision of estimating B? **(B)** Is this limit realized when the physical observable carrying the information on B is the reaction yield? **(C)** If not, can we control the reaction in order to better approach the fundamental limit δB?

8.2.2. RADICAL-PAIR HAMILTONIAN

If we consider a radical pair with n_D nuclear spins in the donor and n_A nuclear spins in the acceptor, the hyperfine Hamiltonian in the presence of an external magnetic field $\mathbf{B} = B\hat{\mathbf{z}}$, where B is to be estimated, is

$$\mathscr{H}_B = -B(s_{Dz} + s_{Az}) + \sum_{j=1}^{n_D} \mathbf{s}_D \cdot \tilde{\mathbf{A}}_j \cdot \mathbf{I}_j + \sum_{k=1}^{n_A} \mathbf{s}_A \cdot \tilde{\mathbf{a}}_k \cdot \mathbf{I}_k \quad . \tag{8.1}$$

Here we denote by $\mathbf{s}_D$ ($\mathbf{s}_A$) the electron spin operator of the donor (acceptor) radical, $\mathbf{I}_j$ ($\mathbf{I}_k$) is the j-th (k-th) nuclear spin operator of the donor (acceptor) radical, and $\tilde{\mathbf{A}}_j$ ($\tilde{\mathbf{a}}_k$) the hyperfine tensor coupling the j-th (k-th) nuclear spin of the donor (acceptor) radical to the donor's (acceptor's) electron spin. The gyromagnetic ratio of the electrons setting the frequency scale, $\gamma/2\pi = 2.8 \times 10^6$ Hz/G, has been set to $\gamma = 1$ in Eq.(8.1) and we will keep this convention from now on. We also set $\hbar = 1$; thus the hyperfine couplings and the magnetic field B have units of frequency, while the spin operators are dimensionless. In the following, in order to get actual magnetic field values, one should divide the derived expressions for B by γ.

Before embarking on our analysis, we will first lay out the tools of quantum parameter estimation and apply them to two pedagogical cases, a single-electron Zeeman interaction and a two-electron Zeeman interaction. These considerations will form a baseline for comparing fundamental sensitivity limits in radical pairs.

8.3. QUANTUM PARAMETER ESTIMATION

The formalism developed by Brun and coworkers [103] is ideally suited to treat the estimation of B, which is not a multiplicative parameter of the radical-pair Hamiltonian (8.1). Specifically, the authors in [103] consider the time-evolution operator, $U_B = e^{-itH_B}$, which obviously depends on the parameter B we wish to estimate. If the initial state of the system is ρ_0, then the time-evolved state will be $\rho_B = U_B \rho_0 U_B^\dagger$, where the subscript in ρ_B reminds us that the time evolved state also depends on B. The generator of B translations is then shown to be $h_B = i(\partial_B U_B)U_B^\dagger$. The utility of this generator is that it directly leads to the *maximum* quantum Fisher information

$$F_B^{\max} = [\lambda_{\max}(h_B) - \lambda_{\min}(h_B)]^2 \quad , \tag{8.2}$$

where $\lambda_{\max}(h_B)$ ($\lambda_{\min}(h_B)$) is the maximum (minimum) eigenvalue of h_B. The authors in [103] then derive two general results. First, knowing the n different eigenvalues, E_k, and corresponding eigenvectors, $|E_k^{(i)}\rangle$ of $\mathscr{H}_B$, where $i = 1,\ldots,d_k$, with d_k being the degeneracy of eigenvalue E_k, one can obtain h_B from

$$h_B = t\sum_{k=1}^{n}\frac{\partial E_k}{\partial B}P_k + 2\sum_{k\neq l}\sum_{i=1}^{d_k}\sum_{j=1}^{d_l} e^{-i(E_k-E_l)t/2} \times \sin\frac{(E_k-E_l)t}{2}\ \langle E_l^{(j)}|\partial_B E_k^{(i)}\rangle\ |E_k^{(i)}\rangle\langle E_l^{(j)}| \quad . \tag{8.3}$$

By $P_k = \sum_{i=1}^{d_k}|E_k^{(i)}\rangle\langle E_k^{(i)}|$ we denote the projector to the k-th eigenspace of $\mathscr{H}_B$. Second, the maximum Fisher information is obtained for the initial state

$$|\psi\rangle = \frac{1}{\sqrt{2}}\left(|\lambda_{\max}\rangle + e^{i\phi}|\lambda_{\min}\rangle\right) \quad , \tag{8.4}$$

where $|\lambda_{\max}\rangle$ and $|\lambda_{\min}\rangle$ are the eigenkets of h_B corresponding to its maximum and minimum eigenvalues, respectively. Finally, the uncertainty δB in estimating B is limited by the Cramér-Rao bound [95]

$$\delta B \geq \frac{1}{\sqrt{\nu F_B^{\max}}} \quad , \tag{8.5}$$

where ν is the number of independent repetitions (number of radical pairs in our case) of the measurement.

8.3.1. SINGLE ELECTRON IN A MAGNETIC FIELD

Before proceeding with radical pairs, we analyze two intuitive and simple examples. Consider first a single electron in a magnetic field $\mathbf{B} = B\hat{\mathbf{z}}$, the Hamiltonian being $\mathscr{H} = -Bs_z$. The eigenvectors and eigenvalues of $\mathscr{H}$ are $|\pm\rangle$ and $\epsilon_\pm = \mp B/2$, respectively. Since the eigenvectors are B-independent, the second term in Eq. 8.3 is zero, while the first term leads to $h_B = t\sum_{j=\pm}\frac{d\epsilon_j}{dB}|j\rangle\langle j| = -ts_z$. The maximum and minimum eigenvalues of h_B are $t/2$ and $-t/2$, respectively, hence $F_B^{\max} = t^2$. Thus, we recover the well-known time-scaling limit; namely the magnetic sensitivity resulting from measuring the electron's Larmor frequency during a time interval t is limited by $\delta B \geq 1/\sqrt{F_B^{\max}} = 1/t$. Repeating this measurement ν times, the so-called shot-noise-limited sensitivity will be $\delta B \geq 1/\sqrt{\nu}t$.

8.3.2. TWO ELECTRONS IN A MAGNETIC FIELD

We will now demonstrate the particle-number scaling limit by considering a 4-dimensional Hamiltonian consisting of the Zeeman interaction of two electrons, $\mathscr{H} = -B(s_z\otimes\mathbb{1}+\mathbb{1}\otimes s_z)$. Now the eigenvalues are $\epsilon_{++} = -B$ with corresponding eigenstate $|++\rangle$, $\epsilon_{--} = B$ with corresponding eigenstate $|--\rangle$, and $\epsilon_0 = 0$, which is doubly degenerate, with corresponding eigenstates $|+-\rangle$ and $|-+\rangle$. Again, the eigenstates are B-independent, hence $h_B =$

$-t\big(|++\rangle\langle++|-|--\rangle\langle--|\big)$. The eigenvalues of h_B are $\pm t$, hence now it is $F_B^{\max}=4t^2$. The magnetic sensitivity is now $\delta B \geq 1/2t$.

This is $\sqrt{2}$ times better than repeating the one-electron measurement two times. Generalizing to an N-electron system, where $\mathscr{H}=-B(s_z\otimes\mathbb{1}\otimes\mathbb{1}\otimes\cdots\otimes\mathbb{1}+\mathbb{1}\otimes s_z\otimes\mathbb{1}\otimes\cdots\otimes\mathbb{1}+\cdots+\mathbb{1}\otimes\mathbb{1}\otimes\cdots\otimes s_z)$, we find $\delta B\geq 1/Nt$. This is $\sqrt{N}$ times better than repeating the one-electron measurement N times. This enhancement is due to a possible multi-partite entanglement in the N-electron state. That is, a notable feature of $F_B^{\max}$ is that it automatically takes into account such a possibility in the system's state preparation.

It should be noted that the scaling with the particle number should not be confused with the scaling with the number ν of the experiment's repetition. Since the experimental realizations are independent, the scaling with ν is the ordinary statistical scaling $1/\sqrt{\nu}$. That is, repeating the 2-electron measurement ν times, the so-called Heisenberg limited magnetic sensitivity will be $\delta B\geq 1/2\sqrt{\nu}t$. Similarly, in the N-electron system, the Heisenberg-limited magnetic sensitivity obtained by averaging ν independent measurements will be $\delta B\geq 1/N\sqrt{\nu}t$.

8.4. FUNDAMENTAL MAGNETIC SENSITIVITY OF RADICAL-PAIR REACTIONS

As shown previously with the simple scenario of free electrons in a magnetic field, the sensitivity δB depends on the measurement time t. In radical-pair reactions there is a natural time scale limiting the magnetic sensitivity, the radical pair's lifetime. This is determined by the recombination rates k_S and k_T. For the reasons outlined in Sec. 8.2.1, we here consider the so-called exponential model, where $k_S=k_T\equiv k$. When $k_S=k_T=k$, the quantum dynamics of the radical-pair reaction simplify considerably. This is because, neglecting singlet-triplet decoherence which we understand is inherent in the system (even when $k_S=k_T$), in the exponential model radical pairs can be considered to evolve unitarily by the magnetic Hamiltonian $\mathscr{H}_B$, while their population decays exponentially at the rate k. Equivalently, at the single-molecule level, each radical pair evolves unitarily until the random instant in time when it recombines. This time follows the exponential distribution $(dt/\tau)e^{-t/\tau}$, where $\tau=1/k$.

Since the quantum Fisher information is time-dependent, we have to take into account the fact that from each radical pair in the ensemble we can extract a different Fisher information, depending on the time it recombined. If ν_t is the radical-pair population at time t and ν_0 is the initial population, then in each time interval dt there will be $k\nu_t dt$ radical pairs contributing to $F_B^{\max}$. If the variance of the magnetic field estimate resulting from one molecule is $1/F_B^{\max}$, then the $k\nu_t dt$ molecules contribute independently to the measurement during dt. The inverse uncertainties of B add in quadrature, hence the inverse variance stemming from those $k\nu_t dt$ molecules will be $1/(\delta B)_t^2=F_B^{\max}k\nu_t dt$. Since

$\nu_t = \nu_0 e^{-kt}$, the magnetic sensitivity for the whole reaction is

$$\delta B = \frac{1}{\left[\nu_0 \int_0^\infty F_B^{\max} k e^{-kt} dt\right]^{1/2}} \quad . \tag{8.6}$$

Clearly, we are not concerned with the absolute value of δB as determined by how many molecules participate in the experiment. We rather focus on optimizing $F_B^{\max}$, which depends on the state preparation and measurement scheme. Thus, in the following we will take $\nu_0 = 1$. For those cases where $F_B^{\max} = \alpha t^2$, where α is some constant, it follows that $\delta B = 1/\sqrt{2\alpha}\tau$.

We will first derive exact analytic results for $F_B^{\max}$ and δB for a radical pair with one nuclear spin-1/2 contained in e.g. the donor. The magnetic Hamiltonian is

$$\mathscr{H}_B = -B(s_{Dz} + s_{Az}) + A_x s_{Dx} I_x + A_y s_{Dy} I_y + A_z s_{Dz} I_z \quad .$$

As it formally turns out, the maximum quantum Fisher information does not depend on A_z. Intuitively, this is because the term $A_z s_{Dz} I_z$ just produces a shift in the magnetic field "seen" by the electron spin $\mathbf{s}_D$ along the z-axis and hence does not "produce" any information on B. We therefore have to distinguish two cases: $A_x = A_y$ and $A_x \neq A_y$. After dealing with the single-nuclear-spin radical pair, we generalize to multiple nuclear spins.

8.4.1. SPHEROIDAL HYPERFINE COUPLING ($A_x = A_y$)

For the spheroidal hyperfine coupling it is

$$\mathscr{H}_B = -B(s_{Dz} + s_{Az}) + A s_{Dx} I_x + A s_{Dy} I_y + a s_{Dz} I_z \quad . \tag{8.7}$$

A special case, occurring when $a = A$, is the commonly encountered isotropic hyperfine coupling. The eight eigenvalues of $\mathscr{H}_B$ are given in Appendix A, along with the eigenvalues of h_B calculated from Eq. 8.3 . It is found that the maximum and minimum eigenvalues of h_B are t and $-t$, respectively. Hence in this case, the maximum quantum Fisher information is $F_B^{\max} = 4t^2$, leading to the quantum limit

$$\delta B_F = \frac{1}{\sqrt{8}\tau} \quad . \tag{8.8}$$

This is the first general result of this work: the minimum uncertainty, δB, for determining a magnetic field B by using a radical-ion-pair reaction, the single nuclear spin of the radical pair having a spheroidal hyperfine coupling, is given by Eq. 8.8.

It is worthwhile noting that the maximum Fisher information, $4t^2$, is the same with the case of two free electrons studied in Sec. 8.3.2. One would perhaps expect that having three particles in the system (two electrons and one nucleus), the optimal sensitivity should gain (according to the Heisenberg scaling) a factor of 3 compared to the single-electron case, or a factor of 3/2 compared to the two-electron case. The reason behind the absence of such enhancement is that the nuclear spin does not strongly couple to the magnetic field. Hence

it does not provide any independent information on the magnetic field, but only serves to drive the time evolution of the radical pair's electronic spin state.

The lack of enhancement by the nuclear spin is not because we omitted the nuclear Zeeman interaction in the Hamiltonian. Indeed, if we include the nuclear Zeeman term in $\mathscr{H}_B$, we find that $F_B^{\max} = (2+\gamma_n)^2 t^2$, where γ_n is the nuclear gyromagnetic ratio (scaled to γ). Thus the correction to $F_B^{\max}$ is on the order of 10^{-3} and hence negligible. However, if it were $\gamma_n = 1$, then we would get the expected factor of 3 in sensitivity gain compared to the single-electron case of Sec. 8.3.1. In other words, the information about the magnetic field essentially stems from the strength of the field's coupling to the spins.

8.4.2. ELLIPSOIDAL HYPERFINE COUPLING ($A_x \neq A_y$)

We will now consider the general hyperfine coupling, where $A_x \neq A_y$,

$$\mathscr{H}_B = -B(s_{Dz} + s_{Az}) + A_x s_{Dx} I_x + A_y s_{Dy} I_y + a s_{Dz} I_z. \tag{8.9}$$

Again, we can find analytic expressions for the eigenvalues of h_B, which are given in Appendix B. There it is shown that $\lambda_{\max} \leq t$ and $\lambda_{\min} \geq -t$, hence the resulting maximum quantum Fisher information is bound by $4t^2$, which we found previously for the spheroidal hyperfine coupling. **We thus arrive at our second general result**: for a radical pair with a single nuclear spin-1/2, the spheroidal hyperfine coupling (the isotropic being a special case) leads to the smallest uncertainty, δB, for determining a magnetic field B along the spheroid's symmetry axis. This uncertainty depends only on the radical pair's lifetime τ, and is given by δB_F. As a numerical estimate, for $\tau = 1$ μs and $\nu = 10^{12}$ radical pairs we obtain $\delta B \approx 2$ pT.

8.4.3. RADICAL PAIR WITH MANY NUCLEAR SPINS

Realistic radical pairs contain many (sometimes tens) of nuclear spins. Based on the above, we can readily generalize and state **the third general result of this work**: For any radical pair with a spin-independent lifetime (i.e. $k_S = k_T = k = 1/\tau$), the maximum magnetic sensitivity (minimum δB) that can be obtained with *any measurement method and any initial state* is $\delta B_F = 1/\sqrt{8}\tau$. This follows from the same physical argument used in Sec. 8.4.1, namely that the uncertainty δB is determined just by the two electron spins. The nuclear spins do not couple to the external magnetic field; i.e., they are spectators just driving the spin-state evolution. A formal proof of this general result follows. For any operator $\mathscr{P}(B)$ depending parametrically on B, it is [129] $\frac{d}{dB} e^{\mathscr{P}(B)} = \int_0^1 du\, e^{u\mathscr{P}} \frac{d\mathscr{P}}{dB} e^{(1-u)\mathscr{P}}$. We take $\mathscr{P} = -i\mathscr{H}_B t$, calculate the above derivative with B and multiply with $U_B^\dagger = e^{i\mathscr{H}_B t}$ in order to find $h_B = i(\partial_B U_B) U_B^\dagger = -t\int_0^1 du\, e^{-iut\mathscr{H}_B}(s_{Dz} + s_{Az}) e^{iut\mathscr{H}_B}$. Taking the operator norm we get $||h_B|| \leq t\int_0^1 ||e^{-iut\mathscr{H}_B}|| * ||s_{Dz} + s_{Az}|| * ||e^{iut\mathscr{H}_B}|| du = t$, hence indeed the maximum (minimum) eigenvalue of h_B is smaller (larger) than or equal to t ($-t$).

8.5. REACTION YIELD AS A MAGNETOMETRIC OBSERVABLE

Typically, when studying the magnetic sensitivity of radical-pair reactions, one considers the singlet reaction yield, which quantifies the percentage of the reactants (number of radical pairs starting out in the electronic singlet state at $t = 0$) ending up in the singlet neutral product state. To define the singlet reaction yield, Y_{S}, we first need to introduce two basic operators, the singlet and triplet projectors, Q_S and Q_T, respectively. For a radical pair with a single nuclear spin they are written as $Q_S = |\mathrm{S}\rangle\langle\mathrm{S}| \otimes \mathbb{1}$ and $Q_T = \big(|\mathrm{T}_+\rangle\langle\mathrm{T}_+| + |\mathrm{T}_0\rangle\langle\mathrm{T}_0| + |\mathrm{T}_-\rangle\langle\mathrm{T}_-|\big) \otimes \mathbb{1}$. They leave the nuclear spin state untouched and project out of a general state $|\psi\rangle$ the electronic singlet or triplet component. The expectation value of Q_S in the state $|\psi\rangle$ is thus $\langle\psi|Q_S|\psi\rangle$; hence the singlet reaction yield is written as $Y_{\mathrm{S}} = \int_0^\infty \langle\psi_t|Q_S|\psi_t\rangle k e^{-kt} dt$, where $|\psi_t\rangle = e^{-i\mathscr{H}_B t}|\psi_0\rangle$. It is obviously irrelevant whether one chooses to measure the singlet or the triplet reaction yield, since it is always $Y_{\mathrm{S}} + Y_{\mathrm{T}} = 1$, where $Y_{\mathrm{T}} = \int_0^\infty \langle\psi_t|Q_T|\psi_t\rangle k e^{-kt} dt$.

8.5.1. INSTANTANEOUS VERSUS INTEGRATED YIELD

Now, since the magnetic field enters $|\psi_t\rangle$ through the Hamiltonian, the reaction yield is a function of B. In particular, in order to find the magnetic sensitivity δB, we first need to distinguish two cases. **(A)** If one can measure the instantaneous singlet yield given by $\langle Q_S\rangle_t k e^{-kt} dt = \langle\psi_t|Q_S|\psi_t\rangle k e^{-kt} dt$, one can estimate B just from those radical pairs that recombined into the singlet channel during dt through the relation (error propagation) $1/(\delta B)_t = |\partial_B \langle Q_S\rangle_t|/(\Delta Q_S)_t$, where $(\Delta Q_S)_t^2 = \langle Q_S^2\rangle_t - \langle Q_S\rangle_t^2$ is the variance of Q_S at time t, and $\partial_B\langle Q_S\rangle_t$ is the magnetic sensitivity of the instantaneous singlet fidelity. All such estimates can then be statistically combined (inverse uncertainties add in quadrature) to yield the total uncertainty

$$\delta B = \Big[\int_0^\infty \frac{\big(\partial_B \langle Q_S\rangle_t\big)^2}{\langle Q_S\rangle_t\big(1 - \langle Q_S\rangle_t\big)} k e^{-kt} dt\Big]^{-1/2} \quad , \tag{8.10}$$

where in the expression for the variance of Q_S appearing in the denominator of the integrand in Eq. 8.10, we took into account that $Q_S^2 = Q_S$, since Q_S is a projector. For this measurement scheme to be realistic, the time resolution of the measurement of the instantaneous yield must be much better than $1/k$.

If this is not the case, we are led to case **(B)**, integration over the whole reaction, i.e. measurement of the total yield Y_{S}. Then the magnetic sensitivity δB is given by $\delta B = \delta Y_{\mathrm{S}}/|dY_{\mathrm{S}}/dB|$, where δY_{S} is the precision with which Y_{S} is measured. This is calculated as follows. In each time step dt, the instantaneous yield, proportional to $\langle Q_S\rangle_t$, is a random variable following a binomial distribution with probability $\langle Q_S\rangle_t$. Thus, the total yield follows the sum of binomials having different probabilities, which is the *Poisson binomial*

distribution. Its variance is $\int_0^\infty \langle Q_S\rangle_t\big(1-\langle Q_S\rangle_t\big)ke^{-kt}dt$; hence

$$\delta B = \frac{\left[\int_0^\infty \langle Q_S\rangle_t\big(1-\langle Q_S\rangle_t\big)ke^{-kt}dt\right]^{1/2}}{\left|\frac{\partial}{\partial B}\int_0^\infty \langle Q_S\rangle_t ke^{-kt}dt\right|} \quad . \tag{8.11}$$

It is expected that the magnetic sensitivity of case **(B)** is smaller than case **(A)**, or equivalently $\delta B_{\text{Eq.8.11}} > \delta B_{\text{Eq.8.10}}$, since in case **(A)** we have access to much more information along the reaction than the integrated yield relevant to case **(B)**. Nevertheless, we here opt to provide exact expressions for δB in the integrated case, as we think that this is most relevant for physiological conditions. For completeness, we then report the corresponding sensitivities for case **(A)**.

8.5.2. ISOTROPIC HYPERFINE COUPLING

We first consider an isotropic hyperfine Hamiltonian, $\mathscr{H}_B = -B(s_{Dz}+s_{Az}) + A\mathbf{s}_D\cdot\mathbf{I}$. We calculate δB for initial state (i) $|S\rangle\otimes|\Uparrow\rangle$, (ii) $|S\rangle\otimes|\Downarrow\rangle$, and (iii) an equal mixture of (i) and (ii), which is usually taken to describe the initial state of radical-pair reactions, as it accounts for thermal equilibrium (practically zero) nuclear spin polarization. We denote the respective uncertainties by $\delta B^{\text{iso}}_{\text{S}\Uparrow}$, $\delta B^{\text{iso}}_{\text{S}\Downarrow}$ and $\delta B^{\text{iso}}_{\text{S}}$. The analytic expressions for these uncertainties follow from the analytic expressions for the reaction yields $Y^{\text{iso}}_{\text{S}\Uparrow}$, $Y^{\text{iso}}_{\text{S}\Downarrow}$ and $Y^{\text{iso}}_{\text{S}} = (Y^{\text{iso}}_{\text{S}\Uparrow} + Y^{\text{iso}}_{\text{S}\Downarrow})/2$ and their derivatives with respect to B entering the denominator of Eq.8.11, as well as from the analytic expressions for the respective nominators. The resulting formulas are too cumbersome to list here. In Appendix C we provide for reference the exact expressions for the reaction yields.

We here use the obtained analytic expressions for the uncertainties δB to display their inverses as a function of the Hamiltonian parameters B and A in the contour plots of Fig.8.2 (a)-(c) for the cases (i)-(iii), respectively. We first note that the minimum of $\delta B^{\text{iso}}_{\text{S}\Downarrow}$ (see Fig.8.2b) is smaller by about 30% than the minimum of $\delta B^{\text{iso}}_{\text{S}\Uparrow}$ (see Fig.8.2a), and both minima appear at a finite (and different in each case) value of the hyperfine coupling A and at a different field B. This is due to the different singlet-triplet mixing frequencies caused by the nuclear spin in the $|\Uparrow\rangle$ or in the $|\Downarrow\rangle$ state. In the $|\Downarrow\rangle$ state the nuclear magnetic field opposes B and hence reduces the mixing frequency; thus its B-dependence becomes relatively more significant.

In case (iii), shown in Fig.8.2(c), the minimum of $\delta B^{\text{iso}}_{\text{S}}$ is achieved for $A \gg B$. Although the sensitivity $\partial_B\langle Q_S\rangle$ is linear in the density matrix, the magnetic sensitivity δB depends on the absolute value of $\partial_B\langle Q_S\rangle$; hence $\delta B^{\text{iso}}_{\text{S}}$ is not trivially related to $\delta B^{\text{iso}}_{\text{S}\Uparrow}$ and $\delta B^{\text{iso}}_{\text{S}\Downarrow}$. For example, at low B and A where $\delta B^{\text{iso}}_{\text{S}\Uparrow}$ and $\delta B^{\text{iso}}_{\text{S}\Downarrow}$ are close to their minimum, the respective derivatives $\partial_B\langle Q_S\rangle$ are opposite in sign, and this is why $\delta B^{\text{iso}}_{\text{S}}$ is large in this region.

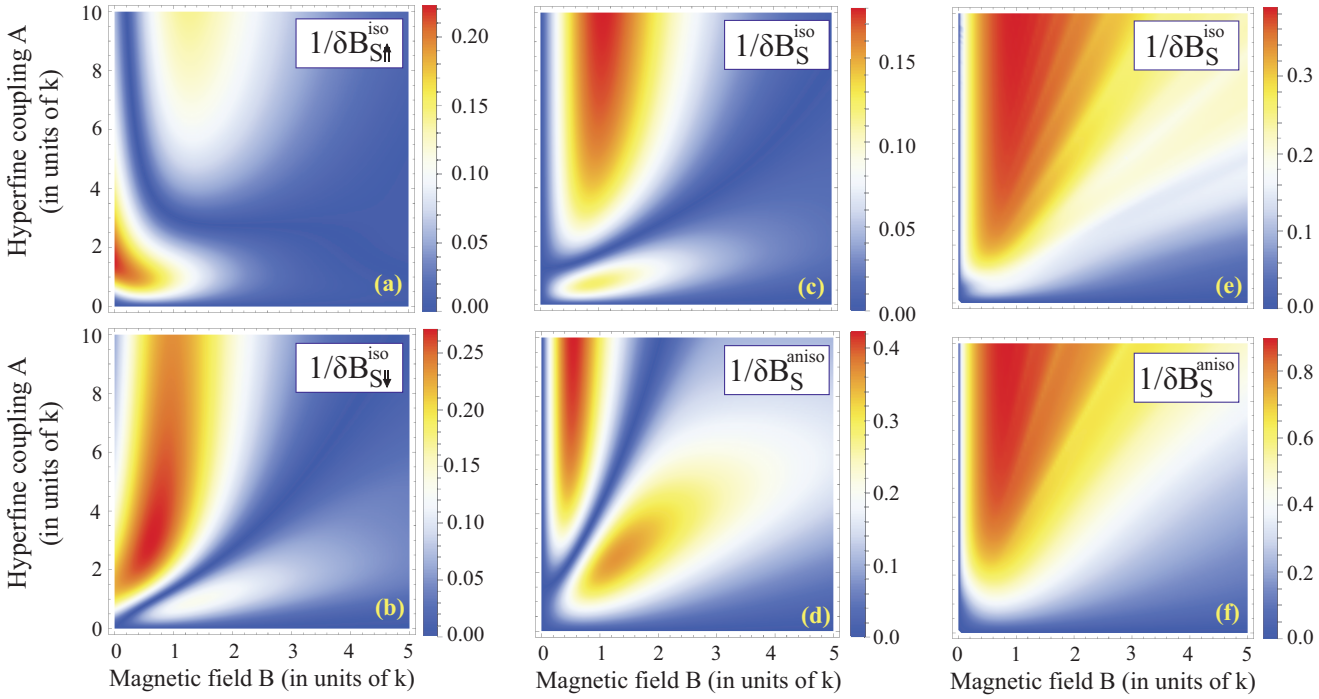

Figure 8.2: Magnetic sensitivity ($1/\delta B$ is better visualized than δB), determined from the singlet reaction yield for a radical pair with one nuclear spin-1/2, having equal recombination rates $k_S = k_T = k$. Isotropic hyperfine coupling ($A_x = A_y = A_z = A$) and initial state (a) $|S\rangle \otimes |\Uparrow\rangle$, (b) $|S\rangle \otimes |\Downarrow\rangle$, (c) an equal mixture of the previous two. (d) Maximally anisotropic hyperfine coupling ($A_x = A$ and $A_y = A_z = 0$, or $A_y = A$ and $A_x = A_z = 0$). In this case δB is the same for all three initial states. (e,f) When a time-resolved measurement of the reaction yield is possible, δB is calculated by Eq.8.10, resulting in (e) and (f) for the isotropic and maximally anisotropic case, respectively, where the mixed singlet initial state (as in (c)) was used for both.

In any case, taking the limit of large A we find the exact expression

$$\delta B_{\rm S}^{\rm iso}(B) \to \frac{(B^2+4k^2)^{3/2}}{16Bk^2}\left[\frac{3}{2}\left(\frac{7B^4+39B^2k^2+28k^4}{B^2+k^2}\right)\right]^{1/2} \quad .$$

The minimum occurs at $B/k = 1.15$ and takes the value

$$\delta B_{\rm S}^{\rm iso} = \frac{5.14}{\tau} \quad . \tag{8.12}$$

This is the fourth main result of this work: For a radical pair with one isotropically coupled nuclear spin-1/2, the maximum possible magnetic sensitivity obtained by measuring the time-integrated reaction yield is almost 15 times lower, $\delta B_{\rm S}^{\rm iso} = 14.5\ \delta B_F$, than the highest possible sensitivity allowed by quantum physics and given by Eq. 8.8. This means that there is ample room for improvement.

8.5.3. ANISOTROPIC HYPERFINE COUPLING

By changing to an anisotropic hyperfine interaction we can already get about a factor of 2 improvement in δB. That is, we repeat the calculation for δB taking $\mathscr{H}_B = -B(s_{Dz} + s_{Az}) + A_x s_{Dx} I_x + A_y s_{Dy} I_y + A_z s_{Dz} I_z$. We find that δB is minimized either for $A_x = A \gg B$ and

$A_y = A_z = 0$ or for $A_y = A \gg B$ and $A_x = A_z = 0$. For both cases the minimum is the same for both initial states (i) $|\mathrm{S}\rangle \otimes |\Uparrow\rangle$ and (ii) $|\mathrm{S}\rangle \otimes |\Downarrow\rangle$, and hence the same for (iii) the mixed singlet initial state. This is expected, since both pure initial states are symmetric with respect to the Hamiltonian anisotropy. We thus denote the uncertainty common to all three initial states (i)-(iii) by $\delta B_{\mathrm{S}}^{\mathrm{aniso}}$. As in the isotropic case, the resulting expressions are long. In Appendix C we provide for reference the reaction yield.

As shown in Fig. 8.2(d), $1/\delta B_{\mathrm{S}}^{\mathrm{aniso}}$ increases with increasing A. Like before, we take the limit $A \gg B$ and find

$$\delta B_{\mathrm{S}}^{\mathrm{aniso}}(B) \to \frac{(B^2+k^2)^{3/2}}{2Bk^2}\left[\frac{7B^4+12B^2k^2+2k^4}{4B^2+k^2}\right]^{1/2} \quad .$$

The minimum occurs at $B/k = 0.58$, and takes the value

$$\delta B_{\mathrm{S}}^{\mathrm{aniso}} = \frac{2.27}{\tau} \quad , \tag{8.13}$$

which is still a factor of 6.4 away from δB_F. **To summarize our fifth main result**: The measurement of the integrated reaction yield can at best provide 6.4 times worse magnetic sensitivity than the absolute quantum limit, and this is achieved for the maximally anisotropic hyperfine interaction. The reason the anisotropic coupling outperforms the isotropic in the reaction-yield magnetic sensitivity will be given in Sec. 8.6.1 after we introduce the optimal measurement strategy. Furthermore, we stress that for a given magnetic field B to be estimated, the optimum reaction-yield sensitivity δB is obtained for a particular lifetime of the radical pair on the order of $1/B$. The reason will be given in Sec. 8.7.4.

For completeness, we produce in Figs. 8.2(e),(f) the results of Eq. 8.10, i.e. the case when our measurement time resolution is enough to monitor the instantaneous yield along the reaction. In both cases studied, isotropic and anisotropic, this kind of measurement yields about a factor of 2 improvement in magnetic sensitivity. Specifically, we find $\delta B_{\mathrm{S}}^{\mathrm{iso}} \approx 2.5/\tau$ and $\delta B_{\mathrm{S}}^{\mathrm{aniso}} \approx 1/\tau$, obtained for $A \gg B$ at $B/k \approx 1$. Moreover, both minimums become broader; i.e., there is a larger range of B values close to the optimal δB.

8.6. OPTIMUM INITIAL STATE AND MEASUREMENT OPERATOR FOR RADICAL-PAIR MAGNETOMETERS

The usual measurement scheme of radical-pair reactions, namely the singlet initial state and the measurement of the singlet reaction yield, is enforced by the very nature of these reactions. As shown in the previous section, this measurement is sub-optimal. Towards a possible improvement in magnetic sensitivity, we first need to point to the optimal initial state and the optimal measurement operator. According to the general result of Eq. 8.4, the optimal initial state for a single-nuclear-spin radical pair is the *Greenberger-Horne-Zeilinger* (GHZ) state $|\psi_0\rangle = \frac{1}{\sqrt{2}}\left(|\uparrow\uparrow\Uparrow\rangle + e^{i\phi}|\downarrow\downarrow\Downarrow\rangle\right)$.

Clearly, $|\psi_0\rangle$ belongs to the triplet manifold, and exhibits maximum tripartite (three-particle) entanglement. It is expected that by measuring the electronic spin precession of

this state in the magnetic field one would obtain the optimum sensitivity. Indeed, for the isotropic hyperfine Hamiltonian, which we know already is optimal (see Sec. 8.4.1), the time-evolved state (taking $\phi = 0$) is $|\psi_t\rangle = \frac{1}{\sqrt{2}}\left(|\uparrow\uparrow\Uparrow\rangle + e^{-i2Bt}|\downarrow\downarrow\Downarrow\rangle\right)$. We choose [92] as measurement operator $\mathscr{X} = |\uparrow\uparrow\Uparrow\rangle\langle\downarrow\downarrow\Downarrow| + |\downarrow\downarrow\Downarrow\rangle\langle\uparrow\uparrow\Uparrow|$.

We will now analyze the two scenarios mentioned in Sec. 8.5, that of a time-resolved measurement and that of an integrated measurement. In the former case we get $\langle\mathscr{X}\rangle_t = \langle\psi_t|\mathscr{X}|\psi_t\rangle = \cos(2Bt)$; hence $\partial_B\langle\mathscr{X}\rangle_t = -2t\sin(2Bt)$. Now during dt there will be $kdte^{-kt}$ molecules contributing to this measurement of $\mathscr{X}$. The resulting inverse variance in B is $1/(\delta B)_t^2 = |\partial_B\langle\mathscr{X}\rangle_t|^2/(\Delta\mathscr{X})_t^2$, where $(\Delta\mathscr{X})_t^2 = \langle\mathscr{X}^2\rangle_t - \langle\mathscr{X}\rangle_t^2 = \sin^2(2Bt)$ is the variance of $\mathscr{X}$. Thus we find $1/(\delta B)_t^2 = 4t^2$, which is exactly equal to the maximum quantum Fisher information, leading to $1/(\delta B)^2 = \int_0^\infty kdte^{-kt}/(\delta B)_t^2 = 8/k^2 = 1/(\delta B_F)^2$. It thus follows that with this measurement strategy one achieves the limit δB_F at any B.

In contrast, an integrated measurement is not as capable. Now the integrated $\mathscr{X}$-"yield" is $Y_{\mathscr{X}} = \int_0^\infty \langle\mathscr{X}\rangle_t ke^{-kt}dt = k^2/(4B^2+k^2)$, and its magnetic sensitivity is $\partial_B Y_{\mathscr{X}} = -8Bk^2/(4B^2+k^2)^2$. The square error in $Y_{\mathscr{X}}$ will be the integrated variance of $\mathscr{X}$, weighted by the exponential population decay, i.e. $\delta Y_{\mathscr{X}} = \left[\int_0^\infty (\Delta\mathscr{X})_t^2 ke^{-kt}dt\right]^{1/2} = \left[8B^2/(16B^2+k^2)\right]^{1/2}$. Finally, the magnetic sensitivity will be $\delta B = \delta Y_{\mathscr{X}}/|\partial_B Y_{\mathscr{X}}| = \frac{1}{\sqrt{8}k^2}\left[\frac{(4B^2+k^2)^4}{16B^2+k^2}\right]^{1/2}$. It is seen that $\delta B \geq \delta B_F$, with the equality sign valid only for $B = 0$. That is, in the integrated measurement with the optimal initial state and optimal measurement operator we achieve the optimal sensitivity only at $B = 0$.

The optimum magnetic sensitivity follows from the optimal measurement strategy outlined before, choosing as initial state a maximally entangled state of the triplet electronic manifold, and measuring its spin coherence while it is evolving, always within the triplet manifold. Clearly, this is far from how radical pairs evolve in reality. This leads to a natural question that we will affirmatively address in the following section; i.e., can we control the reaction in a chemically and physically realistic way in order to approach the optimum magnetic sensitivity?

8.6.1. ANISOTROPIC VERSUS ISOTROPIC HAMILTONIAN

Before addressing the previous question, we will explain the fact that the maximally anisotropic hyperfine interaction gives a factor of 2 improvement in δB, as was demonstrated in Sec. 8.5.3. This can be seen to result from the overlap of the state evolved by the magnetic Hamiltonian $\mathscr{H}_B$, which is $\rho_t = e^{-i\mathscr{H}_B t}\rho_0 e^{i\mathscr{H}_B t}$, with the optimal state $\rho_{\text{opt}} = |\psi_t\rangle\langle\psi_t|$ previously defined. For the isotropic Hamiltonian the overlap is zero, while for the anisotropic Hamiltonian it is $\text{Tr}\{\rho_t\rho_{\text{opt}}\} = \left[A^2/(4A^2+16B^2)\right]\sin^2\left(\sqrt{A^2+4B^2}\,t/4\right)$.

Finally, it might sound contradictory that on the one hand we obtain the maximum quantum Fisher information for the isotropic case, while the maximum *reaction-yield* sin-

glet magnetic sensitivity for the anisotropic case. The latter finding does not contradict the former, as the *reaction-yield* sensitivity limit is well below the quantum limit defined by the Fisher information.

8.7. QUANTUM REACTION CONTROL

In Sec. 8.5 we have rigorously proved that the singlet reaction yield with a maximally anisotropic hyperfine interaction can at most provide a magnetic sensitivity 6.4 times worse than the absolute quantum limit. A natural question is, how can one do better? In particular, given the discussion of the previous section, how can one do better in a chemically realistic way? Towards addressing this question we will (i) take advantage of a very promising approach of optically switching the conformation of the radical pair, recently proposed in [123], and (ii) include a realistic exchange interaction in the Hamiltonian, which changes (a) the initial spin state before the radical pair commences its magnetometric state evolution, and (b) the effective measurement basis before it recombines.

In summary, given the maximally anisotropic coupling that resulted from the optimization of Sec. 8.5.3, the reaction control proposed in [123], and the modified initial state and measurement basis we introduce in the following, we will show that the obtained sensitivity δB is just a factor 2 away from the quantum limit δB_F of Eq. 8.8. Moreover, compared to the approach of [123], we reduce δB by a factor of 3.

8.7.1. THE MAGNETIC SENSITIVITY GAIN RESULTING FROM PULSING THE CONFORMATION OF THE RADICAL PAIR

We briefly reiterate the method of [123], since the added advantage we introduce by the exchange Hamiltonian is based on the same method of optically pulsing the conformation of the radical pair. In particular, the authors in [123] suggest binding the donor and acceptor parts of the radical pair to the two ends of a molecular switch, the conformation of which can be laser-controlled. Schematically, this is shown in Fig. 8.3. The rationale behind this idea is the following. As shown previously, the magnetic sensitivity depends on $g_t(A,B) = \partial_B \langle Q_S \rangle_t$, where $\langle Q_S \rangle_t = \mathrm{Tr}\{\rho_t Q_S\}$ is the so-called singlet fidelity of the radical-pair state at time t, and A, B the hyperfine coupling and the magnetic field, respectively. For reference, the functions g_t are given in Appendix D for the Hamiltonians considered in this work. In Fig. 8.4(a) we plot an example of $g_t(A,B)$, which is seen to be symmetric about zero. Thus, when integrated with the exponential population decay, ke^{-kt}, and the lifetime $1/k$ is long enough to contain many positive and negative swings of $g_t(A,B)$, magnetic sensitivity is suppressed.

The idea of [123] is to pulse the conformation of the molecular switch by an external laser. When the switch is open, the radical pair evolves unitarily by the magnetic Hamiltonian, which for later use we call $\mathscr{H}_{\text{trans}}$. For example, this would be either $\mathscr{H}_{\text{trans}} = -B(s_{Dz}+s_{Az}) + A\mathbf{s}_D\cdot\mathbf{I}$ for the isotropic or $\mathscr{H}_{\text{trans}} = -B(s_{Dz}+s_{Az}) + As_{Dx}I_x$ for the anisotropic

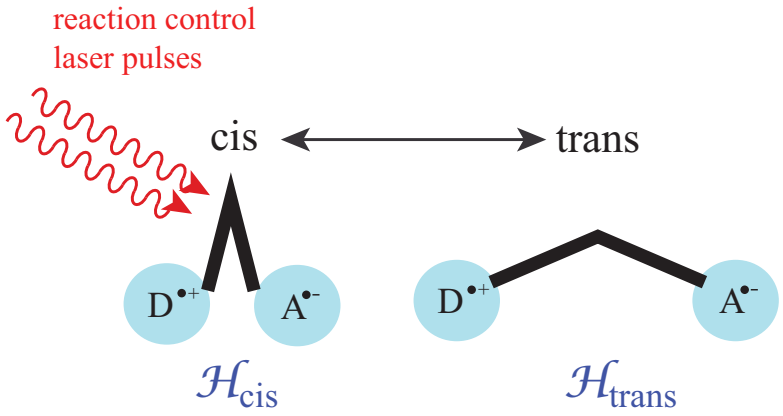

Figure 8.3: According to the proposal of [123], radical-pair reactions can be controlled by binding the two radicals to the two ends of a molecular switch, the conformation of which can be laser-controlled. We here consider that apart from the Zeeman and hyperfine coupling term in the magnetic Hamiltonian, in the *cis*-conformation there is also a finite exchange coupling, which the authors in [123] take to be infinite.

case. When the switch is closed, the authors in [123] argue, the short distance between D and A will turn on the exchange interaction [57], $J\mathbf{s}_D \cdot \mathbf{s}_A$. For large exchange coupling J, pertinent to the small D-A separation at the closed switch position, the singlet and triplet energy levels separate by J and singlet-triplet mixing is suppressed, so only recombination can take place. If the reaction control laser is turned on at those instances (Fig. 8.4b) where $g_t(A,B)$ is positive (and does not have fast oscillations, as in the middle part of Fig. 8.4a), then the reaction-yield magnetic sensitivity will be enhanced, as demonstrated in [123].

8.7.2. MEASUREMENT SCHEME INVOLVING OPTIMAL STATE PREPARATION AND READ OUT

Taking advantage of the cis $\rightleftarrows$ trans modulation that can be externally controlled by the reaction control laser pulses, we now analyze our measurement scheme approaching the absolute quantum limit δB_F. As shown in Fig. 8.5, we first prepare the radical-pair state in the electron singlet state. The nuclear spin is usually in an equal mixture of the states $|\Uparrow\rangle$ and $|\Downarrow\rangle$. Towards better exhibiting the connection of this biochemical reaction with quantum metrology, we take the quantum circuit perspective and depict the electron singlet state as produced from $|\downarrow\downarrow\rangle$ by a Hadamard gate followed by a controlled-NOT gate. In radical pairs, this state preparation is naturally realized by the electron transfer producing the charge-separated state, since the precursor neutral molecule is already in the singlet state.

Step 1 At $t = 0$ all molecular switches are in the "closed" conformation and the radical pairs in the state $\rho_0 = Q_S/\mathrm{Tr}\{Q_S\} = |\mathrm{S}\rangle\langle\mathrm{S}| \otimes \frac{1}{2}\mathbb{1}$, which describes a singlet state for the electrons and a maximally mixed state for the nuclear spin-1/2. Now, while the authors in [123] open the switch at this time, using a laser pulse strong enough to open all molecular switches, we wait for a time τ_1 and act on the initial state with the Hamiltonian $\mathscr{H}_{\rm cis}$. While the authors in [123] consider an exchange coupling J too large to allow any S-T mixing, we take J to be a finite optimization parameter. We thus take $\mathscr{H}_{\rm cis} = -B(s_{Dz} + s_{Az}) + As_{Dx}I_x + J\mathbf{s}_A \cdot \mathbf{s}_D$. The

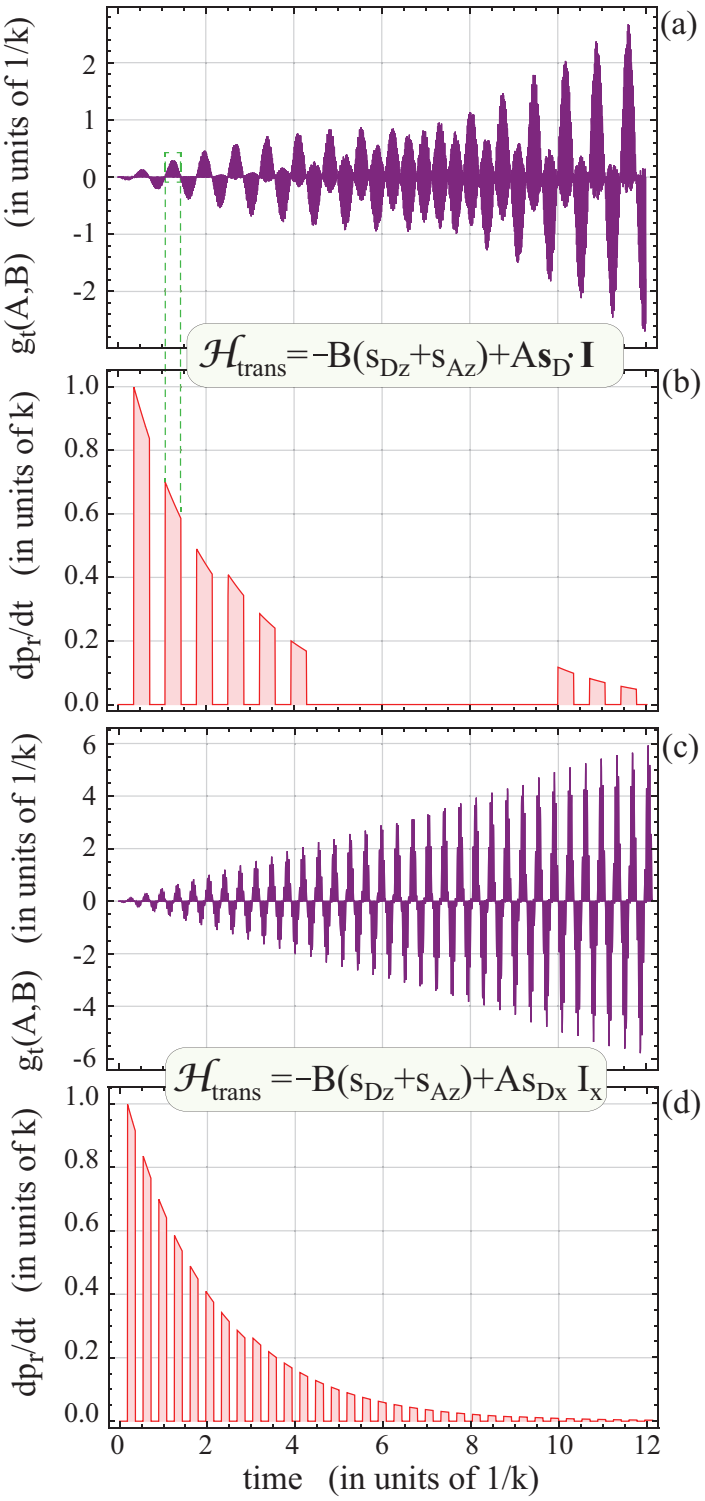

Figure 8.4: Time-dependence of $g_t(A,B) = \partial_B \mathrm{Tr}\{\rho_t Q_S\}$, where $\rho_t = e^{-i\mathcal{H}_{\mathrm{trans}}t}\rho_0 e^{i\mathcal{H}_{\mathrm{trans}}t}$, for a mixed singlet initial state $\rho_0 = Q_S/\mathrm{Tr}\{Q_S\}$, and (a) an isotropic and (c) a maximally anisotropic hyperfine interaction. In (b) and (d) we depict the corresponding probability per unit time, $dp_r/dt = ke^{-kt}$, for the molecular switches to close by the reaction control laser pulses, which are tuned to coincide with the positive swings of g_t. In the middle of trace (b) there are a number of pulses missing, since there the corresponding g_t is on average zero and hence will not contribute to the singlet-yield magnetic sensitivity. For all plots it was $A = 352k$ and $B = 17.6k = A/20$.

duration τ_1 of the action of $\mathscr{H}_{\text{cis}}$ is a free parameter, however constrained by $\tau_1 \ll 1/k$, so that the radical pairs do not have enough time to recombine through the singlet channel. Essentially, the action of $\mathscr{H}_{\text{cis}}$ for a time τ_1 prepares the initial state of the radical pair in a state other than ρ_0.

Step 2 At time $t = \tau_1$ a strong reaction control laser pulse opens all molecular switches, and the two radicals are now far apart, so that $J \to 0$ is a good approximation, given the exponential dependence of J on inter-radical distance [57]. From $t = \tau_1$ until $t = \tau_1 + \tau_2$ the Hamiltonian $\mathscr{H}_{\text{trans}}$ effects the singlet-triplet conversion forming the main magnetometric state evolution.

Step 3 At time $t = \tau_1 + \tau_2$ a weak reaction control laser pulse closes some of the switches. The pulse energy is chosen so that the rate of closing is equal to the radical-recombination rate k. This pulse is the first pulse shown in the pulse sequence of Fig. 8.4(d). Now in our model, the Hamiltonian $\mathscr{H}_{\text{cis}}$ will act again until the radical pairs of those switches that closed recombine. In the model of [123], the radical pairs just recombine at some time after the switches close without any state evolution taking place before recombination.

Step 4 The radical pairs of those switches that did not close in step 3 continue to evolve under $\mathscr{H}_{\text{trans}}$. Step 3 is then repeated with the next weak reaction control pulse, and so on. Thus, the pulse repetition period is $2\pi/B$, which is the envelope period of the function $g_t(A,B)$ shown in Fig. 8.4(c), while the pulse width is π/B, so that only the positive swings of $g_t(A,B)$ contribute to the yield's magnetic sensitivity. Hence for any given radical pair, the time τ_2 during which $\mathscr{H}_{\text{trans}}$ is acting is some odd multiple of π/B, plus the time within the pulse, at which this radical pair recombines.

8.7.3. RESULTS AND INTERPRETATION

The magnetic sensitivity resulting from the quantum circuit of Fig. 8.5 is shown in Fig. 8.6 in two equivalent ways. In Fig. 8.6(a) we plot the yield sensitivity $\Lambda_B = |dY_S/dB|$, in order to directly compare with the result of [123]. In Fig. 8.6(b) we plot the absolute value of δB, normalized to the optimum quantum limit δB_F. It is evident that (a) the choice of the maximally anisotropic Hamiltonian and (b) the inclusion of the action of the exchange interaction in $\mathscr{H}_{\text{cis}}$ lead to an enhancement by a factor of 3 compared to [123], and put the scheme of Fig. 8.5 a factor of 2 away from the absolute quantum limit. The factor of 3 is equally attributed to (a) and (b).

The physical interpretation of the enhancement of the magnetic sensitivity by the exchange interaction is the initial phase difference between the singlet and triplet states resulting from the initial action of $\mathscr{H}_{\text{cis}}$. Due to this phase difference, the action of $\mathscr{H}_{\text{trans}}$ fully transforms the $|S\rangle$ into a $|T_0\rangle$ state, thus sensitively affecting the results of the recombination measurement. Without this phase, i.e. setting $J = 0$, the singlet and triplet states both have significant populations at the end of the circuit and dilute the magnetic sensitivity of the recombination products. Our quantum circuit scheme of Fig. 8.5 reminds one of Ramsey spectroscopy, where an initial $\pi/2$ pulse produces an atomic hyperfine coherence,

which evolves under the clock transition hyperfine Hamiltonian, and is refocused by the final $\pi/2$ pulse. To further clarify the workings of this quantum reaction control the following remarks are in order.

(**1**) The pulse sequence of the reaction control laser shown in Fig. 8.4(d) is synchronized with the positive swings of g_t shown in Fig. 8.4(c). This necessitates some prior (and approximate) knowledge of the magnetic field, a feature common with the reaction control scheme of [123].

(**2**) The time interval τ_1 during which $\mathscr{H}_{\rm cis}$ acts before the molecular switch opens is taken $1/10k$, so that radical-pair recombination is negligible (it actually increases the obtained δB by 5%) . After the switch closes, $\mathscr{H}_{\rm cis}$ acts for time τ_3 before the radical pairs recombine. This time is taken to follow the exponential distribution with parameter k, i.e. $\mathscr{H}_{\rm cis}$ acts for a time as long as the radical pair takes to recombine on average, i.e. $\tau_3 \approx 1/k$.

(**3**) The inclusion of $H_{\rm cis}$, which includes the exchange interaction, was motivated by (i) other works [130], where a controlled-NOT gate is shown to be a crucial element in metrology, and (ii) the fact that the controlled-NOT gate is naturally realized by the exchange interaction, as analyzed in [131].

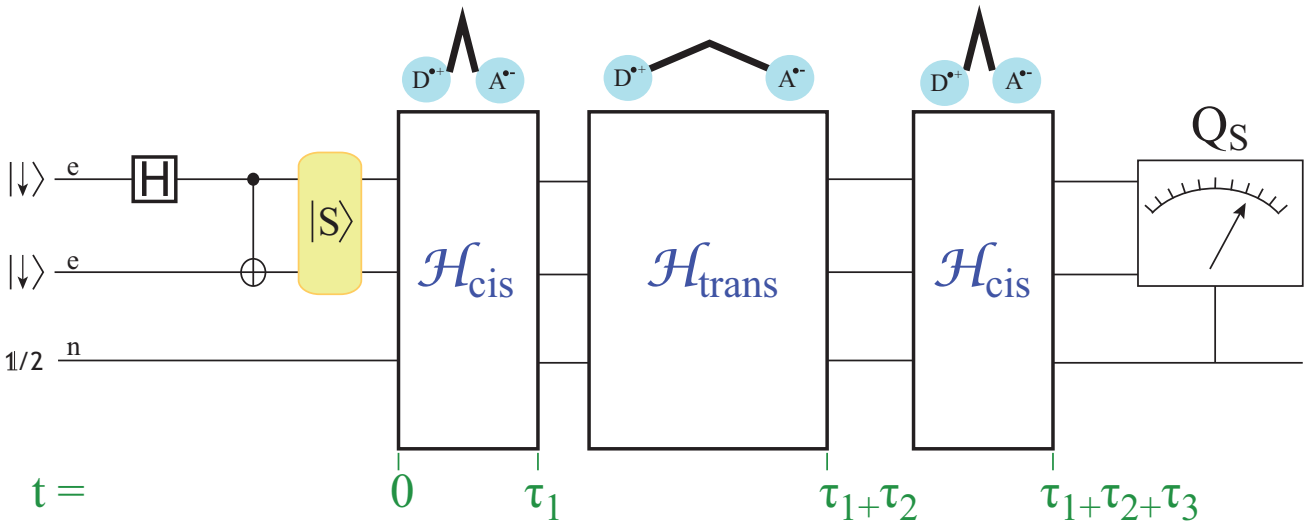

Figure 8.5: Quantum circuit for a quantum-limited biochemical magnetometer, approaching the absolute quantum limit on δB by a factor of 2. The two unpaired electron spins of the radical pair start out in the singlet state. Circuit-wise, this follows from $|\downarrow\downarrow\rangle$ by application of a Hadamard and a controlled-NOT gate. The nuclear spin is unpolarized, compactly denoted by the 2×2 unit matrix divided by 2, $\mathbb{1}/2$ (equivalently, there are two such circuits for each of the two nuclear spin states). The Hamiltonian $\mathscr{H}_{\rm cis}$, including a finite exchange interaction, acts upon the initial radical-pair state for a time τ_1. A reaction control laser pulse opens all molecular switches, and the magnetometric Hamiltonian $\mathscr{H}_{\rm trans}$ acts for a time τ_2. Another reaction control pulse closes some switches, and upon closure the radical-pair spin state evolves again by $\mathscr{H}_{\rm cis}$ until it recombines. The singlet recombination yield, i.e. the measurement of the singlet projector Q_S, carries the magnetic field information.

We let the exchange coupling J be a free optimization parameter. The minimum δB was found for $J = 0.65A$. For a typical hyperfine coupling A of several Gauss, the resulting value of J is also on the order of several Gauss. Now, $J = J_0 e^{-\beta r}$, where r is the donor-acceptor distance, and typical values [57] of J_0 and β are 8×10^{13} μT and 14 nm^{-1}, respectively. For J to be on the order of several Gauss, the distance r in the closed position of the switch must be around 1.8 nm. This is quite larger than the D-A distance of 0.5 nm in the closed position of azobenzene [132], proposed in [123] as a molecular switch. So for the reaction control studied here azobenzene is not an ideal candidate, and other candidates [133–136] should be investigated for D-A separation and chemical affinity with the radical pair.

Furthermore, in Fig. 8.6(c) we plot the minimum value of the obtained sensitivity, $\delta B_{\min}$ (i.e. the minimum of the red solid trace of Fig. 8.6b) as a function of the exchange coupling J. However, as the exchange coupling depends on inter-radical separation, which is modulated by molecular vibrations, in reality we have to average the trace of Fig. 8.6(c). Indeed, evaluating $J = J_0 e^{-\beta r}$ around $r = 1.8$ nm, and taking a variation of r by 0.05 nm, which is typical for studies on the relaxation effect of J-modulation due to molecular vibrations [137], leads to a factor of 2 change in J, similar to the J-range of Fig. 8.6(c). We thus obtain a final $\delta B = 2.2\ \delta B_F$, i.e. 10% higher than the value for a constant (and optimum) J.

(**4**) Further, there are two points that might cause a misunderstanding. We first note that although the reaction control pulse sequence introduces a timing in the measurement of reaction yields, the measurement is not of the instantaneous type described in Sec. 8.5.1, since we still measure an integrated yield, as does the scheme in [123]. Second, the reader might argue that we use an exchange interaction, which was absent in the optimization presented in Secs. 8.4 and 8.5. However, the exchange interaction is used in $\mathscr{H}_{\text{cis}}$, which is just a state-preparation process, changing the initial singlet state and the final measurement basis. We thus engineer an initial state which is more optimal than ρ_0, and the actual magnetometry takes place during the action of $\mathscr{H}_{\text{trans}}$, which does not include any spin exchange.

8.7.4. WHEN IS REACTION CONTROL NECESSARY?

Finally, we elaborate on a subtle point regarding practical implementation. In Sec. 8.5, evaluating the optimum sensitivity of the reaction yield in the case of the maximally anisotropic coupling, we found $\delta B_{\text{S}}^{\text{aniso}}$ to be 6.4 times away from the absolute quantum limit δB_F. This optimum, however, is realized for a specific value of B, e.g. $B = 0.58k$ for the anisotropic case, and a hyperfine coupling $A \gg B$. In other words, if one wants to realize the limit $\delta B_{\text{S}}^{\text{aniso}}$ at e.g. earth's field, one needs to find a radical pair having a lifetime $\tau = 0.58/B_{\text{earth}}$. We can now explain this earlier finding: because at that lifetime the reaction is almost complete during one (positive or negative) swing of the sensitivity function g_t, and further swings do not suppress sensitivity.

Now, it is evident by looking at Fig. 8.6(b) that the optimum sensitivity $\delta B_{\text{S}}^{\text{aniso}}$ we obtain just by using the optimal RP lifetime (i.e. without any reaction control) is the same as the one achieved by the authors of [123] using the reaction control, but taking $B = 17.6k$, which

is far from the magnetic field value at which $\delta B_{\mathrm{S}}^{\mathrm{aniso}}$ is optimized. This leads to the following statement summarizing our findings: One can realize the optimum uncertainty δB at a desired magnetic field B if it is possible to engineer a radical pair with the specified lifetime and an anisotropic hyperfine coupling approaching the maximal anisotropy. For example, the lifetime engineering could result from molecular bridges [82] interleaving the donor and acceptor. On the other hand, if such experimental control of the radical pair's lifetime is not possible, then the reaction control scheme of [123] and its modification presented here offer a generally useful alternative.

8.8. DISCUSSION

In this work we introduced the tools of quantum metrology to put formal and fundamental limits to the magnetic sensitivity of radical-pair reactions, a class of spin-dependent biochemical reactions central in the field of spin chemistry and relevant to the avian compass mechanism. Knowing what is the fundamental limit is crucial for understanding how successful a particular measurement scheme is, and for motivating the search for new measurement schemes if there is room for improvement. This has been shown to be the case with the reaction-yield measurement, which we have shown to be sub-optimal by almost an order of magnitude. We then took advantage of a recently proposed reaction control scheme, modified the scheme by inclusion of the exchange interaction along the lines of a quantum circuit and Ramsey interferometry, and demonstrated a close approach to the absolute quantum limit. Regarding future work, we point to two venues of research naturally following from here.

8.8.1. IS ENTANGLEMENT A RESOURCE?

A recurring discussion [29, 34] in the quantum dynamics of radical-pair reactions, in particular in relevance to the avian compass, is whether electron spin entanglement is a resource. In other words, whether the initial singlet electron state, which is maximally entangled, and its subsequent evolution, more or less maintaining the initial entanglement, enhances whatever biological performance radical-pair reactions have. Regarding the radical-pair magnetometer we have considered in this work, the answer is clear: Considering a radical pair with a spin-independent lifetime ($k_S = k_T = k = 1/\tau$), and neglecting the intrinsic singlet-triplet decoherence mechanism we introduced [26, 55], electron spin entanglement obviously helps *in principle*. Indeed, based on the discussion of Sec. 8.3.1 and Sec. 8.3.2, for a system consisting of just two *uncorrelated* electron spins the optimum magnetic sensitivity is $\tau\delta B = 1/2$. Allowing quantum correlations one can in principle obtain a $\sqrt{2}$ improvement, i.e. $\tau\delta B = 1/2\sqrt{2} = 0.35$. Our reaction control scheme of Fig. 8.5 leads to $\tau\delta B = 0.78$, but this does not imply that entanglement "does not help". In other words, it is not straightforward to arrive at a definitive statement with such comparisons. On the one hand it is inconceivable how to experiment with two free electron spins in a chemical environment. Radical pairs offer such a possibility. Similarly, there is no immediate way to controllably "switch-off" entanglement within the radical-pair reactions. Put

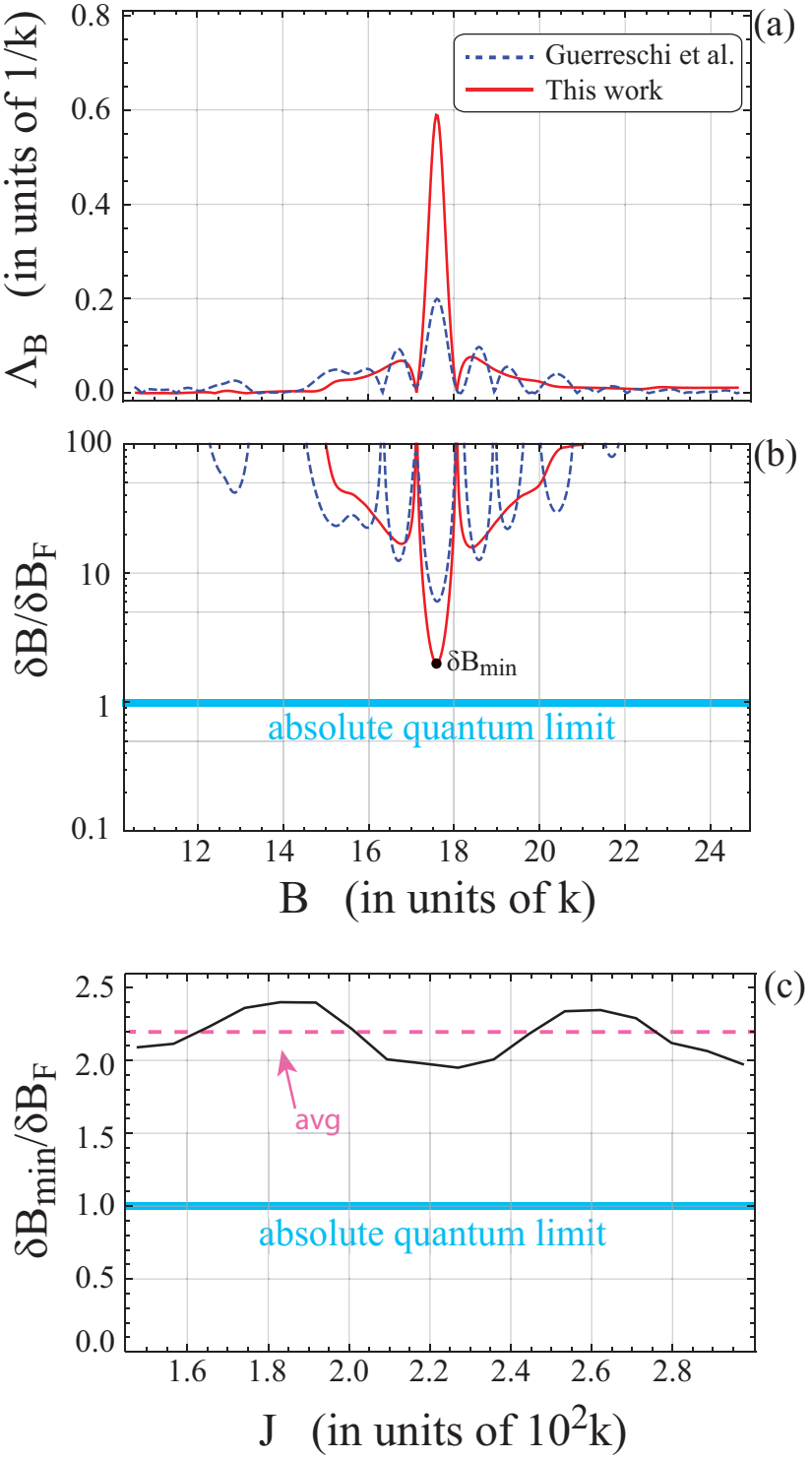

Figure 8.6: (a) Magnetic sensitivity of the singlet reaction yield, $\Lambda_B = |dY_S/dB|$, and (b) error δB in the estimation of the magnetic field, normalized by the absolute quantum limit δB_F. The blue dashed line reproduces the result of the reaction control scheme of [123], while the red solid line is the result of this work. Our reaction control scheme approaches δB_F within a factor of 2. (c) The minimum of the red solid line in (b) is plotted as a function of the exchange coupling J. For $J = 0.65A = 229k$, we obtain $\delta B = 2\delta B_F$. But nearby values of J are induced by molecular vibrations; hence averaging trace (c) leads to the realistic uncertainty 2.2 times away from δB_F.

differently, even though the achieved sensitivity $\tau\delta B = 0.78$ happens to be worse than the two-uncorrelated-spins case, further analysis is required to demonstrate whether or not (or what part of) $\tau\delta B = 0.78$ is attributed to entanglement.

Moreover, according to our understanding [55], singlet-triplet decoherence is an unavoidable feature of the radical-pair mechanism itself, and in the case of equal recombination rates ($k_S = k_T = k$) leads to a master equation for ρ that reads $d\rho/dt = -i[\mathscr{H}, \rho] - k(Q_S\rho + \rho Q_S - 2Q_S\rho Q_S) - k\rho$. In other words, in this work we omitted the second term of the previous equation, first because its validity is not generally accepted and we wish to decouple this work from the relevant debate, second because omitting it considerably simplifies the calculations, and third we obtain the sought after fundamental limits in the idealized and intuitive physical context of unitary evolution.

Nevertheless, the role of decoherence in the magnetic sensitivity δB ought to be addressed in detail, as it is known that the advantage due to entangled states might deteriorate [138]. Hence it remains an unsettled issue whether entanglement is a resource for this kind of biochemical magnetometer.

8.8.2. CHEMICAL COMPASS

A natural extension of this work is to study the fundamental limit $\delta\phi$ in estimating the angle of the magnetic field with respect to a molecular frame of reference. This is directly relevant to the avian compass function of radical-pair reactions, and the relevant study will be undertaken elsewhere.

IV

APPENDIX

A

SPHEROIDAL HYPERFINE INTERACTION

For the spheroidal hyperfine interaction (8.7) considered in Sec. 8.4.1,

$$\mathscr{H}_B = -B(s_{Dz} + s_{Az}) + As_{Dx}I_x + As_{Dy}I_y + as_{Dz}I_z$$

the eigenvalues of $\mathscr{H}_B$ are $a/4$ (doubly degenerate), $a/4 \pm B$, $\left(-a - 2B \pm 2\sqrt{A^2+B^2}\right)/4$ and $\left(-a + 2B \pm 2\sqrt{A^2+B^2}\right)/4$.

Taking care of the degeneracy in the calculation of h_B (8.3), the eigenvalues of h_B are found to be:

0 (doubly degenerate),

$\lambda_{\pm}^{(1)} = \pm t$,

$\lambda_{\pm}^{(2)} = \pm t/2 \pm \frac{\left[(A^2+B^2)B^2t^2+2A^2-2A^2\cos\left(\sqrt{A^2+B^2}\,t\right)\right]^{1/2}}{2(A^2+B^2)}$, and

$\lambda_{\pm}^{(3)} = \pm t/2 \mp \frac{\left[(A^2+B^2)B^2t^2+2A^2-2A^2\cos\left(\sqrt{A^2+B^2}\,t\right)\right]^{1/2}}{2(A^2+B^2)}$.

By inspection it is seen that $|\lambda_{\pm}^{(2)}| \geq |\lambda_{\pm}^{(3)}|$, but due to the cosine term it is not immediately obvious how $|\lambda_{\pm}^{(1)}|$ compares to $|\lambda_{\pm}^{(2)}|$. We can prove that for all times $|\lambda_{\pm}^{(1)}| \geq |\lambda_{\pm}^{(2)}|$. Indeed, take $\lambda_{+}^{(1)}$ and $\lambda_{+}^{(2)}$ and subtract from both the common term $t/2$. We need to show that $\left[(A^2+B^2)B^2t^2+2A^2-2A^2\cos\left(\sqrt{A^2+B^2}\,t\right)\right]^{1/2}/2(A^2+B^2)$ is less than $t/2$, or their ratio smaller than 1. The maximum value of the term involving the cosine occurs at $t = (2n+1)\pi/\sqrt{A^2+B^2}$, where $n = 0, 1, \ldots$. Then the maximum value of the ratio is

$$\sqrt{\frac{4A^2+(2n+1)^2\pi^2B^2}{(2n+1)^2\pi^2A^2+(2n+1)^2\pi^2B^2}} < 1 \quad \forall\ n \quad .$$

Thus the maximum and minimum eigenvalues of h_B are t and $-t$, respectively.

B

Ellipsoidal Hyperfine Interaction

For the ellipsoidal hyperfine coupling (8.9) discussed in Sec. 8.4.2, the eigenvalues of h_B are found to be:

$$\lambda_{\pm}^{(1)} = t/2 \pm \frac{Bt}{\sqrt{(A_x-A_y)^2+4B^2}},$$

$$\lambda_{\pm}^{(2)} = t/2 \pm \frac{\left[B^2\left((A_x+A_y)^2+4B^2\right)t^2+4(A_x+A_y)^2\sin^2\left(\frac{1}{4}\sqrt{(A_x+A_y)^2+4B^2}\,t\right)\right]^{1/2}}{\left[(A_x+A_y)^2+4B^2\right]},$$

$$\lambda_{\pm}^{(3)} = -t/2 \pm \frac{\left[B^2\left((A_x+A_y)^2+4B^2\right)t^2+4(A_x+A_y)^2\sin^2\left(\frac{1}{4}\sqrt{(A_x+A_y)^2+4B^2}\,t\right)\right]^{1/2}}{\left[(A_x+A_y)^2+4B^2\right]}, \text{ and}$$

$$\lambda_{\pm}^{(4)} = -t/2 \pm \frac{\left[B^2\left((A_x-A_y)^2+4B^2\right)t^2+4(A_x-A_y)^2\sin^2\left(\frac{1}{4}\sqrt{(A_x-A_y)^2+4B^2}\,t\right)\right]^{1/2}}{\left[(A_x-A_y)^2+4B^2\right]}.$$

Now it is less straightforward to find the maximum (and similarly the minimum) eigenvalue, as for some times $\lambda_+^{(1)}$ is the maximum, while at other times it is $\lambda_+^{(2)}$. However, we can prove as in Appendix A that *at any time* the maximum eigenvalue is smaller than or equal to t, and similarly the minimum eigenvalue is larger than or equal to $-t$. Hence the ellipsoidal case cannot exceed the spheroidal $F_B^{\max}$.

C

Singlet Reaction Yield

For the Hamiltonian $\mathscr{H}_B = -B(s_{Dz}+s_{Az}) + A\mathbf{I}\cdot\mathbf{s}_D$, we calculate the singlet reaction yields $Y_{\mathrm{S}\Uparrow}^{\mathrm{iso}}$ and $Y_{\mathrm{S}\Downarrow}^{\mathrm{iso}}$ corresponding to the initial states $|\mathrm{S}\rangle\otimes|\Uparrow\rangle$ and $|\mathrm{S}\rangle\otimes|\Downarrow\rangle$, respectively. For the Hamiltonian $\mathscr{H}_B = -B(s_{Dz}+s_{Az}) + As_{Dx}I_x$, and for all three initial states considered before we find a common singlet reaction yield $Y_{\mathrm{S}}^{\mathrm{aniso}}$. The results are

$$Y^{\rm iso}_{\rm S\Uparrow\Downarrow}=\frac{1}{8}\Big[\frac{3A^2+4B^2}{A^2+B^2}+\frac{A^2k^2}{(A^2+B^2)(A^2+B^2+k^2)}+\frac{8(A^2\pm 2AB+2B^2)k^2+16k^4}{A^2B^2+4(A^2\pm AB+B^2)k^2+4k^4}\Big] \tag{C.1}$$

$$Y^{\rm aniso}_{\rm S}=1-\frac{A^2B^2}{4(A^2+4B^2)(B^2+k^2)}-\frac{A^4(A^2+8B^2+4k^2)}{4(A^2+4B^2)(A^4+8(A^2+8B^2)k^2+16k^4)}-\frac{A^2}{4(A^2+4B^2+4k^2)} \tag{C.2}$$

The + (−) sign in the third term of (C.1) corresponds to $|{\rm S}\rangle\otimes|\Uparrow\rangle$ ($|{\rm S}\rangle\otimes|\Downarrow\rangle$). Taking the average $(Y^{\rm iso}_{\rm S\Uparrow}+Y^{\rm iso}_{\rm S\Downarrow})/2$, we reproduce the result of [139].

D

Instantaneous Magnetic Sensitivity

The magnetic field sensitivity of the singlet fidelity $g_t(A,B)=\partial_B{\rm Tr}\{\rho_t Q_S\}$, where $\rho_t=e^{-i\mathscr{H}_B t}\rho_0 e^{i\mathscr{H}_B t}$, is given (after setting $\alpha^2=A^2+B^2$) by the expressions

$$g_t(A,B)=-\frac{A^2}{4\alpha^4}\Big[\alpha t\cos\Big(\frac{\alpha t}{2}\Big)-2\sin\Big(\frac{\alpha t}{2}\Big)\Big]\Big[\alpha\sin\Big(\frac{(A+B)t}{2}\Big)+B\sin\Big(\frac{\alpha t}{2}\Big)\Big]\quad , \tag{D.1}$$

$$g_t(A,B)=\frac{A^2}{4\alpha^4}\Big[\alpha t\cos\Big(\frac{\alpha t}{2}\Big)-2\sin\Big(\frac{\alpha t}{2}\Big)\Big]\Big[\alpha\sin\Big(\frac{(A-B)t}{2}\Big)-B\sin\Big(\frac{\alpha t}{2}\Big)\Big]\quad , \tag{D.2}$$

$$g_t(A,B)=-\frac{A^2}{4\alpha^4}\Big[\alpha t\cos\Big(\frac{\alpha t}{2}\Big)-2\sin\Big(\frac{\alpha t}{2}\Big)\Big]\Big[\alpha\cos\Big(\frac{At}{2}\Big)\sin\Big(\frac{Bt}{2}\Big)+B\sin\Big(\frac{\alpha t}{2}\Big)\Big]\quad , \tag{D.3}$$

for the isotropic Hamiltonian $\mathscr{H}_B=-B(s_{Dz}+s_{Az})+A\mathbf{s}_D\cdot\mathbf{I}$, and initial states (a) $|{\rm S}\rangle\otimes|\Uparrow\rangle$, (b) $|{\rm S}\rangle\otimes|\Downarrow\rangle$, and (c) an equal mixture of (a) and (b), respectively.

For the maximally anisotropic Hamiltonian $\mathscr{H}_B=-B(s_{Dz}+s_{Az})+As_{Dx}I_x$, all three initial states produce the same expression for g_t, given (after setting $\beta^2=A^2+4B^2$) by

$$g_t(A,B)=-\frac{A^2}{\beta^4}\sin\Big(\frac{Bt}{2}\Big)\Big[\beta t\cos\Big(\frac{\beta t}{4}\Big)-4\sin\Big(\frac{\beta t}{4}\Big)\Big]\Big[\beta\cos\Big(\frac{Bt}{2}\Big)\cos\Big(\frac{\beta t}{4}\Big)+2B\sin\Big(\frac{Bt}{2}\Big)\sin\Big(\frac{\beta t}{4}\Big)\Big]\quad . \tag{D.4}$$

BIBLIOGRAPHY

[1] N. Lambert, Y.-N. Chen, Y.-C. Cheng, C.-M. Li, G.-Y. Chen, and F. Nori, *Quantum biology,* Nature Physics **8**, 10 (2012).

[2] S. Huelga and M. Plenio, *Vibrations, quanta and biology,* Contemporary Physics **54**, 181 (2013).

[3] J. Cai, *Quantum biology: explore quantum dynamics in biological systems,* Science China Information Sciences **59**, 1 (2016).

[4] G. S. Engel, T. R. Calhoun, E. L. Read, T.-K. Ahn, T. Mancal, Y.-C. Cheng, R. E. Blankenship, and G. R. Fleming, *Evidence for wavelike energy transfer through quantum coherence in photosynthetic systems,* Nature **446**, 782 (2007).

[5] H. Lee, Y.-C. Cheng, and G. R. Fleming, *Coherence Dynamics in Photosynthesis: Protein Protection of Excitonic Coherence,* Science **316**, 1462 (2007).

[6] Z.-q. Yin and T. Li, *Bringing quantum mechanics to life: from Schroedinger's cat to Schroedinger's microbe,* Contemporary Physics **00**, 1 (2016).

[7] M. Mohseni, P. Rebentrost, S. Lloyd, and A. Aspuru-Guzik, *Environment-assisted quantum walks in photosynthetic energy transfer,* Journal of Chemical Physics **129**, 174106 (2008).

[8] M. B. Plenio and S. F. Huelga, *Dephasing-assisted transport: Quantum networks and biomolecules,* New Journal of Physics **10**, 1 (2008).

[9] J. Wu, F. Liu, J. Ma, R. J. Silbey, and J. Cao, *Efficient energy transfer in light-harvesting systems: Quantum-classical comparison, flux network, and robustness analysis,* Journal of Chemical Physics **137**, 174111 (2012).

[10] J. S. Briggs and A. Eisfeld, *Equivalence of quantum and classical coherence in electronic energy transfer,* Physical Review E **83**, 4 (2011).

[11] M. M. Wilde, J. M. McCracken, and A. Mizel, *Could light harvesting complexes exhibit non-classical effects at room temperature?* Proceedings of the Royal Society A: Mathematical, Physical and Engineering Science **466**, 1347 (2010).

[12] M.-J. Tao, Q. Ai, F.-G. Deng, and Y.-C. Cheng, *Proposal for probing energy transfer pathway by single-molecule pump-dump experiment,* Scientific Reports **6**, 27535 (2016).

[13] W. Wiltschko and R. Wiltschko, *Magnetic compass of European robins,* Science **176**, 62 (1972).

[14] R. Wiltschko and W. Wiltschko, *Sensing Magnetic Directions in Birds: Radical Pair Processes Involving Cryptochrome,* Biosensors **4**, 221 (2014).

[15] R. Wiltschko, K. Stapput, P. Thalau, and W. Wiltschko, *Directional orientation of birds by the magnetic field under different light conditions,* Journal of the Royal Society Interface **7**, 163 (2010).

[16] K. Schulten, C. E. Swenberg, and A. Weller, *A Biomagnetic Sensory Mechanism Based on Magnetic Field Modulated Coherent Electron Spin Motion,* Zeitschrift für Physikalische Chemie **111**, 1 (1978).

[17] W. Wiltschko, R. Wiltschko, and U. Munro, *Light-dependent magnetoreception in birds: Does directional information change with light intensity?* Naturwissenschaften **87**, 36 (2000).

[18] W. Wiltschko, K. Stapput, P. Thalau, and R. Wiltschko, *Avian magnetic compass: fast adjustment to intensities outside the normal functional window.* Die Naturwissenschaften **93**, 300 (2006).

[19] T. Ritz, *Quantum effects in biology: Bird navigation,* Procedia Chemistry **3**, 262 (2011).

[20] T. Ritz, P. Thalau, J. B. Phillips, R. Wiltschko, and W. Wiltschko, *Resonance effects indicate a radical-pair mechanism for avian magnetic compass,* Nature **429**, 177 (2004).

[21] W. Wiltschko, J. Traudt, O. Güntürkün, H. Prior, and R. Wiltschko, *Lateralization of magnetic compass orientation in a migratory bird,* Nature **419**, 467 (2002).

[22] S. Engels, N.-L. Schneider, N. Lefeldt, C. M. Hein, M. Zapka, A. Michalik, D. Elbers, A. Kittel, P. J. Hore, and H. Mouritsen, *Anthropogenic electromagnetic noise disrupts magnetic compass orientation in a migratory bird,* Nature **509**, 353 (2014).

[23] E. M. Gauger, E. Rieper, J. J. L. Morton, S. C. Benjamin, and V. Vedral, *Sustained Quantum Coherence and Entanglement in the Avian Compass,* Physical Review Letters **106**, 040503 (2011).

[24] J. N. Bandyopadhyay, T. Paterek, and D. Kaszlikowski, *Quantum Coherence and Sensitivity of Avian Magnetoreception,* Physical Review Letters **109**, 110502 (2012).

[25] E. M. Gauger and S. C. Benjamin, *Comment on "Quantum Coherence and Sensitivity of Avian Magnetoreception",* Physical Review Letters **110**, 178901 (2013).

[26] I. K. Kominis, *Quantum Zeno effect explains magnetic-sensitive radical-ion-pair reactions,* Physical Review E **80**, 056115 (2009).

[27] I. K. Kominis, *Radical-ion-pair reactions are the biochemical equivalent of the optical double-slit experiment,* Physical Review E **83**, 056118 (2011).

[28] J. Cai, G. G. Guerreschi, and H. J. Briegel, *Quantum Control and Entanglement in a Chemical Compass,* Physical Review Letters **104**, 220502 (2010).

[29] J. Cai and M. Plenio, *Chemical Compass Model for Avian Magnetoreception as a Quantum Coherent Device,* Physical Review Letters **111**, 230503 (2013).

[30] C. Y. Cai, Q. Ai, H. T. Quan, and C. P. Sun, *Sensitive chemical compass assisted by quantum criticality,* Physical Review A **85**, 022315 (2012).

[31] I. K. Kominis, *Reactant-product quantum coherence in electron transfer reactions,* Physical Review E **86**, 026111 (2012).

[32] J. A. Pauls, Y. Zhang, G. P. Berman, and S. Kais, *Quantum coherence and entanglement in the avian compass,* Physical Review E **87**, 062704 (2013).

[33] Y. Zhang, G. P. Berman, and S. Kais, *The radical pair mechanism and the avian chemical compass: Quantum coherence and entanglement,* International Journal of Quantum Chemistry **115**, 1327 (2015).

[34] H. J. Hogben, T. Biskup, and P. J. Hore, *Entanglement and Sources of Magnetic Anisotropy in Radical Pair-Based Avian Magnetoreceptors ,* Physical Review Letters **109**, 220501 (2012).

[35] U. E. Steiner and T. Ulrich, *Magnetic Field Effects in Chemical Kinetics and Related Phenomena,* Chem. Rev. **89**, 51 (1989).

[36] K. Maeda, K. B. Henbest, F. Cintolesi, I. Kuprov, C. T. Rodgers, P. A. Liddell, D. Gust, C. R. Timmel, and P. J. Hore, *Chemical compass model of avian magnetoreception,* Nature **453**, 387 (2008).

[37] H. G. Hiscock, S. Worster, D. R. Kattnig, C. Steers, Y. Jin, D. E. Manolopoulos, H. Mouritsen, and P. J. Hore, *The quantum needle of the avian magnetic compass,* Proceedings of the National Academy of Sciences **113**, 4634–4639 (2016).

[38] T. Ritz, S. Adem, and K. Schulten, *A model for photoreceptor-based magnetoreception in birds,* Biophysical Journal **78**, 707 (2000).

[39] C. T. Rodgers and P. J. Hore, *Chemical magnetoreception in birds: the radical pair mechanism.* Proceedings of the National Academy of Sciences of the United States of America **106**, 353 (2009).

[40] T. Ritz, M. Ahmad, H. Mouritsen, R. Wiltschko, and W. Wiltschko, *Photoreceptor-based magnetoreception: optimal design of receptor molecules, cells, and neuronal processing,* Journal of the Royal Society Interface **7**, 135 (2010).

[41] L.-Q. Wu and J. D. Dickman, *Neural Correlates of a Magnetic Sense,* Science **336**, 1054 (2012).

[42] D. A. Kishkinev and N. S. Chernetsov, *Magnetoreception systems in birds: a review of current research,* Biology Bulletin Reviews **5**, 46 (2015).

[43] K. Mouloudakis and I. K. Kominis, *Revealing the properties of the radical-pair magnetoreceptor using pulsed photo-excitation timed with pulsed rf,* Bio Systems **147**, 35 (2016).

[44] S. Fletcher, *The theory of electron transfer,* Journal of Solid State Electrochemistry **14**, 705 (2010).

[45] R. M. Williams, *Introduction to Electron Transfer*, Ph.D. thesis (2007).

[46] C. T. Rodgers, *Magnetic field effects in chemical systems,* Pure and Applied Chemistry **81**, 19 (2009).

[47] R. A. Marcus, *Electron transfer reactions in chemistry. Theory and experiment,* Pure and Applied Chemistry **69**, 13 (1997).

[48] M. Andrea, *Marcus Theory for Electron Transfer – A short introduction* (2008).

[49] J. P. Allen and J. C. Williams, *Photosynthetic reaction centers,* Federation of European Biochemical Societies Letters **438**, 5 (1998).

[50] W. Hillier and G. T. Babcock, *Photosynthetic reaction centers,* Plant physiology **125**, 33 (2001).

[51] G. L. Closs and L. E. Closs, *Induced dynamic nuclear spin polarization in reactions of photochemically and thermally generated triplet diphenylmethylene,* Journal of the American Chemical Society **91**, 4549 (1969).

[52] R. Kaptein and J. L. Oosterhoff, *Chemically induced dynamic nuclear polarization II: (Relation with anomalous ESR spectra),* Chemical Physics Letters **4**, 195 (1969).

[53] Z. Schulten and K. Schulten, *The generation, diffusion, spin motion, and recombination of radical pairs in solution in the nanosecond time domain,* The Journal of Chemical Physics **66**, 4616 (1977).

[54] K. Schulten, *Magnetic field effects in chemistry and biology,* Advanced Solid State Physics **22**, 61 (1982).

[55] I. K. Kominis, *The radical-pair mechanism as a paradigm for the emerging science of quantum biology,* Modern Physics Letters B **29**, 1 (2015).

[56] V. S. Poonia, D. Saha, and S. Ganguly, *State transitions and decoherence in the avian compass,* Physical Review E **91**, 052709 (2015).

[57] O. Efimova and P. J. Hore, *Role of exchange and dipolar interactions in the radical pair model of the avian magnetic compass.* Biophysical journal **94**, 1565 (2008).

[58] R. Haberkorn, *Density matrix description of spin-selective radical pair reactions,* Molecular Physics **32**, 1491 (1976).

[59] W. H. Zurek, *Decoherence and the transition from quantum to classical,* Phys. Today , 36 (1991).

[60] W. Zurek, *Decoherence and the transition from quantum to classical–Revisited,* Los Alamos Science , 2 (2002).

[61] K. Hornberger, *Introduction to Decoherence Theory* (Springer Berlin Heidelberg, 2009) pp. 221–276.

[62] M. Schlosshauer, *The quantum-to-classical transition and decoherence,* (2014), arXiv:1404.2635 .

[63] H. Breuer and F. Petruccione, *The Theory of Open Quantum Systems* (Oxford University Press, Oxford, 2002).

[64] M. Schlosshauer, *Decoherence and the Quantum-To-Classical Transition* (Springer Berlin Heidelberg, 2007).

[65] I. K. Kominis, *Comment on 'Spin-selective reactions of radical pairs act as quantum measurements' (Chemical Physics Letters 488 (2010) 90-93),* Chemical Physics Letters **508**, 182 (2011).

[66] I. K. Kominis, *Magnetic sensitivity and entanglement dynamics of the chemical compass,* Chemical Physics Letters **542**, 143 (2012).

[67] I. K. Kominis, *Quantum measurement corrections to CIDNP in photosynthetic reaction centers,* New Journal of Physics **15**, 075017 (2013).

[68] G. E. Katsoprinakis, A. T. Dellis, and I. K. Kominis, *Coherent triplet excitation suppresses the heading error of the avian compass,* New Journal of Physics **12**, 085016 (2010).

[69] A. T. Dellis and I. K. Kominis, *Photon statistics as an experimental test discriminating between theories of spin-selective radical–ion-pair reactions,* Chemical Physics Letters **543**, 170 (2012).

[70] A. T. Dellis and I. K. Kominis, *The quantum Zeno effect immunizes the avian compass against the deleterious effects of exchange and dipolar interactions,* BioSystems **107**, 153 (2012).

[71] J. Jones and P. Hore, *Spin-selective reactions of radical pairs act as quantum measurements,* Chemical Physics Letters **488**, 90 (2010).

[72] J. Cai, F. Caruso, and M. B. Plenio, *Quantum limits for the magnetic sensitivity of a chemical compass,* Physical Review A **85**, 040304 (2012).

[73] B. M. Xu, J. Zou, J. G. Li, and B. Shao, *Estimating the hyperfine coupling parameters of the avian compass by comprehensively considering the available experimental results,* Physical Review E **88**, 032703 (2013).

[74] W. Wiltschko and R. Wiltschko, *Magnetic orientation and magnetoreception in birds and other animals,* Journal of Comparative Physiology A **191**, 675 (2005).

[75] H. Mouritsen, *Sensory biology: Search for the compass needles,* Nature **484**, 320 (2012).

[76] S. Boxer, C. E. Chidsey, and M. G. Roelofs, *Magnetic field effects on reaction yields in the solid state: an example from photosynthetic reaction centers,* Annual Review of Physical Chemistry **34**, 389 (1983).

[77] E. Daviso, S. Prakash, A. Alia, P. Gast, J. Neugebauer, G. Jeschke, and J. Matysik, *The electronic structure of the primary electron donor of reaction centers of purple bacteria at atomic resolution as observed by photo-CIDNP ^{13}C NMR.* Proceedings of the National Academy of Sciences of the United States of America **106**, 22281 (2009).

[78] K. L. Ivanov, M. V. Petrova, N. N. Lukzen, and K. Maeda, *Consistent treatment of spin-selective recombination of a radical pair confirms the Haberkorn approach,* Journal of Physical Chemistry A **114**, 9447 (2010).

[79] A. I. Shushin, *Effect of state-selective reactive decay on the evolution of quantum systems,* Journal of Chemical Physics **133**, 044505 (2010).

[80] V. A. Bagryansky, V. I. Borovkov, and Y. N. Molin, *On the verification of different approaches describing spin-selective radical recombination,* Chemical Physics Letters **570**, 141 (2013).

[81] J. Jortner, *Dynamics of electron transfer in bacterial photosynthesis.* Biochimica et Biophysica Acta **594**, 193 (1980).

[82] M. Bixon and J. Jortner, *Charge separation and recombination in isolated supermolecules,* Journal of Physical Chemistry **97**, 13061 (1993).

[83] M. Bixon, J. Jortner, J. Cortes, H. Heitele, and M. E. Michel-Beyerle, *Energy Gap Law for Nonradiative and Radiative Charge Transfer in Isolated and in Solvated Supermolecules,* The Journal of Physical Chemistry **98**, 7289 (1994).

[84] J. H. Golbeck, *Chapter 3: Photosynthetic Reaction Centers: So little time, so much to do.*

[85] M. Goldman, *Formal Theory of Spin-Lattice Relaxation,* Journal of Magnetic Resonance **149**, 160 (2001).

[86] R. A. Fisher, *On the Mathematical Foundations of Theoretical Statistics,* Philosophical Transactions of the Royal Society A **222**, 309 (1922).

[87] H. Cramer, *Mathematical Methods of Statistics* (Princeton University, Princeton, 1946).

[88] C. R. Rao, *Linear Statistical Inference and its Applications, 2nd Edition* (Wiley, New York, 1973).

[89] B. M. Escher, R. L. de Matos Filho, and L. Davidovich, *Quantum Metrology for Noisy Systems,* Brazilian Journal of Physics **41**, 229 (2011).

[90] B. M. Escher, R. L. de Matos Filho, and L. Davidovich, *General framework for estimating the ultimate precision limit in noisy quantum-enhanced metrology,* Nature Physics **7**, 406 (2011).

[91] V. Giovannetti, S. Lloyd, and L. Maccone, *Quantum-Enhanced Measurements : Beating the Standard Quantum Limit,* Science **306**, 1330 (2004).

[92] V. Giovannetti, S. Lloyd, and L. Maccone, *Quantum Metrology,* Physical Review Letters **96**, 010401 (2006).

[93] G.-Y. Xiang and G.-C. Guo, *Quantum metrology,* Chinese Physics B **22**, 110601 (2013).

[94] L.-J. Zhang and M. Xiao, *Towards quantum-enhanced precision measurements: Promise and challenges,* Chinese Physics B **22**, 110310 (2013).

[95] C. W. Helstrom, *Quantum Detection and Estimation Theory* (Academic Press, New York, 1976).

[96] A. S. Holevo, *Probabilistic and Statistical Aspects of Quantum Theory* (North-Holland, Amsterdam, 1982).

[97] S. Braunstein and C. Caves, *Statistical Distance and the Geometry of Quantum States,* Physical Review Letters **72**, 3439 (1994).

[98] S. L. Braunstein, C. M. Caves, and G. J. Milburn, *Generalized uncertainty relations: Theory, examples, and Lorentz invariance,* Annals of Physics **247**, 135 (1996).

[99] Q. Zheng, L. Ge, Y. Yao, and Q. J. Zhi, *Enhancing parameter precision of optimal quantum estimation by direct quantum feedback,* Physical Review A **91**, 033805 (2015).

[100] M. A. Taylor and W. P. Bowen, *Quantum metrology and its application in biology,* Physics Reports **615**, 1 (2015).

[101] B. R. Frieden, *Science from Fisher Information: A Unification, 2nd edition* (Cambridge University Press, Cambridge, 2004).

[102] J. Liu, X. Jing, W. Zhong, and X. Wang, *Quantum Fisher information for density matrices with arbitrary ranks,* Communications in Theoretical Physics **61**, 45 (2014).

[103] S. Pang and T. A. Brun, *Quantum metrology for a general Hamiltonian parameter,* Physical Review A **90**, 022117 (2014).

[104] S. Johnsen and K. J. Lohmann, *Magnetoreception in animals,* Physics Today **61**, 29 (2008).

[105] R. Haberkorn and M. E. Michel-Beyerle, *On the mechanism of magnetic field effects in bacterial photosynthesis,* Biophysical Journal **26**, 489 (1979).

[106] T. Polenova and A. E. McDermott, *A Coherent Mixing Mechanism Explains the Photoinduced Nuclear Polarization in Photosynthetic Reaction Centers,* The Journal of Physical Chemistry B **103**, 535 (1999).

[107] J. Matysik, A. Diller, E. Roy, and A. Alia, *The solid-state photo-CIDNP effect,* Photosynthesis Research **102**, 427 (2009).

[108] I. F. Céspedes-Camacho and J. Matysik, *Spin in Photosynthetic Electron Transport, in The biophysics of photosynthesis, by J. Goldbeck & Art van der Est* (Springer Science+ Business Media, New York, 2014).

[109] K. M. Vitalis and I. K. Kominis, *Lamb shift in radical-ion pairs produces a singlet-triplet energy splitting in photosynthetic reaction centers,* European Physical Journal Plus **129**, 187 (2014).

[110] M. Kritsotakis and I. K. Kominis, *Retrodictive derivation of the radical-ion-pair master equation and Monte Carlo simulation with single-molecule quantum trajectories,* Physical Review E **90**, 042719 (2014).

[111] D. Budker and M. V. Romalis, *Optical Magnetometry,* Nature Physics **3**, 227 (2007).

[112] D. Budker, D. F. Kimball, S. M. Rochester, V. V. Yashchuck, and M. Zolorotev, *Sensitive magnetometry based on nonlinear magneto-optical rotation,* Physical Review A **62**, 043403 (2000).

[113] J. C. Allred, R. N. Lyman, T. W. Kornack, and D. Budker, *High-Sensitivity Atomic Magnetometer Unaffected by Spin-Exchange Relaxation,* Physical Review Letters **89**, 130801 (2002).

[114] V. Shah, S. Knappe, P. D. D. Schwinndt, and J. Kitching, *Subpicotesla atomic magnetometry with a microfabricated vapour cell,* Nature Photonics **1**, 649 (2007).

[115] W. Wasilewski, K. Jensen, H. Krauter, J. J. Renema, M. V. Balabas, and E. S. Polzik, *Quantum Noise Limited and Entanglement-Assisted Magnetometry,* Physical Review Letters **104**, 133601 (2010).

[116] Z. D. Grujić, P. A. Koss, G. Bison, and A. Weiss, *A sensitive and accurate atomic magnetometer based on free spin precession,* European Physical Journal D **69**, 135 (2015).

[117] V. G. Lucivero, R. Jiménez-Martínez, J. Kong, and M. W. Mitchell, *Squeezed-light spin noise spectroscopy,* Physical Review A **93**, 053802 (2016).

[118] K. Fang, V. M. Acosta, C. Santori, Z. Huang, K. M. Itoh, H. Watanabe, S. Shikata, and R. G. Beausoleil, *High-Sensitivity Magnetometry Based on Quantum Beats in Diamond Nitrogen-Vacancy Centers,* Physical Review Letters **110**, 130802 (2013).

[119] K. Jensen, N. Leefer, A. Jarmola, Y. Dumeige, V. M. Acosta, P. Kehayias, B. Patton, and D. Budker, *Cavity-Enhanced Room-Temperature Magnetometry Using Absorption by Nitrogen-Vacancy Centers in Diamond,* Physical Review Letters **112**, 160802 (2014).

[120] T. Wolf, P. Neumann, K. Nakamura, H. Sumiya, T. Ohshima, J. Isoya, and J. Wrachtrup, *Subpicotesla Diamond Magnetometry,* Physical Review X **5**, 041001 (2015).

[121] B. Teklu, S. Olivares, and M. G. A. Paris, *Bayesian estimation of one-parameter qubit gates,* Journal of Physics B **42**, 035502 (2009).

[122] S. Gammelmark and K. Mølmer, *Fisher Information and the Quantum Cramér-Rao Sensitivity Limit of Continuous Measurements,* Physical Review Letters **112**, 170401 (2014).

[123] G. G. Guerreschi, M. Tiersch, U. E. Steiner, and H. J. Briegel, *Optical switching of radical pair conformation enhances magnetic sensitivity,* Chemical Physics Letters **572**, 106 (2013).

[124] K. Maeda, S. R. T. Neil, K. B. Henbest, S. Weber, E. Schleicher, P. J. Hore, S. R. Mackenzie, and C. R. Timmel, *Following Radical Pair Reactions in Solution: A Step Change in Sensitivity Using Cavity Ring-Down Detection,* Journal of the American Chemical Society **133**, 17807 (2011).

[125] K. Maeda, A. J. Robinson, K. B. Henbest, H. J. Hogben, T. Biskup, M. Ahmad, E. Schleicher, S. Weber, C. R. Timmel, and P. J. Hore, *Magnetically sensitive light-induced reactions in cryptochrome are consistent with its proposed role as a magnetoreceptor,* Proceedings of the National Academy of Sciences of the United States of America **109**, 4774 (2012).

[126] Y. Wang, K. Sahin-Tiras, N. J. Harmon, M. Wohlgenannt, and M. E. Flatté, *Immense Magnetic Response of Exciplex Light Emission due to Correlated Spin-Charge Dynamics,* Physical Review X **6**, 011011 (2016).

[127] G. Jeschke, *Comment on "Quantum trajectory tests of radical-pair quantum dynamics in CIDNP measurements of photosynthetic reaction centers" [Chem. Phys. Lett. 640 (2015) 40–45],* Chemical Physics Letters **648**, 200 (2016).

[128] I. K. Kominis, *Reply to the comment on "Quantum trajectory tests of radical-pair quantum dynamics in CIDNP measurements of photosynthetic reaction centers" by G. Jeschke,* Chemical Physics Letters **648**, 204 (2016).

[129] R. R. Puri, *Mathematical Methods of Quantum Optics* (Springer, Berlin, 2001).

[130] T. Unden, P. Balasubramanian, D. Louzon, Y. Vinkler, M. B. Plenio, M. Markham, D. Twitchen, A. Stracey, I. Lovchinsky, A. O. Sushkov, M. D. Lukin, A. Retzker, B. Naydenov, L. P. McGuinness, and F. Jelezko, *Quantum Metrology Enhanced by Repetitive Quantum Error Correction,* Physical Review Letters **116**, 230502 (2016).

[131] M. Twardy and D. Olszewski, *Realization of controlled NOT quantum gate via control of a two spin system,* Bulletin of the Polish Academy of Sciences. Technical Sciences **61**, 379 (2013).

[132] E. Merino and M. Ribagorba, *Control over molecular motion using the cis–trans photoisomerization of the azo group,* Beilstein Journal of Organic Chemistry **8**, 1071 (2012).

[133] F. M. Raymo and S. Giordani, *All-optical processing with molecular switches,* Proc. Natl. Acad. Sci. U.S.A. **99**, 4941 (2002).

[134] H. Li and D. H. Qu, *Recent advances in new-type molecular switches,* Sci. China Chem. **58**, 916 (2015).

[135] D. Bléger and S. Hecht, *Visible-light-activated molecular switches,* Angew. Chem. Int. Ed. **54**, 11338 (2015).

[136] J. L. Zhang, J. Q. Zhong, J. D. Lin, W. P. Hu, K. Wu, G. Q. Xu, A. T. S. Wee, and W. Chen, *Towards single molecule switches,* Chem. Soc. Rev. **44**, 2998 (2015).

[137] D. R. Kattnig, J. K. Sowa, I. A. Solov'yov, and P. J. Hore, *Electron spin relaxation can enhance the performance of a cryptochrome-based magnetic compass sensor,* New Journal of Physics **18**, 063007 (2016).

[138] S. F. Huelga, C. Macchiavello, T. Pellizzari, A. K. Ekert, M. B. Plenio, and J. I. Cirac, *Improvement of Frequency Standards with Quantum Entanglement,* Physical Review Letters **79**, 3865 (1997).

[139] C. R. Timmel, U. Till, B. Brocklehurst, K. A. Mclauchlan, and P. J. Hore, *Effects of weak magnetic fields on free radical recombination reactions,* Molecular Physics **95**, 71 (1998).